



AGU Advances

First Revision of

Column-Compound Extremes in the Global Ocean

Joel Wong¹, Matthias Münnich¹, and Nicolas Gruber¹

¹Environmental Physics, Institute of Biogeochemistry and Pollutant Dynamics, ETH Zurich, Zurich, Switzerland

Column-Compound Extremes in the Global Ocean

Joel Wong¹, Matthias Münnich¹, and Nicolas Gruber¹

¹Environmental Physics, Institute of Biogeochemistry and Pollutant Dynamics, ETH Zurich, Zürich, Switzerland

Key Points:

- Column-compound extremes (CCX)- extremes in multiple parameters within the top 300 m, may reduce habitable space by up to 75%.
- From 1961 to 2020, CCX have become more intense, longer, and occupy more volume, driven by the trends in ocean warming and acidification.
- Triple CCX are largely confined to the tropics and the North Pacific, have high intensity, and severely reduce habitable space.

Abstract

Marine extreme events such as marine heatwaves, ocean acidity extremes and low oxygen extremes can pose a substantial threat to marine organisms and ecosystems. Such extremes might be particularly detrimental (i) when they are compounded in more than one stressor, and (ii) when the extremes extend substantially across the water column, restricting the habitable space for marine organisms. Here, we use daily output of a hindcast simulation (1961-2020) from the ocean component of the Community Earth System Model to characterise such column-compound extreme events (CCX), employing a relative threshold approach to identify extremes and requiring them to extend vertically over at least 50 m. The diagnosed CCX are prevalent, occupying worldwide in the 1960s about 1% of the volume contained within the top 300 m. Over the duration of our simulation, CCX become more intense, last longer, and occupy more volume, driven by the trends in ocean warming and ocean acidification. For example, the triple CCX expanded 39-fold, now last 3-times longer, and became 6-times more intense since the early 1960s. Removing this effect with a moving baseline permits us to better understand the key characteristics of CCX, revealing a typical duration of 10-30 days and a predominant occurrence in the Tropics and high latitudes, regions of high potential biological vulnerability. Overall, the CCX fall into 16 clusters, reflecting different patterns and drivers. Triple CCX are largely confined to the tropics and the North Pacific, and tend to be associated with the El Niño-Southern Oscillation.

Plain Language Summary

The global ocean is becoming warmer, more acidic, and losing oxygen due to climate change. On top of this trend, sudden increases in temperature, or drops in pH or oxygen adversely affect marine organisms when they cannot quickly adapt to these extreme conditions. These conditions are worse for marine organisms when such extremes occur together in the vertical water column, leading to column-compound extreme (CCX) events, severely reducing the available habitable space. To investigate such CCX, we used a numerical model simulation of the global ocean during the historical period of 1961 to 2020. Singular extreme events are identified primarily with relative percentile thresholds, while CCX require a 50 m minimum depth threshold in the water column. We find that CCX have been increasing in volume, occupying up to 20% of the global ocean volume toward 2020. We then remove the climate trend to better understand the drivers behind CCX. Many CCX occur in the tropics and high latitudes, lasting 10 to 30 days and reducing habitable space by up to 75%. This study is the first to systematically detect compound extremes in the water column and may form the basis for determining their detrimental effects on marine organisms and ecosystems.

1 Introduction

Climate change has measurably heated the ocean, increased its acidity, and decreased its oxygen content (Masson-Delmotte et al., 2021). These trends are punctuated by extreme events whose intensities and rapid onsets may impact marine organisms and ecosystems more than slowly evolving trends (Collins et al., 2019; Gruber et al., 2021). The study of marine extremes has emerged strongly in the last decade, with the vast majority of studies focusing on marine heat waves (Hobday et al., 2016; Holbrook, Sen Gupta, et al., 2020; Oliver et al., 2021), their drivers (Holbrook et al., 2019; Sen Gupta et al., 2020), and impacts (Smale et al., 2019; K. E. Smith et al., 2023). Receiving increased attention are extremes in ocean acidity (OAX) (Hauri et al., 2013; Kwiatkowski & Orr, 2018; Negrete-García et al., 2019; Burger et al., 2020; Desmet et al., 2022, 2023) and low oxygen (LOX) (Chan et al., 2008; Hofmann et al., 2011; Leung, Mislán, et al., 2019; Köhn et al., 2022), with a particular emerging concern about compound marine extremes, when

61 conditions are extreme in more than one stressor (Gruber et al., 2021; Le Grix et al., 2021;
62 Burger et al., 2022; Le Grix et al., 2022; Hauri et al., 2024).

63 Such compounded extreme events can have a large impact on marine biota. When
64 different stressors act synergistically, they can cause a disproportionately larger impact
65 than that of individual stressors (Crain et al., 2008; Boyd & Brown, 2015; Pirotta et al.,
66 2022). A well-known example is the decrease in aerobic metabolic rates with increasing
67 temperature and decreasing oxygen (Pörtner & Knust, 2007; Deutsch et al., 2015), mak-
68 ing ectotherms especially susceptible to compounded MHW and LOX. Bednaršek et al.
69 (2018) also showed biological implications for pteropods during anomalously high tem-
70 perature and acidity events (the latter corresponding to anomalously low pH events, with
71 $\text{pH} = -\log[\text{H}^+]$, and $[\text{H}^+]$ being the concentration of the hydrogen ion). Multiple ex-
72 tremes occurring at the same time and place have been explored with properties such
73 as temperature and pH (Burger et al., 2022), temperature and chlorophyll (Le Grix et
74 al., 2021), pH and oxygen (Nam et al., 2011; Köhn et al., 2022), and for triple extremes
75 involving pH, oxygen, and temperature (Gruber et al., 2021).

76 Warming of the ocean in the past 150 years and the strong trend of ocean acidi-
77 fication have led to substantial increases in MHW and OAX associated with these stres-
78 sors (Oliver et al., 2018; Gruber et al., 2021) and are certain to increase in the future
79 as long as these driving trends continue (Frölicher et al., 2018). For example, Oliver et
80 al. (2018) showed on a fixed baseline approach that between 1925 and 2016, the frequency
81 and duration of MHW increased by 34% and 17%, respectively, resulting globally in a
82 greater than 50% increase in the number of MHW days. For OAX, the trends are even
83 stronger, increasing from a pre-industrial situation of about 4 extreme days a year to a
84 nearly permanent state of extremes (Gruber et al., 2021; Burger et al., 2022). Correspon-
85 ding trends are also expected for LOX events driven by ocean deoxygenation (Gruber et
86 al., 2021), but global ocean deoxygenation trends tend to be smaller compared to the
87 level of variability, leading to smaller, and not yet well-established trends in LOX. As
88 a consequence of these trends in the single stressor extremes, increasing compound ex-
89 tremes naturally follow. For example, Gruber et al. (2021) attributed the development
90 of widespread double compound extremes in the Northeast Pacific over the past 40 years,
91 and especially the triple compound extreme at the height of the 'Blob' event (2013-2016),
92 in part, to the underlying trends of ocean warming, acidification, and deoxygenation. They
93 speculated that part of the broad ecological impacts of the "Blob" might be caused by
94 these compound extremes. To better understand the mechanisms driving these extremes,
95 we remove the underlying trends using a so-called moving baseline (Oliver et al., 2021;
96 Burger et al., 2020; Gruber et al., 2021; Burger et al., 2022). Analysis of extremes and
97 especially compound extremes on a moving baseline is also appropriate when consider-
98 ing the impact of these extremes on organisms that have the capacity to adapt to the
99 more slowly evolving changes in temperature, ocean acidification, and oxygen (see also
100 the discussion by Sen Gupta (2023)).

101 So far, the vast majority of MHW studies have focused on the surface ocean only,
102 although many organisms might have the potential to migrate to colder temperatures
103 at deeper depths when a surface heat wave affects them (Jorda et al., 2020). Further-
104 more, the habitat of vertically migrating organisms can be considered to include the wa-
105 ter column down to about 400 m (Bianchi et al., 2013; Bianchi & Mislán, 2016). Detect-
106 ing extremes across the vertical dimension is thus an important step towards understand-
107 ing the compression of habitable space during such extremes. Some MHW studies have
108 looked into the subsurface, (Schaeffer & Roughan, 2017; Elzahaby et al., 2021; Scannell
109 et al., 2020; McAdam et al., 2022; Fragkopoulou et al., 2023; Amaya et al., 2023; Köhn
110 et al., 2024), while the concept of habitat compression has been considered with respect
111 to temperature and oxygen changes (Jorda et al., 2020; Köhn et al., 2022). However, a
112 consistent definition of compound extremes in the column has yet to be defined. The well-

113 studied surface MHW may extend into the subsurface, vertically compounding with OAX
114 and LOX to deteriorate the habitable conditions of the water column.

115 Marine extremes can be driven by various mechanisms, and the study of extremes
116 compounded in the vertical dimension increases the complexity of this task (Gruber et
117 al., 2021). Surface MHW are understood to be driven primarily from the atmosphere through
118 anomalous air-sea heat fluxes, or by lateral heat advection (Sen Gupta et al., 2020; Hol-
119 brook, Sen Gupta, et al., 2020; Marin et al., 2022). Such surface MHW may cause higher
120 stratification in the upper ocean, suppressing the upwelling of carbon-rich and low-oxygen
121 waters and hence decreasing the likelihood of surface OAX and LOX. However, temper-
122 ature anomalies have been shown to influence OAX occurrence by shifting the carbon-
123 ate chemistry equilibrium or modulating dissolved organic carbon (DIC) (Burger et al.,
124 2022), thus increasing or decreasing $[H^+]$ respectively. At depth, vertical or lateral dis-
125 placement of waters across strong temperature gradients, $[H^+]$, or oxygen tends to be
126 an important driver of subsurface extremes, with the orientation of the gradients being
127 key to determine the nature of the compound extreme. In terms of generating and main-
128 taining marine extremes at depth, other biological-physical mechanisms (e.g., mesoscale
129 eddies (Gruber et al., 2021; Köhn et al., 2022; Desmet et al., 2022)) are critical.

130 Taking into account the various physical, chemical, and biogeochemical processes
131 in the ocean, inferring the mechanisms behind compound extreme events can be a com-
132 plex task. Extremes that are compounded may share a common driver, be driven by one
133 another, or co-occur in the column with different drivers (Gruber et al., 2021). With per-
134 centile thresholds, some detected compound extremes may arise purely out of statisti-
135 cal chance (Burger et al., 2022). Extremes with affiliated drivers have a higher propen-
136 sity of co-occurrence above such a random signal. Such compound extremes are signif-
137 icant and merit investigation.

138 Extreme events across the globe have been linked to large-scale climate modes, the
139 dominant one being the El Niño-Southern Oscillation (ENSO) (Santoso et al., 2017; Hol-
140 brook, Claar, et al., 2020). The prevalence of ENSO in the study of marine extremes is
141 due in part to the large area it affects in the Pacific, but also to its teleconnections with
142 other ocean basins (Roy & Reason, 2001; Luo et al., 2010). ENSO events are triggered
143 by changes in winds in the eastern tropical Pacific, but they affect many remote regions
144 through connected changes in large-scale ocean and atmospheric circulations (aka tele-
145 connections). Although ENSO might not directly cause the extreme, ENSO-driven changes
146 in the mean state can make the occurrence of extremes more likely or prolong and in-
147 tensify existing extremes. A good example is the 2013-2015 "Blob" marine heatwave in
148 the Northeast Pacific, which became one of the largest and longest lasting MHW owing
149 to the coalescence of regional circulation changes and ENSO-driven warming (Di Lorenzo
150 & Mantua, 2016; Holbrook et al., 2019; Gruber et al., 2021). ENSO has also been as-
151 sociated with MHW in the Indian and Southern Oceans (Holbrook et al., 2019; Sen Gupta
152 et al., 2020; Oliver et al., 2021). Furthermore, ENSO has been shown to be strongly cor-
153 related with OAX and LOX in the Pacific Ocean, especially at depth (Turi et al., 2018;
154 Leung, Thompson, et al., 2019; Köhn et al., 2022; Desmet et al., 2023).

155 Here, we extend the existing work on marine extremes by simultaneously expand-
156 ing our analysis in two directions. We expand in depth by analyzing extremes across the
157 upper water column, and we expand in terms of stressors by focusing on compound events.
158 Thus, we will define and characterise column-compound extreme events in the vertical
159 water column at the global scale, and aim to understand their drivers. To this end, we
160 will use results from a hindcast simulation undertaken with a global ocean coupled physical-
161 biogeochemical model, sampled at high temporal frequency to permit us to identify ex-
162 tremes. We rely on model simulation results, since there are no observational records avail-
163 able across all parameters or depth that would permit us to undertake this study.

164 We also develop a framework to analyze such events, which we call Column-Single
 165 eXtreme events (CSX) in the case of a single parameter being extreme across a good por-
 166 tion of the water column and column-compound eXtreme events (CCX) when more than
 167 one CSX is detected in the same column at the same time. We will show that these events
 168 are prevalent in the ocean, primarily occurring at low latitudes, and that their frequency,
 169 duration, and intensity have increased in recent decades. While we cannot yet identify
 170 the potential impacts of these extremes on marine organisms and ecosystems, the com-
 171 pounding of extreme conditions is expected to push marine organisms to their limits. We
 172 will show the places and times where these column extremes tend to occur, giving in-
 173 sights into where and when one should look for these ecological impacts.

174 2 Detecting Extreme Events in the Water Column

175 No consistent definition of single or compound marine extreme events exists so far,
 176 much less if they are co-occurring in the same vertical column. We thus first review the
 177 issues at hand and then illustrate the framework we have used to identify the Column-
 178 Single eXtreme events (CSX) and the Column-Compound eXtreme events (CCX).

179 A common issue to be resolved in all studies is the choice of thresholds and base-
 180 lines. Regarding the threshold, MHW-related studies have relied on a relative percentile
 181 threshold approach, with the majority of studies using a seasonally-varying threshold (Oliver
 182 et al., 2018; Holbrook, Sen Gupta, et al., 2020), so that extreme conditions can be de-
 183 tected regardless of the season. On the contrary, absolute thresholds remain pertinent
 184 to extremes such as LOX, where the metabolic requirement for organisms tends to be
 185 fixed (Hofmann et al., 2011), with some degree of variability with temperature (Seibel,
 186 2011; Deutsch et al., 2015). Absolute thresholds have also been used to detect extremes
 187 in aragonite saturation state (Hauri et al., 2013; Negrete-García et al., 2019; Desmet et
 188 al., 2022), where a thermodynamic threshold determines the state of dissolution of the
 189 shells of calcifying organisms. Thus, there are clear grounds for using either relative or
 190 absolute thresholds, and we make use of both in this study.

191 The baseline, that is, the time period used to identify thresholds, is also a critical
 192 choice in detecting extremes (Jacox, 2019; Oliver et al., 2021; Sen Gupta, 2023). In the
 193 case of a fixed baseline, the thresholds remain invariant, such that trends in tempera-
 194 ture, pH, and oxygen imply an increase in the frequency and intensity of extreme events
 195 (Gruber et al., 2021). This could be problematic when cold spells in subsequent years
 196 are potentially marked as heatwaves (Jacox, 2019), or when waters become classified as
 197 permanently extreme with respect to ocean acidification (Hauri et al., 2013; Burger et
 198 al., 2020, 2022; Gruber et al., 2021). An alternative is the use of a moving baseline, that
 199 is, where the reference period used to identify the relative thresholds is shifting in time
 200 with the analysis, or alternatively, where the thresholds are computed based on detrended
 201 data. An analysis with such a moving baseline gives equal weight to extreme events through-
 202 out the time period (Burger et al., 2020; Rosselló et al., 2023), and is more suitable for
 203 the investigation of drivers (Chiswell, 2022). It is also more relevant to organisms that
 204 are able to adapt to the gradually changing conditions (Holbrook, Sen Gupta, et al., 2020;
 205 Oliver et al., 2021), but are still affected by sudden changes in conditions during an ex-
 206 treme event. In this study, we first present our results on a fixed baseline, illustrating
 207 the response of extreme events to the climate trend. Then, we primarily use the mov-
 208 ing baseline to analyse extreme events and postulate drivers. A quadratic moving base-
 209 line is chosen to fit the long-term trend in $[H^+]$ (Hauri et al., 2021) (Text S1 and Fig-
 210 ures S1-S2).

211 The next choices concern the vertical structure and compounding of the stressors.
 212 For the vertical structure, we define columns to be Column-Single eXtreme events (CSX)
 213 of a particular type (MHW, OAX, or LOX) when the grid cells considered extreme with
 214 respect to this particular parameter occupy more than 50 m of the upper 300 m of the

215 water column. For the compounding, we identify columns to be Column-Compound eX-
 216 treme events (CCX) when more than one CSX is detected in the same column at the same
 217 time. This leads to three types of double stressor CCX, that is, MHW-OAX, MHW-LOX,
 218 and OAX-LOX, and one type of triple stressor CCX, i.e., MHW-OAX-LOX.

219 In Figure 1a, a conceptual sketch of the various types of defined extremes is shown
 220 for a single column over time. Grid cell extreme events are coloured within the Hovmoller
 221 diagram, where they occur. However, this does not necessarily mean that a column ex-
 222 treme is occurring. For example, a CSX-MHW starts at day 20 from the surface, while
 223 a CSX-OAX and CSX-LOX start from the bottom of the column at days 35 and 47 re-
 224 spectively. The durations of the CSX and CCX are marked with arrow ranges below Fig-
 225 ure 1b.

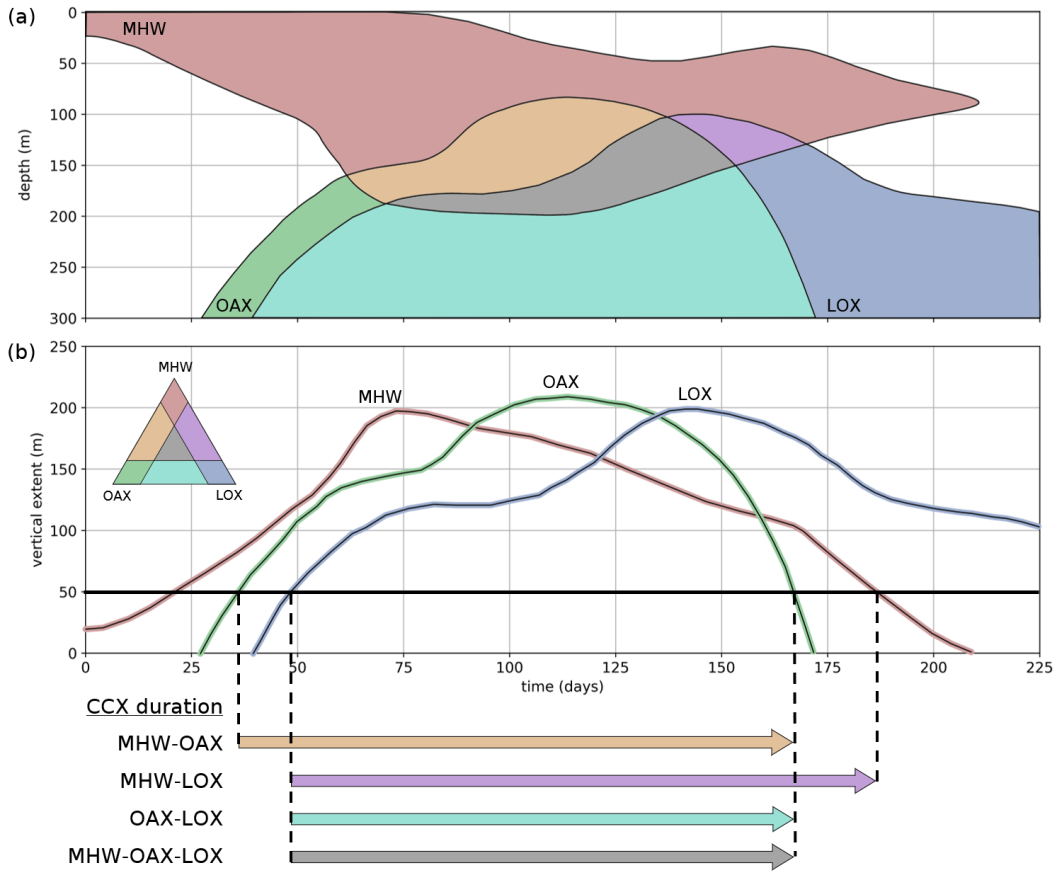


Figure 1. Illustration of the concepts used to detect and analyze column compound extremes. (a) Idealized Hovmoller diagram illustrating the time-depth evolution of extreme conditions in a hypothetical water column from the surface down to 300 m depth. The coloured regions within the plot are considered extreme, with the colours brown, green and blue representing pure MHW, OAX and LOX, respectively. The areas where the different extremes overlap are given colours according to the mixing diagram in panel (b). (b) Timeseries of the total vertical extent (within the top 300 m of the water column) for each extreme type. When the vertical extent for a particular type of extreme exceeds 50 m, we call it a *Column-single eXtreme event (CSX)* of this parameter and when more than one of these occur at the same time a *Column-Compound eXtreme event (CCX)*. The duration of the four different types of CCX is indicated by arrows.

3 Methods

3.1 Model Simulations

To identify the CSX and CCX, we used results from a hindcast simulation performed with the ocean component of the global Community Earth System Model (CESM) Version 1.2 (Gent et al., 2011). The ocean component consists of the Parallel Ocean Program 2 (POP2) (R. Smith & Gent, 2010) that simulates ocean circulation and mixing, the Community Ice Code 4 (CICE4) model, also known as the Los Alamos Sea Ice Model (Hunke & Lipscomb, 2008) simulating the presence and thickness of sea ice, and the Biological Elemental Cycling (BEC) model (Moore et al., 2004, 2013) representing ocean ecology and biogeochemistry. The model has a nominal meridional resolution of 0.5° near the poles, refined to 0.3° at the equator, and a nominal zonal resolution of 1° . There are 60 depth levels in the vertical dimension, extending from the surface to 5375 m. BEC includes three phytoplankton functional types that are grazed by one zooplankton type. Temperature and dissolved oxygen fields are prognostic variables of the coupled model, while the hydrogen ion concentration (on the total scale) was obtained from the simulated inorganic carbon parameters by applying calculations of the carbonate system based on the OCMIP2 routines (Orr et al., 2005). Details of the model can be found in Yang and Gruber (2016).

The model simulation started from a spun-up preindustrial state (Yang & Gruber, 2016) and was brought forward from 1850 to 1957 with cyclically repeated 3-hourly atmospheric forcing from the Japanese 55-year Re-analysis (JRA-55) product (Ebita et al., 2011) and atmospheric CO_2 prescribed according to observations provided by the Global Carbon Project (Friedlingstein et al., 2022). The hindcast simulation was then produced with daily output for the years 1958 to 2020 also using the historical JRA-55 forcing. To allow the ocean state to relax from the cyclic atmospheric forcing during the spinup, we discard the first three years and limit our analysis to the 60-year period between 1961 and 2020. The results of this simulation were also used for the Global Carbon Budgets 2020 and 2021 (Friedlingstein et al., 2022) in Hauck et al. (2020) and in RECCAP2 papers DeVries et al. (2023); Hauck et al. (2023).

3.2 Extreme Events Detection

In the first step, single extreme events of MHW, OAX, and LOX are detected for each grid cell for each day. For MHW and OAX, a 95th percentile threshold is applied to temperature and $[\text{H}^+]$, respectively, using seasonally-varying thresholds. For LOX, we require the oxygen concentration to be below the 5th percentile value (again seasonally varying), after which values above $150 \mu\text{M}$ ($\sim 3.5 \text{ ml/L}$) are masked. The absolute threshold for LOX was added because LOX at high oxygen levels have very little biological impact. The chosen value is the hypoxic threshold of some larger fish species such as yellowfin and skipjack tuna, marlin, and sailfish (Braun et al., 2015; Leung, Mislán, et al., 2019; Rose et al., 2019). The absolute threshold for LOX is applied directly on the (non-detrended) model output. The detection thresholds for single events in the grid cell are summarised in Table 1. In this work, we do not impose additional criteria, such as minimum duration (Hobday et al., 2016), since one goal of this study is to identify drivers behind exceedances of the threshold. For fixed baseline thresholds, the data are detrended with a quadratic trend to a reference year of 1958 prior to computing the percentile thresholds. For the moving baseline results, the thresholds change with time with respect to the fitted quadratic trend. A detailed description of the detrending for fixed and moving baselines and the computation of thresholds can be found in Text S1.

Table 1. Single extremes and the thresholds used for their detection

Single Extreme Type	Variable	Percentile Threshold	Additional Absolute Threshold
Marine Heatwave (MHW)	T	> 95 th	-
Ocean Acidification Extreme (OAX)	[H ⁺]	> 95 th	-
Low Oxygen Extreme (LOX)	[O ₂]	< 5 th	< 150 μ M

273 To define extreme events in the vertical column, we require that at least 50 m of
 274 the top 300 m be extreme with respect to each stressor. The analysis range of 300 m re-
 275 flects the vertical habitat range of epipelagic and other vertically migrating organisms
 276 (Bertrand et al., 2010; Bianchi et al., 2013; Bianchi & Mislan, 2016). This choice is ar-
 277 guably somewhat subjective, but it encompasses the depth range of the vast majority
 278 of marine organisms. The value of the minimum extension of 50 m is also subjective, but
 279 aims to capture the occasion when a substantial fraction of the water column is extreme,
 280 affecting the organisms that live within this water column in a major way. Adjusting this
 281 minimum extension modulates the number of column extremes detected, but does not
 282 significantly change their spatial or temporal distribution (Text S2 and Figures S3-S6).
 283 When the 50 m vertical threshold is met for a single stressor, it is denoted as a column-
 284 single extreme event (CSX), illustrated in Figure 2a. The criteria for a CCX are met when
 285 two or more CSX occur in the same vertical column at the same time. Various config-
 286 urations of CCX are illustrated in Figure 2b. CSX can be located separately in column
 287 (c) or have some overlap (e). The single extreme grid cells do not need to be vertically
 288 connected to meet the 50 m threshold, as seen in (b) and (d).

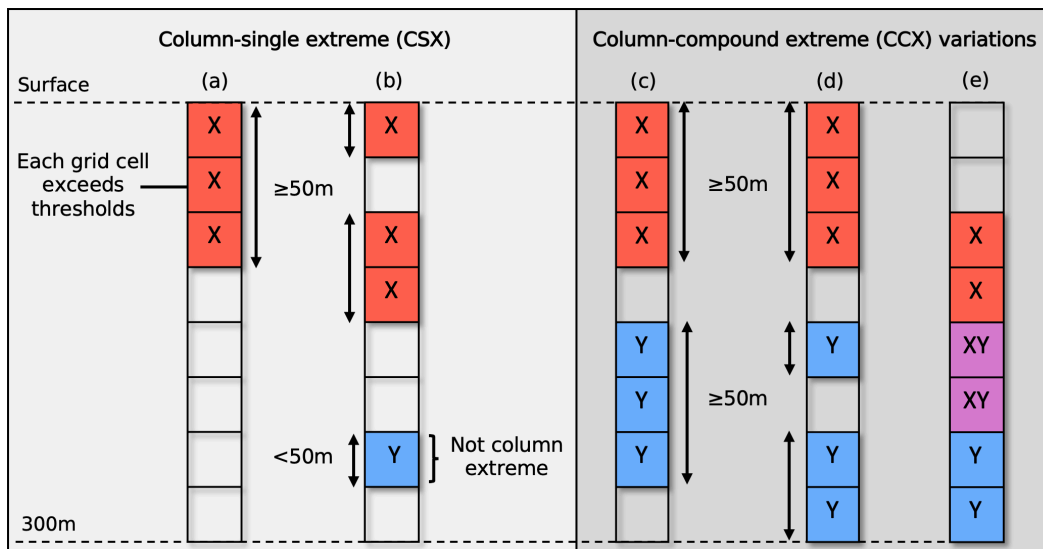


Figure 2. Illustration of different types of column-extreme events within the water column. (a) Column-single extreme (CSX), (b) CSX with discontinuous grid cells of extreme type 'X', (c) Column-compound extreme (CCX), (d) CCX with discontinuous grid cells of extreme type 'Y', (e) CCX with overlapping 'X' and 'Y' type extremes.

289

3.3 Extreme Event Metrics

290

291

292

293

294

295

296

297

298

The metrics used to characterise extreme events can be broadly grouped into frequency, intensity, and temporal categories. Regarding the extremes in the vertical column, we also quantify their size, location, and remaining contiguous habitable space (see Table 2). Although many of these metrics are commonly used in extreme studies, some had to be redefined in the context of our work on column extremes. We do not include severity in our analyses, that is, the cumulative sum of the intensity value over the duration of the event (Hobday et al., 2016; Hauri et al., 2013; Samuels et al., 2021), since it strongly correlates with the event duration in our analyses. Note that triple CCX are also double CCX and are thus included in their metrics.

Table 2. Metrics used in the analysis of extreme events

Name	Symbol	Definition
<i>Frequency metrics</i>		
Days per year	N	Mean number of extreme days per year
Co-occurrence propensity	CP	Likelihood of two or more CSX occurring within the same vertical water column at the same time
Enhancement (Suppression) of CCX during ENSO	ΔN	Mean increase (decrease) in the number of extreme days per year during ENSO events, compared to that in the neutral phase
<i>Intensity metrics</i>		
Intensity index	ψ_i	Ratio of an event variable's i difference from its climatological value to the difference between the threshold and the climatological value.
Compound intensity index	Ψ	Square-root of the sum of squares of the intensity index of individual events that make up a compound event
Maximum intensity index	ψ^{\max}	Maximum value of the intensity index over time and the vertical column
<i>Temporal metrics</i>		
Duration	D	Lifetime of an event for which the thresholds are met continuously
<i>Size and location metrics</i>		
Volume fraction	f_V	Fraction of total volume (top 300 m) of a defined region that is affected by extremes
Vertical fraction	f_z	Fraction of top 300 m of a column occupied by extremes
Contiguous habitable space fraction	f_h	Fraction of the top 300 m within a column contiguously unaffected by extremes

299

300

301

302

The duration of an event refers to the total length of time for which the specified extreme type exists in the water column. For example, a MHW-OAX event starts from the time CSX-MHW and CSX-OAX both exist in the water column, even if the CSX-MHW started earlier (see Figure 1). The same applies to the end of a CCX.

303

304

305

The intensity index expresses the strength of an extreme event in a unitless way. It is inspired by the MHW categories of Hobday et al. (2018), and defined as the continuous severity index by Sen Gupta et al. (2020). Using the intensity index as a mea-

306 sure of event intensity permits us to compare the intensities of multiple extremes and
 307 even combine them. For a single grid cell, it is expressed as:

$$\psi_X = \frac{X - X_c}{X_t - X_c}, \quad (1)$$

308 where X is the parameter of interest, X_c is its climatological value for that day of the
 309 year, and X_t is the threshold value. For the climatology, we use the median value to avoid
 310 instances where it is skewed by exceptionally intense extreme events. The median value
 311 is obtained from a seasonally varying 11-day rolling window. To express the intensity
 312 index of multiple extremes occurring in the same grid cell, we take the Euclidean norm
 313 of ψ of the single extremes:

$$\Psi = \sqrt{\psi_X^2 + \psi_Y^2 + \psi_Z^2}, \quad (2)$$

314 where ψ_X , ψ_Y , and ψ_Z are the intensity index values of single extremes.

315 The co-occurrence propensity (CP) is a central metric for the study of compound
 316 extremes, as it allows us to assess whether two extremes co-occur by chance, or whether
 317 they co-occur as a result of a common process forcing them. Likewise, the propensity
 318 can be used to assess whether two extremes co-occur much less frequently than expected
 319 by chance, since the process forcing one extreme may lead to conditions that suppress
 320 its co-occurrence with another. The CP metric is defined as the likelihood that two (or
 321 three) different CSX occur in the vertical column at the same time. It is scaled to the
 322 range of $[-1,1]$. A value of 1 indicates that the CSX always occur together whenever they
 323 occur, while a value of -1 indicates that they never occur together. A value of 0 suggests
 324 that their occurrences are independent, as if randomly distributed in time. A positive
 325 value suggests that the CSX in consideration have similar or related drivers, while a neg-
 326 ative value suggests that they have opposing drivers.

327 First, the independent (random) value of CCX days per year is computed using the
 328 mean number of CSX days per year:

$$N_r = \begin{cases} \frac{N_1}{D_Y} \frac{N_2}{D_Y} \times D_Y, & \text{for double extremes,} \\ \frac{N_1}{D_Y} \frac{N_2}{D_Y} \frac{N_3}{D_Y} \times D_Y, & \text{for triple extremes,} \end{cases} \quad (3)$$

329 where N_1 , N_2 , N_3 are the mean number of days per year of different CSX, and $D_Y =$
 330 365 is the number of days in a year. The CP metric is then defined as:

$$CP = \begin{cases} \frac{N - N_r}{N_{\max} - N_r}, & N \geq N_r \\ \frac{N - N_r}{N_r}, & N < N_r \\ 0, & N_r = 0 \end{cases} \quad (4)$$

331 where N is the mean number of days per year of the CCX, and N_{\max} is the global max-
 332 imum value of N . The CESM hindcast does not simulate leap years. The CP metric is
 333 similar in concept to the likelihood multiplication factor (LMF) (Zscheischler & Senevir-
 334 ratne, 2017; Burger et al., 2022), but differs in that the maximum value of CP is 1.0,
 335 giving us the view of how far away a grid cell is from the constituent CSX always oc-
 336 ccurring together. On the other hand, the LMF value directly indicates the change in like-
 337 lihood of compound events.

338 The fraction of contiguous habitable space is calculated by identifying vertically
 339 connected non-extreme grid cells within the column. This metric quantifies the amount

of space within the 300 m deep column an organism can inhabit before it encounters waters under extreme conditions. An organism that performs diel vertical migration may not be impacted if 25% of the column is extreme at the bottom of the column. However, if these extreme conditions occur in the middle of the column, the organism is more likely to encounter extreme conditions during its migration.

3.4 Clustering of Extremes

To find commonalities of the detected CCX with regard to their vertical structure and to help us identify the underlying drivers, we cluster the detected CCX with a k-means clustering approach (MacQueen, 1967). The clustering algorithm is performed on the vertical locations of single extreme events in the column, exclusively during CCX and for grid cells with a positive co-occurrence propensity. In detail, the water column is first divided into 6 bins of 50 m each, and then, over the 60-year analysis period, the number of occurrences of single extremes in each bin during CCX is counted and weighted by their intensity index. These bins of vertical locations are then used as the clustering dimensions, with 12 dimensions for the double CCX and 18 dimensions for the triple CCX. These dimensions are chosen as the vertical locations of single extremes reflect the conditions under which they occur and allude to their drivers. More information on the clustering approach and the choice of the number of clusters is provided in Text S3 and Figure S19.

3.5 Model Evaluation

Given our reliance on model simulation results for detecting single and compound extremes across the upper water column, it behooves us to evaluate the model with regard to its ability to represent extremes. However, our evaluations are largely limited to the surface. For MHW, we used daily observations of sea-surface temperature from the Optimally Interpolated Sea Surface Temperature (OISSTv2) product (Huang et al., 2021) covering the period 1982 to 2020. For OAX, we relied on the OceanSODA-ETHZ dataset (Gregor & Gruber, 2021) that covers the period 1982 to 2020. Surface daily MHW and monthly OAX are detected in the observational products with a seasonally-varying 95th percentile threshold on a quadratic moving baseline, analogous to how this was done for the model output (see Section 3.2). Furthermore, the climatological distributions of pH and $[O_2]$ are evaluated with respect to the Global Ocean Data Analysis Project for Carbon (GLODAPv2) (Lauvset et al., 2016) and Gridded Ocean Biogeochemistry from Artificial Intelligence (GOBAI-O2) (Sharp et al., 2022) respectively. In particular, we evaluated the depths where $[O_2] = 150 \mu\text{M}$ since this value is used as an absolute threshold in this study. As the El Niño-Southern Oscillation (ENSO) turns out to be a major driver for the variability in extremes, we also evaluate the model with respect to ENSO, using the Oceanic Niño Index (ONI) and the depth of the 20 °C isotherm across the equatorial Pacific.

The model captures the observed variations and global coverage of surface MHW with high fidelity (Figure 3(a)). In particular, the model captures well the strong year-to-year fluctuations, which tend to be closely coupled to ENSO, for example, in the years 1998 and 2015-2016. The model also correctly simulates the spatial pattern of the mean duration of these surface MHW (Figure 3(b-c)). However, the model overestimates the duration across the globe, particularly in the eastern tropical Pacific (Figure 3(d)). This is a common shortcoming of models for reasons not yet established firmly (Frölicher et al., 2018; Gruber et al., 2021; Köhn et al., 2024). It is also possible that observations tend to underestimate the duration due to observational gaps (Gruber et al., 2021). We also need to point out that the MHW durations reported here on the basis of OISSTv2 tend to be shorter than those reported elsewhere on the basis of the same data (Oliver et al., 2018; Holbrook et al., 2019). This is due to our use of a higher percentile threshold and not filling in gaps between events (Hobday et al., 2016). Finally, the model represents

391 well the distribution of surface MHW intensities (Figure 3 (ef)), with higher intensities
 392 seen in the tropics and subtropics. It underestimates the mean annual maximum intensi-
 393 ty almost everywhere by about 0.3°C (Figure 3(g)), likely a result of our using a rela-
 394 tively coarse resolution model, except in the eastern tropical Pacific where it overes-
 395 timates the intensity by up to 0.6°C in a small area.

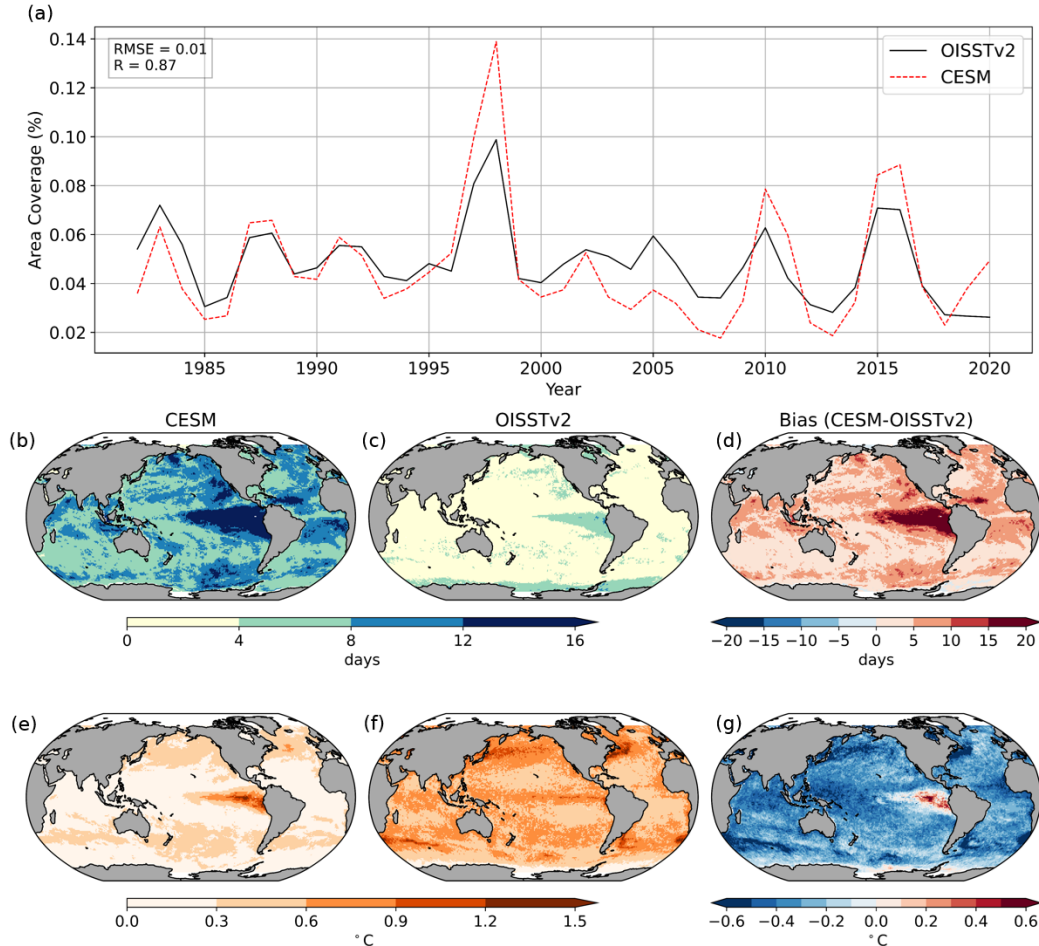


Figure 3. Evaluation of the hindcast model CESM with regard to its representation of surface marine heatwaves (MHW). (a) Timeseries of annual global area coverage of surface MHW identified by the OISSTv2 observational product compared to those diagnosed in the CESM hindcast. (b) CESM and (c) OISSTv2 mean duration of surface MHW and (d) the corresponding bias. (e) CESM and (f) OISSTv2 mean annual maximum MHW intensity and (g) the corresponding bias. The MHW were diagnosed in the observations in the same manner as done for the model.

396 The evaluation of surface OAX with the observation-based product OceanSODA-
 397 ETHZ (Gregor & Gruber, 2021) confirms the fidelity of the model simulations, but also
 398 reveals more differences than those seen for surface MHW. However, one needs to note
 399 that the uncertainties associated with this product are much larger than those associ-
 400 ated with SST. This is a consequence of the several orders of magnitude fewer observa-
 401 tions available to construct the space-time distribution of $[\text{H}^+]$. Still, the model-based
 402 time-series of the global area coverage of surface OAX (based on $[\text{H}^+]$) agrees remark-
 403 ably well with that inferred from the observation-based product, both in terms of mean

404 and year-to-year variations (Figure 4(a)). However, the peak values differ by up to about
405 50%, with this difference especially apparent in the years 1988-1989 and 1997. The sur-
406 face OAX detected with CESM have a spatial pattern similar to that inferred from the
407 observation-based product, especially with regard to the locations of the longest and most
408 intense OAX found in the tropical Pacific (Figure 4(b-c) and (e-f)). However, there is
409 a mismatch in the high latitudes, especially in the North Pacific and the Southern Ocean,
410 where the model identifies long-lasting and intense surface OAX, whereas they are not
411 detected in the observation-based product. We suspect that this difference is probably
412 a consequence of the observation-based product underestimating the variability of $[H^+]$
413 (Ma et al., 2023), thus detecting fewer and less intense OAX. It may also be a consequence
414 of biases in the model and should be taken into account during the analysis. Regardless,
415 biases in intensity tend to have a minor effect on most conclusions drawn in this study,
416 especially those related to the propensity or mechanisms of OAX. However, biases in in-
417 tensity will impact derived metrics such as the compound intensity index of compound-
418 OAX.

419 We also evaluate the model’s ability to reproduce the climatological distributions
420 of pH and $[O_2]$ at various depths, since they are less directly related to the forcing ap-
421 plied to the model. Overall, we find that the model captures well the spatial distribu-
422 tion of pH and $[O_2]$ (Figures S7-S10). In general, the biases are low, about $\pm 40 \mu M$ for
423 $[O_2]$ and ± 0.1 for pH. In addition to pH on the surface, we find a high correlation ($R >$
424 0.8) for both properties at all depths. In certain regions such as the oxygen-deficient zones
425 (ODZs) and the Southern Ocean, we find an increasing bias with depth, up to $\pm 60 \mu M$
426 for $[O_2]$ and ± 0.4 for pH. The sign and location of the biases between the two proper-
427 ties are similar, suggesting that they probably arise from physical processes such as mix-
428 ing and stratification. For example, a positive bias in the Pacific upwelling regions in-
429 dicates a deeper oxycline in the hindcast, which may have resulted from too much mix-
430 ing at the surface. Examining the seasonal variability of $[O_2]$ (Figure S11), we find that
431 the model reproduces the relative changes well on a monthly time scale and therefore
432 accurately represents the seasonal variations of physical and biogeochemical cycles.

433 Although the absolute value of the bias is less important for relative thresholds in
434 extremes, we use an absolute threshold of $150 \mu M$ for $[O_2]$ in this study and hence con-
435 duct a further evaluation of the hindcast. The depths at which $[O_2] = 150 \mu M$ (Figures
436 S12-S13) are typically deeper by about 30 m in the hindcast especially at the location
437 of ODZs, confirming our observations in the previous paragraph. This bias reverses in
438 the western tropical and north Pacific, where the hindcast reaches $150 \mu M$ at a shallower
439 depth of about 30 m. These biases, although generally low, may potentially include or
440 exclude LOX in the hindcast, especially near the boundaries of the absolute threshold.

441 The hindcast model simulates the time-series of the Oceanic Niño index ONI well
442 with a bias of $0.11^\circ C$, and a correlation coefficient of $R^2 = 0.91$, based on ORAS5 (Zuo
443 et al., 2019)). It also replicates the variation of the thermocline structure in the east-
444 ern Pacific. Concretely, we assess the ability of the model to reproduce the depth of the
445 $20^\circ C$ isotherm at monthly resolution (Figure S14). The interannual variability of the
446 isotherm depth is comparable between the two, and the time scales of ENSO events are
447 similar. We find a weaker zonal gradient in the CESM hindcast with a deeper thermo-
448 cline in the east and shallower in the west. Overall, we conclude that the hindcast model
449 is capable of capturing not only the mean state of the ocean’s physical and biogeochem-
450 ical state, but also its variability, which is a critical requirement for investigating extremes.

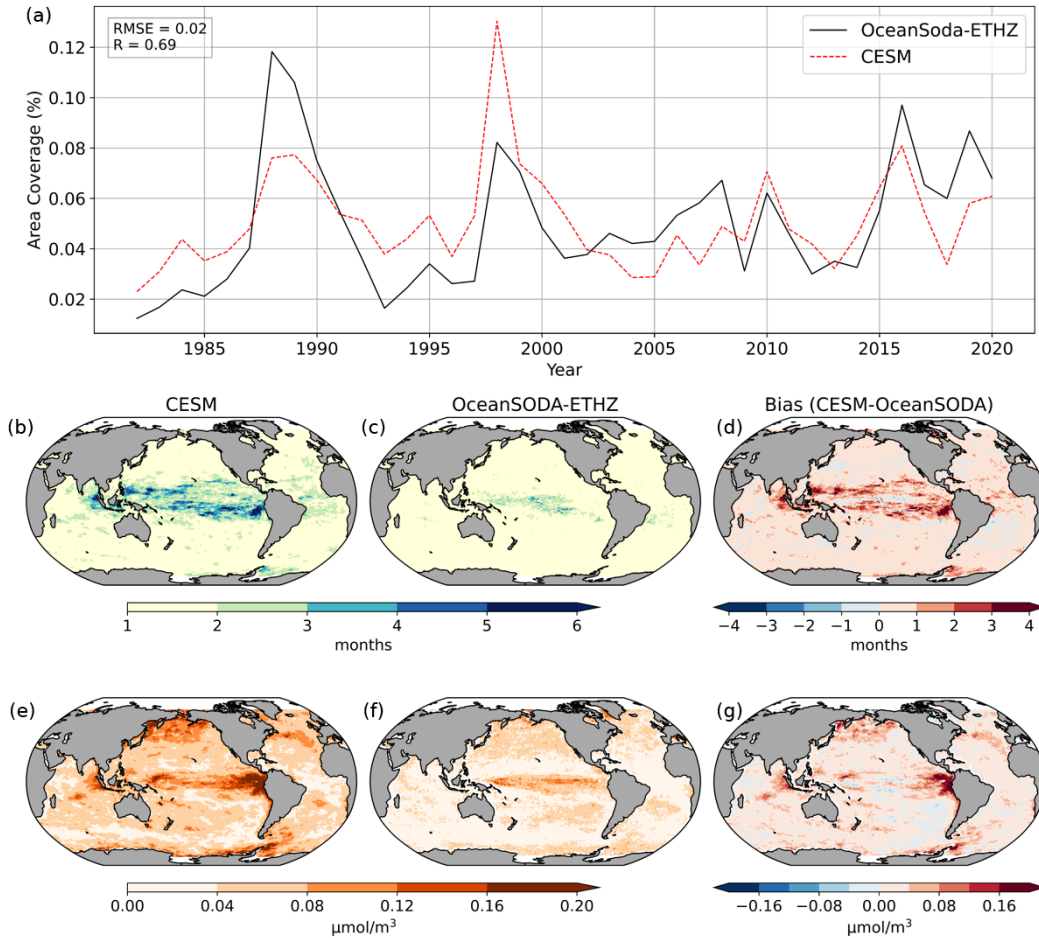


Figure 4. Evaluation of the hindcast model CESM with regard to its representation of surface ocean acidification extreme events (OAX) (a) Time-series of annual global area coverage of surface OAX identified on the basis of the OceanSODA-ETHZ observational product (Gregor & Gruber, 2021) compared to those diagnosed in the CESM hindcast. (b) CESM and (c) OceanSODA-ETHZ mean duration of surface OAX and (d) the corresponding bias. (e) CESM and (f) OceanSODA-ETHZ mean annual maximum OAX intensity and (g) the corresponding bias.

451

4 Results and Analysis

452

4.1 Trends of Column Extremes

453

454

455

456

457

458

459

460

461

462

The volumes occupied by all single-parameter column extremes are modeled to have increased substantially over the 60 years of our analysis (Figure 5a). Extreme volume fractions started from values of a few percent in the 1960s and doubled for LOX, more than quadrupled for MHW to more than 20% and reached almost 100% for OAX at the end of the simulation in 2020. As these metrics were calculated with a fixed baseline reflecting the conditions of the 1950s, these increases are a direct consequence of the underlying changes in temperature, oxygen, and acidity. Specifically, averaged over the top 300 m, temperature increased by $0.18\text{ }^{\circ}\text{C}$, $[\text{H}^+]$ increased by $1.56\text{ }\mu\text{molm}^{-3}$, and $[\text{O}_2]$ decreased by $1.18\text{ }\mu\text{M}$ between the first and last decade (Figure S15-S16). The rapid changes in OAX and the more moderate increases in MHW diagnosed for the column extremes

463 mirror the results obtained for the surface (Oliver et al., 2018; Burger et al., 2020; Gruber
 464 et al., 2021). This reflects the fact that ocean warming and ocean acidification are
 465 not limited to the surface, but extend over much of the upper ocean (Gleckler et al., 2016;
 466 Kwiatkowski et al., 2020), causing strong trends also in column extremes. The trend is
 467 particularly strong for the volume fraction of OAX, reflecting the rapid forcing through
 468 ocean acidification relative to the magnitude of the natural variability of $[\text{H}^+]$, an effect
 469 seen in previous work (Burger et al., 2020; Gruber et al., 2021). The trend of the LOX
 470 volume fraction is comparatively muted due to smaller global trends in oxygen. Further-
 471 more, the trend in $[\text{O}_2]$ is not homogeneous across the globe and could be stronger (or
 472 even increasing) in certain basins, leading to a muted global average trend. The over-
 473 all volume fraction of LOX is also relatively smaller in magnitude compared to the other
 474 CCX due to the additional absolute threshold of $150 \mu\text{M}$ used in this study.

475 The increasing volume fraction of single parameter CSX also causes the volume frac-
 476 tion of column compound extremes (CCX) to increase, but the increases are less steep
 477 and also not as monotonic (Figure 5b). In the 1960s and 1970s, the volume fractions of
 478 the different combinations hover around 0.1–2%, with OAX-LOX events being the most
 479 prevalent at around 1%, and the triple compound extreme occupying less than 0.1% of
 480 the water column, on average. Then at various points in time, the prevalence of these
 481 CCX suddenly increased. In the case of the MHW-OAX events, this occurred around
 482 1980 with a relatively steady growth thereafter, reaching a volume fraction of nearly 50%
 483 in 2020. The volume fraction of OAX-LOX more than doubled in 1998, and then remained
 484 fairly constant near 10%. The smallest increases are seen for the volume fraction of MHW-
 485 LOX and MHW-OAX-LOX, but they still increased 4.5 and 32 times when comparing
 486 the first and last 20 years.

487 As the volume of CCX has increased over the last 60 years, their duration has also
 488 increased (Figure 5c). MHW-OAX and OAX-LOX events lasted on average less than 50
 489 days before ~ 1995 , but saw a sudden increase in 1997. Thereafter, the mean duration
 490 of these CCX rarely fell below 50 days and instead achieved new records with durations
 491 of close to 200 days. MHW-LOX and the triple compound events have also increased in
 492 duration over the hindcast period, averaging close to 50 days per event towards 2020.

493 The starkest changes in the CCX properties occurred with the maximum intensity
 494 index (Figure 5d). In the 1960s and 1970s, it hovered around 2 for all compound extremes,
 495 except for OAX-LOX. But then, as the intensity of OAX began to increase rapidly due
 496 to strong trends in ocean acidification (Ma et al., 2023), the maximum intensities of all
 497 CCX began to increase rapidly as well, reaching a nearly 10-fold increase by 2020. The
 498 exception is MHW-LOX, which experienced "only" a doubling in their maximum inten-
 499 sity.

500 In summary, column compound extremes used to be relatively rare, but have be-
 501 come much more prevalent and frequent over the last few decades and, in particular, have
 502 become much more intense. This is best illustrated for the triple column compound ex-
 503 tremes that have expanded 39-fold, now last 3-times longer, and have become 6-times
 504 more intense since the early 1960s. This strong increase is driven to a substantial degree
 505 by the increase in the intensity of the OAX. 2.3% of the volume of the global upper ocean
 506 is now under conditions of triple compound extremes, corresponding to a volume of $2\,300\,000 \text{ km}^3$.
 507 This is much greater than, for example, the volume of the ocean that is considered 'dead'
 508 as a consequence of coastal eutrophication (Diaz & Rosenberg, 2008). Thus, while many
 509 studies have already shown the increasing frequency, duration, and intensities of surface
 510 extremes, especially those of MHW, our work now shows that this leads to severe reduc-
 511 tions in habitable space below the surface, restricting the ability of organisms to cope
 512 with, for example, surface MHW by migrating to deeper depths. These analyses also show
 513 how important it is to better understand the impact of compound extremes on marine
 514 organisms, as these compound extremes are becoming more common (Hauri et al., 2024).

Fixed Baseline

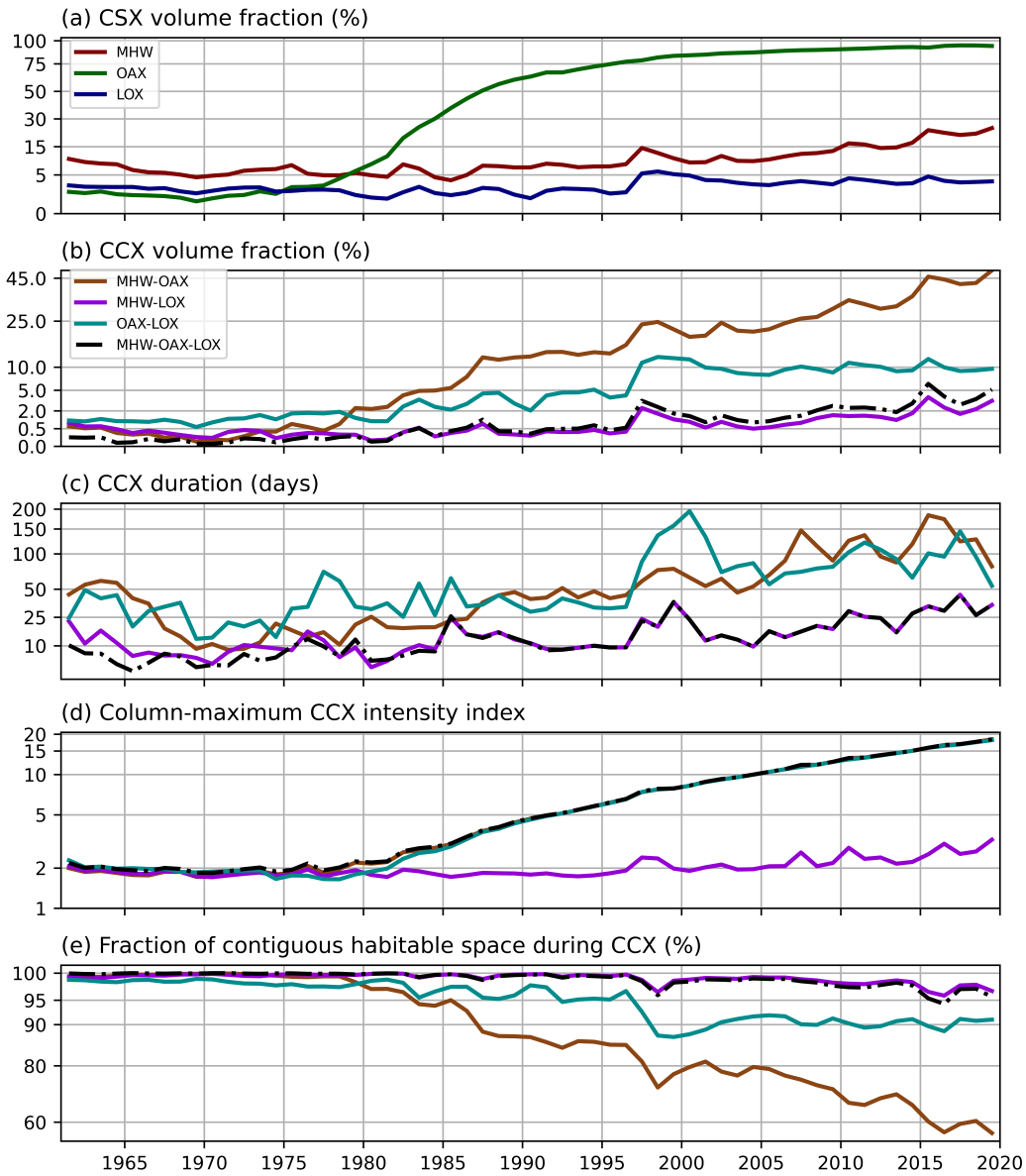


Figure 5. Temporal evolution of model simulated column extremes over the past 60 years on a fixed baseline. Shown are the timeseries of (a) annual mean global volume fraction of the three single column extremes (CSX), (b) annual mean global volume fraction of column compound extremes (CCX) of the four different types, (c) mean CCX duration, and (d) annual column-maximum CCX intensity index.

515 Next, we would like to investigate the processes behind these events, and also un-
 516 derstand what causes, e.g., also the strong year-to-year variations in the trends. We also
 517 would like to characterize the events more specifically with regard to where they occur
 518 and what properties they have. To this effect, we change our perspective to a moving
 519 baseline, which removes the long-term trend. We do this without the intention of un-
 520 derstating the increasing severity of marine extremes under climate change.

4.2 Temporal Variability of Column-Compound Extremes

By removing the underlying climate trend through the use of a moving baseline, the strong year-to-year variability of the column-compound extremes becomes clearer (Figure 6). In particular, local peaks in the global volume fraction, duration, and intensities of CCX coincide with strong ENSO events of high Oceanic Niño index (ONI). Most visible are the alignments of the peaks during moderate and strong ENSO events in 1972-1973, 1982-1985, 1997-1998, 2009-2011, and 2015-2016. The global volume fractions of CCX are strongly correlated with positive ONI (Pearson $R = 0.50$ to 0.68), and less so with negative ONI (Pearson $R = -0.06$ to -0.27). The negative R indicates an increase in volume fraction with more negative ONI, i.e. La Niña. We examine ENSO as a driver of CCX on a regional scale in Section 4.5.

OAX-LOX events affect the water column more than any other type of CCX. On average, they have the highest mean volume fraction of 1.2% ($1\,208\,000\text{ km}^3$), reaching up to 4.7% ($4\,732\,000\text{ km}^3$) during the strong consecutive El Niño/La Niña events of 1997-1998. They also last the longest, having a duration of about 18 days on average but exceeding 40 days during some periods. Due to their large volume, they also contract the habitable space the most out of all the CCX types. The maximum intensity of OAX-LOX is among the highest of double CCX, at about 2.5. The second most extensive type of CCX is MHW-OAX, which typically occupies about 0.9% of the global volume ($906\,000\text{ km}^3$), and lasts 11 days, on average. Together with the triple CCX, they are also one of the most intense CCX types, with a maximum intensity index typically higher than 2. Although some peaks may be seen coinciding with major ENSO events, their association with ENSO is weaker than that of OAX-LOX. Finally, there is a relatively smaller mean volume of MHW-LOX and triple CCX (MHW-OAX-LOX), of 0.16% ($161\,000\text{ km}^3$) and 0.11% ($111\,000\text{ km}^3$) respectively. These two CCX types have the same interannual variability, suggesting that many MHW-LOX events are also triple compound events.

4.3 Spatiotemporal Distribution of Column-Compound Extremes

The four different types of CCX have rather different global distributions in terms of annual extreme days (Figure 7a,c,e,g), and in terms of the co-occurrence propensity (Figure 7b,d,f,h) (see also Table 2). MHW-OAX occur globally, but most frequently in the subtropics and the high-latitude Southern Ocean, where between 7 to more than 28 days per year are characterised as MHW-OAX events. In contrast, the number of MHW-OAX days in the equatorial regions is low, typically less than 7 days. The co-occurrence propensity (later referred to as just propensity) helps to explain these distributions. For example, the strongly negative propensity of MHW-OAX events in the eastern tropical Pacific explains well why the number of CCX days in this region is so low (Figure 7a,b). This negative propensity means that whenever there is, for example, a heatwave in this region, the likelihood that this region also has an OAX is substantially lower than by chance. This is a result of the fact that most MHW in the eastern tropical Pacific are associated with El Niño, which tend to push the thermocline and therefore also the waters with high $[\text{H}^+]$ down, thereby suppressing the formation of subsurface OAX (Burger et al., 2022). Similarly, the negative propensities in the boundary upwelling regions are the result of surface OAX events that are typically driven by strong upwelling events (Desmet et al., 2022), which tend to cool the surface ocean and therefore suppress the formation of MHW.

The OAX-LOX events have nearly the opposite spatial pattern to that of the MHW-OAX events. The OAX-LOX events occur primarily in the tropics, in the Eastern Boundary Upwelling Systems (EBUS), and the north subpolar Pacific, typically more than 14 days per year under CCX conditions. On the contrary, OAX-LOX events are entirely absent in the North Atlantic and the ocean south of about 30°S . This absence is a consequence of the high level of oxygenation in these regions with $[\text{O}_2]$ staying generally above the $150\text{ }\mu\text{M}$ threshold. This contrasts with the low-latitude regions, many of which are

Moving Baseline

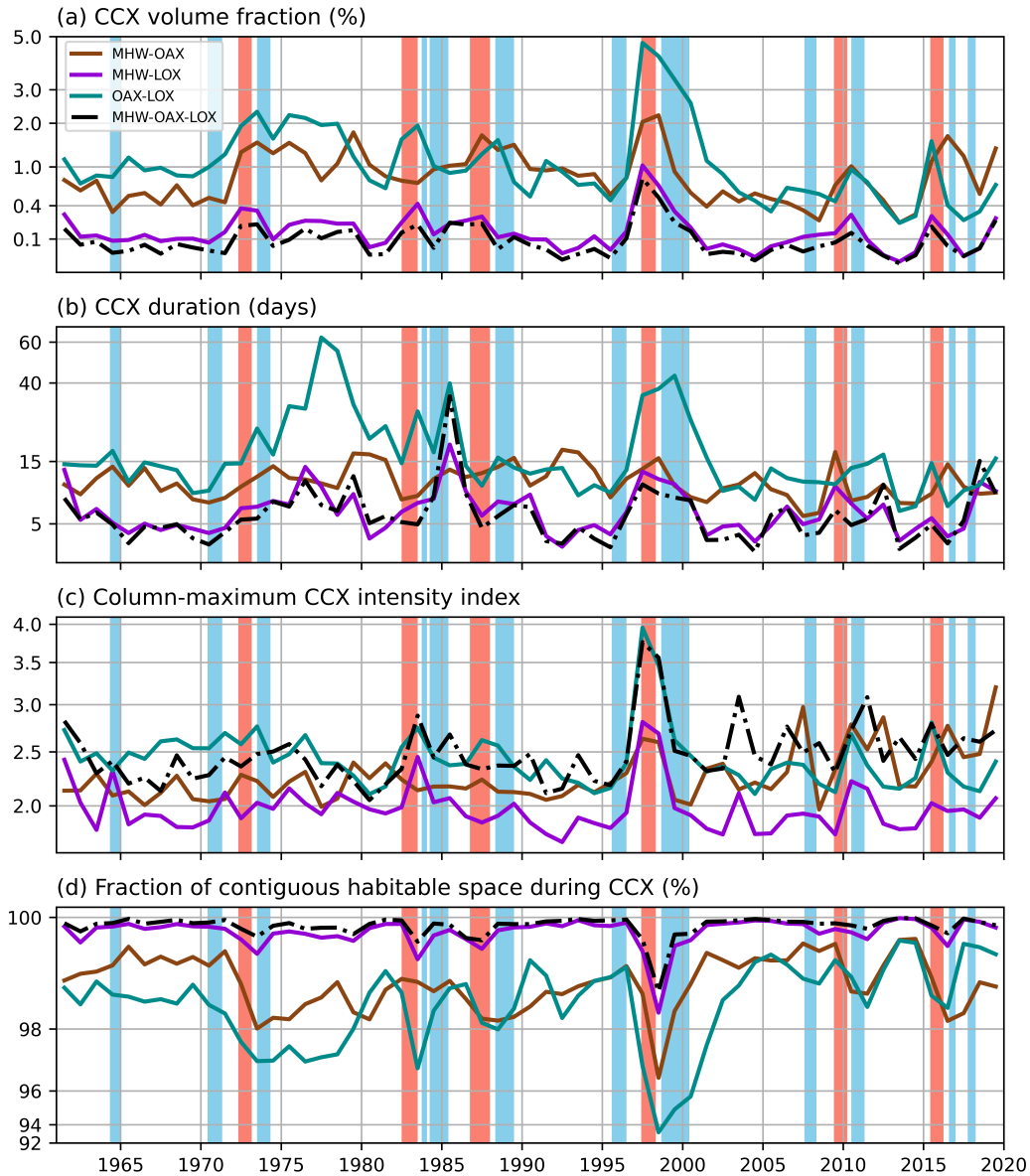


Figure 6. As Figure 5, but for a moving baseline, i.e., when the trends are removed using a quadratic fit. Strong El Niño events ($\text{ONI} \geq 1.5^\circ\text{C}$) are shaded in red, and strong La Niña events ($\text{ONI} \leq -1.0$) are shaded in blue.)

572 characterised as oxygen-deficient zones (ODZs) (Paulmier & Ruiz-Pino, 2009), foster-
 573 ing the presence of LOX (Köhn et al., 2022). The high prevalence of the OAX-LOX events
 574 in the low latitudes can be understood by their very positive propensity, which means
 575 that when there is a LOX, there is a very high chance that there is also an OAX. This
 576 can be understood from the fact that OAX and LOX tend to be generated by the same
 577 processes, such as remineralisation, upwelling, or thermocline heaving (Gruber et al., 2021),
 578 substantially increasing the likelihood that the two extremes occur together.

579 Compared to these first two CCX types, MHW-LOX and the triple compound occur
 580 substantially less frequently and have durations of typically less than 7 days. The
 581 spatial pattern is similar to that of the OAX-LOX events with a low-latitude focus, sug-
 582 gesting that the absence of LOX in the high latitudes due to the oxygen threshold is also
 583 an important determinant for the triple compound events. However, the propensity plots
 584 exhibit a clear difference, with most areas having substantially lower propensity than those
 585 exhibited by the OAX-LOX events, and some regions even having a negative propensity.
 586 The reasons behind this distribution are complex and will be discussed later in this study.

587 Thus, we can identify two general patterns of the occurrence and propensity of CCX.
 588 A more global and high-latitude pattern for MHW-OAX events and a more low-latitude/tropical
 589 pattern for the other three CCX types due to the oxygen concentration threshold. This
 590 allows us to focus on only two of the four types in the following discussion of the full sets
 591 of CCX metrics, i.e. MHW-OAX events (Figure 8) and MHW-OAX-LOX triple com-
 592 pounds (Figure 9). Figures for the other two CCX types, i.e., OAX-LOX and MHW-
 593 LOX, can be found in Figures S17-S18.

594 MHW-OAX events in the subtropics and Antarctic zone last the longest (more than
 595 21 days) (Figure 8a). In these regions, we also see the highest maximum intensity index
 596 of 2 to 4 (Figure 8b), which means that the intensity of the combined events is approx-
 597 imately 2 to 4 times the intensity of the threshold for a single event. This shows that
 598 where MHW-OAX occur most frequently, they are also long and intense. Likewise, in
 599 tropical regions where the number of CCX days is small and where the CCX events are
 600 short (Figure 8a,c) they are also relatively weaker, between 1 and 3 in the maximum in-
 601 tensity index. This is also the region of very low propensity (Figure 8d). But while the
 602 CCX events in the tropics are less frequent, shorter, and less intense, they still contract
 603 the habitable space, between 25 % to 75 % of the column (Figure 8e). In some areas, the
 604 remaining contiguous habitable space is less than 25 % (Figure 8f).

605 The spatial distribution of the triple compound events (MHW-OAX-LOX) can be
 606 understood in conjunction with that of the OAX-LOX. OAX-LOX events are unique from
 607 the other CCX types due to their high number of days per year (Figure 7c) and posi-
 608 tive propensity everywhere they occur (Figure 7d). This means that when either OAX
 609 or LOX occurs, the other almost always occurs together with it. Thus, the triple com-
 610 pound occurs when an MHW is induced in the same column. We see this more frequently
 611 in the tropics and the Bering Sea, up to 21 days a year in some areas (Figure 9c). When
 612 triple CCX occur, they typically have moderate maximum intensity indices of 2 to 3, but
 613 can exceed 4 in the central tropical Pacific (Figure 9b). In the equatorial regions, they
 614 typically last up to 10 days (Figure 9c). However, their durations are more than dou-
 615 ble in the Bering Sea and along the boundaries of the subtropical gyres. The triple com-
 616 pound events contract the habitable space by far the most (Figure 9f). During such events,
 617 less than 50 % remains habitable, with some regions going to 0% in some areas.

618 4.4 Vertical Structure and Clustering of CCX

619 The k-means clustering for the MHW-OAX events according to the vertical dis-
 620 tribution of extreme conditions results in four clusters (see Figure 10 left column) with
 621 distinct properties and spatial distributions. This clear separation confirms our choice
 622 of clustering only on the basis of the vertical distribution of the extremes. Cluster 2 (24%)
 623 occupies much of the subtropical gyres, while clusters 3 (14%) and 4 (5%) occur in the
 624 Subantarctic zone of the Antarctic Circumpolar Current (ACC) and in the Antarctic zone,
 625 respectively. Cluster 1 occurs along the borders of the other clusters, accounting for nearly
 626 60% of the total area of all MHW-OAX events. However, it also has the shortest aver-
 627 age duration, the lowest average days per year, and the lowest maximum intensity in-
 628 dex. In contrast, cluster 4 is the highest in these metrics, with the other two clusters in

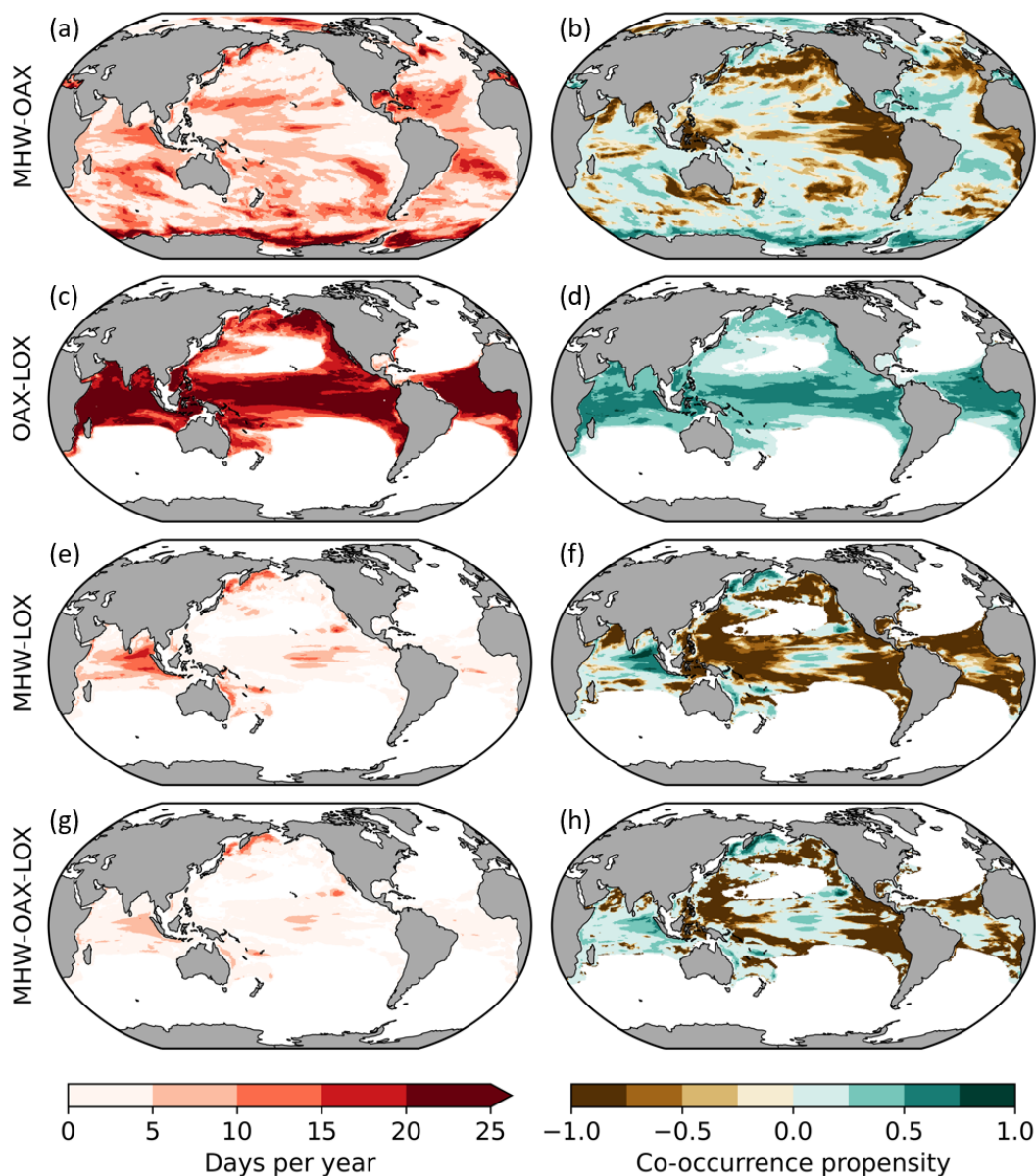


Figure 7. Spatial distribution of CCX illustrated by: CCX days per year (left column) and mean co-occurrence propensity (CP) of CCX (right column). A positive CP indicates two column-single extremes occurring in the same column more frequently than by random occurrence. Conversely, a negative CP indicates a lower frequency than random occurrence. (Section 3.3). Each row corresponds to one CCX type, i.e. (a,b): MHW-OAX, (c,d): OAX-LOX, (e,f): MHW-LOX, (g,h): MHW-OAX-LOX.

629 between. In terms of vertical fraction, the four clusters are similar, ranging between 41%
 630 and 46%.

631 We discuss these clusters in turn, using their characteristics as an indication of the
 632 likely processes driving them. Since increases in temperature during MHW directly lead
 633 to an increase in $[H^+]$ through shifts in the carbonate chemistry equilibrium, some of the
 634 OAX must be driven by the MHW (Burger et al., 2022; Burger & Frölicher, 2023). As

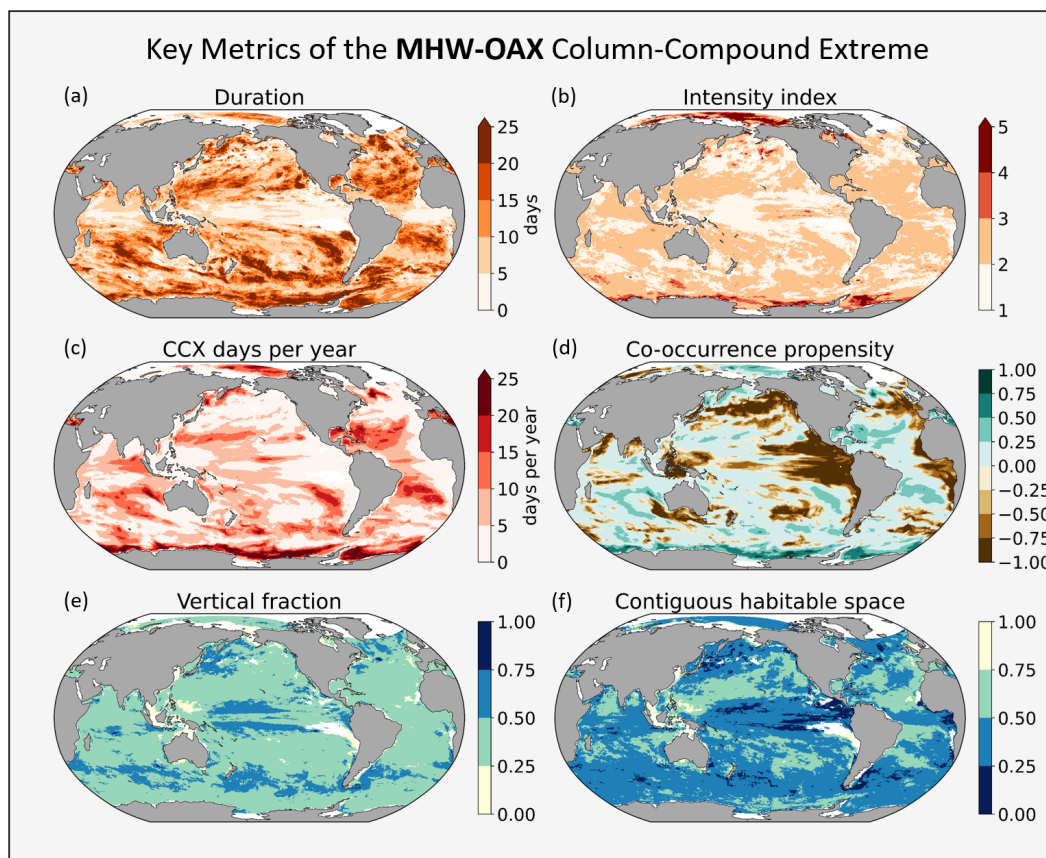


Figure 8. Key metrics of MHW-OAX events in the global ocean. (a) Mean duration, (b) mean annual maximum intensity index, (c) mean annual CCX days, (d) mean co-occurrence propensity, (e) mean fraction of water column occupied by extremes, and (f) mean fraction of contiguous habitable space in the vertical column. (c) and (d) are the same plots as Figure 7(a) and 7(b).

635 the isochemical sensitivity of $[\text{H}^+]$ is well known, we can compute the fractional contribu-
 636 tion of the temperature changes to the changes in $[\text{H}^+]$ (Text S4) (Orr & Epitalon,
 637 2015). We do not have sufficient information stored during the simulation to determine
 638 all the processes that drive the changes in DIC and Alk underlying the non-thermal changes
 639 in $[\text{H}^+]$ (Burger & Frölicher, 2023), but we use anomalies in the export and sinking of
 640 particulate organic carbon (POC) and a logistic regression (Mahlstein et al., 2012; Filho
 641 et al., 2013; Le Grix et al., 2023) to infer the potential contribution of changes in the bi-
 642 ological pump to the OAX (Text S5).

643 Cluster 1 is characterised by the bimodal depth distribution of the MHW and OAX
 644 signals, with a surface signal similar to cluster 2, and a weaker maximum in the subsur-
 645 face reminiscent of the signals in clusters 3 and 4. Since the violin plots reflect the sum
 646 of extreme signals over the hindcast period, these modes do not necessarily occur at the
 647 same time. In general, the warming associated with MHW can account for nearly 80%
 648 of the OAX (Figure S21), suggesting that it is primarily the MHW that drives this CCX
 649 cluster. We did not find a strong relationship between the events in Cluster 1 and POC
 650 export (Table S1), leaving advection and mixing processes as the most likely processes
 651 driving the remaining 20% of the OAX signal in this cluster. Potential mechanisms in-
 652 clude the advection of surface waters with MHW or OAX characteristics from adjacent

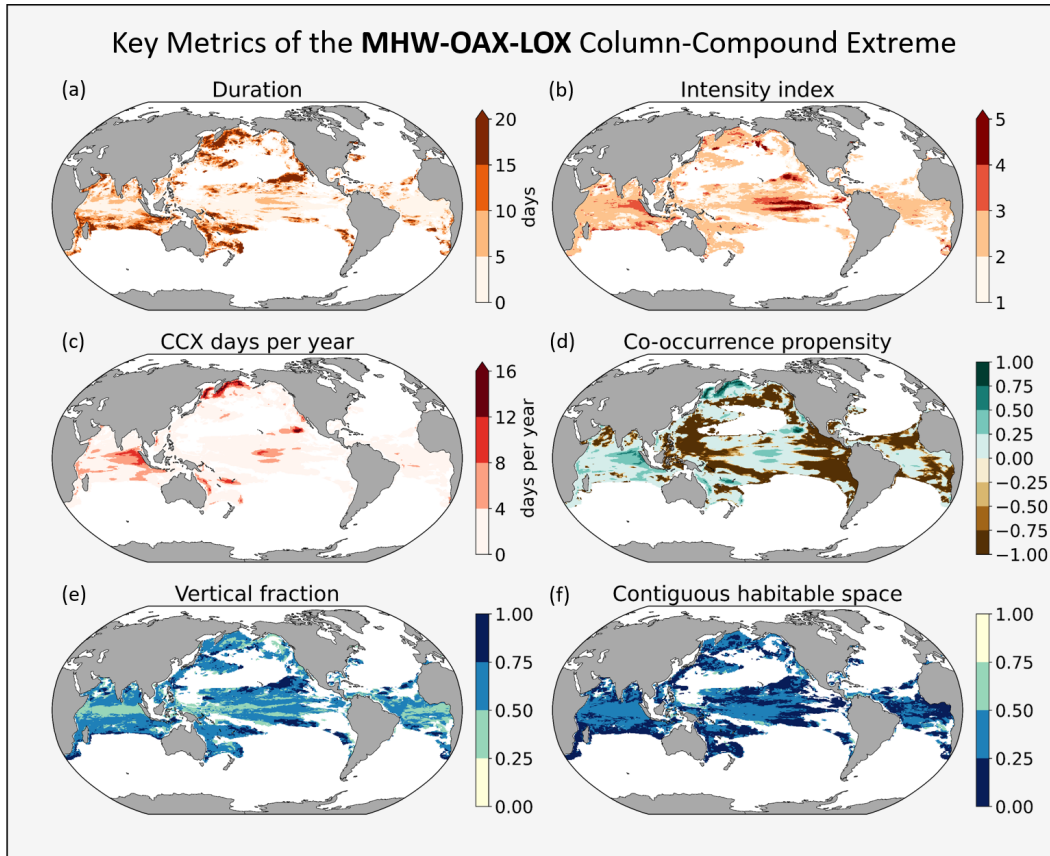


Figure 9. As Figure 8, but for triple compound events. (c) and (d) are the same plots as Figure 7(g) and 7(h).

653 regions (Holbrook et al., 2019; Sen Gupta et al., 2020; Elzahaby et al., 2021), possibly
 654 combined with downwelling Kelvin and Rossby waves that can propagate, maintain, and
 655 and deepen the extreme signals (Holbrook et al., 2019; Zhang et al., 2021; Maulida et al., 2022;
 656 Qi et al., 2022).

657 Cluster 2 has a pure surface intensified signal, with MHW and OAX co-occurring
 658 from the surface down to 100 m. More than 100 % of the change in $[H^+]$ can be explained
 659 by the warming (Figure S21), suggesting that a surface ocean driven MHW is the key
 660 process driving this type of CCX. Compound surface MHW and OAX have previously
 661 been detected by Burger et al. (2022) in similar regions of the tropics and subtropics,
 662 and our analysis shows that these events tend to extend further below the surface.

663 MHW-OAX cluster 3 is the opposite of cluster 2, with a strong subsurface intensi-
 664 fied signal. In cluster 3, MHW occur beneath the surface between 50 –300 m, and OAX
 665 occur in the lower half of the water column below 100 m. The spread across the water
 666 column causes this cluster to have the highest vertical fraction of 46 %. Up to 60 % of
 667 the change in $[H^+]$ in co-occurring OAX can be attributed to the increase in tempera-
 668 ture (Figure S21). In addition, enhanced export and remineralisation appears to be driv-
 669 ing part of the OAX signal, as indicated by the positive correlation between MHW-OAX
 670 events and increased POC export (Table S1). Another contribution might stem from anoma-
 671 lous advection and mixing. In fact, the regions occupied by this cluster, such as the Sco-
 672 tia Sea, Drake Passage, and Macquarie Ridge, stand out as regions with enhanced di-
 673 apycnical mixing (Ledwell et al., 2011). Strong wind-driven currents and rough bathymetry

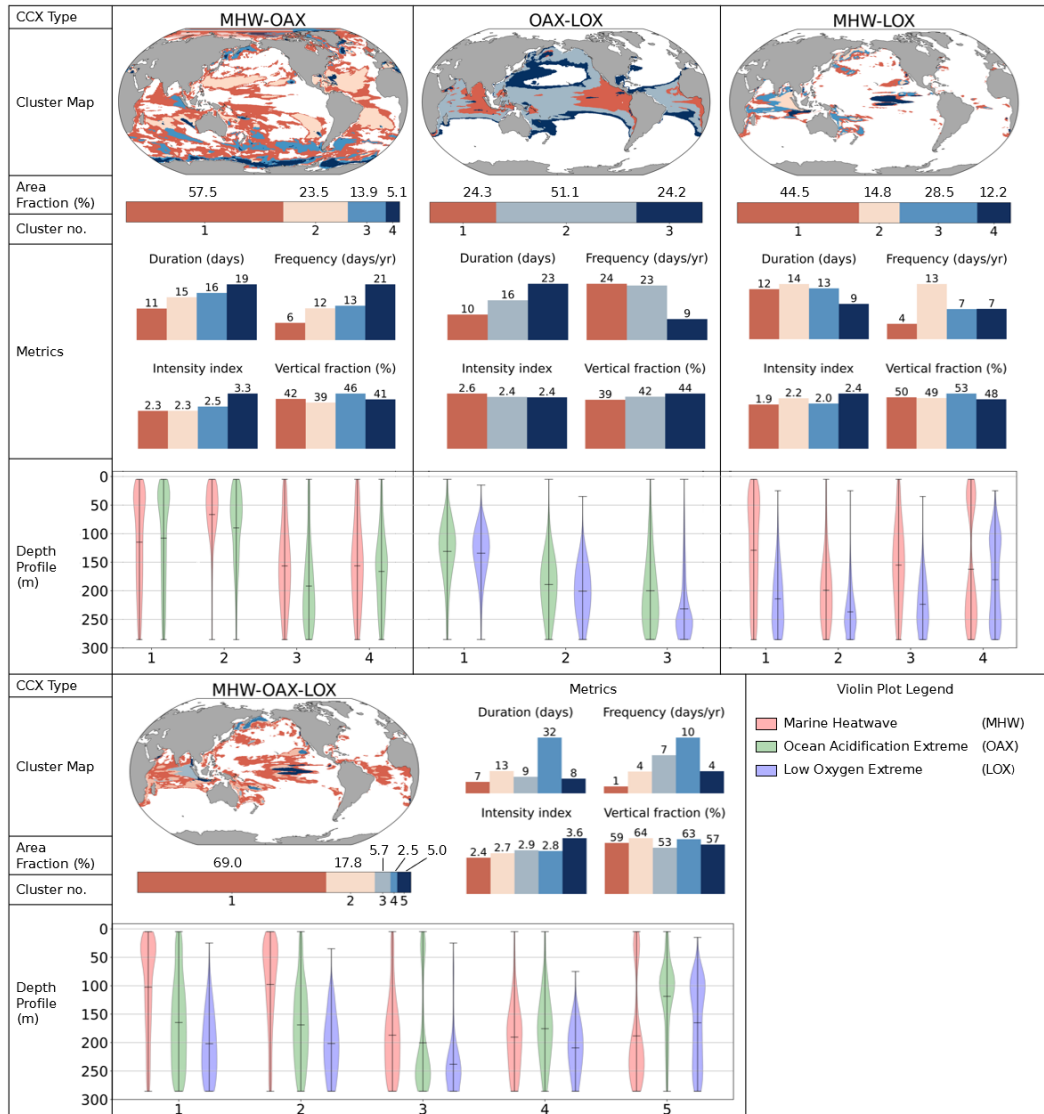


Figure 10. Summary of the main cluster characteristics identified by k-means clustering for each CCX type, i.e., MHW-LOX (top left column), OAX-LOX (top middle column), MHW-LOX (top right column), and the triple CCX MHW-OAX-LOX (bottom row). For each type, four groups of characteristics are provided (from the top): Horizontal distribution by a cluster map, cluster numbers and the area fraction occupied by each cluster as a horizontal bar plot, key metrics including cluster-averaged values of mean duration, mean days per year, mean annual column-maximum intensity index, and mean vertical fraction occupied by extremes as a vertical bar plots, and vertical distribution in the form of vertical violin plots. The latter show the sum of single grid-cell extreme occurrences during CCX, weighted by their intensity index.

674 have been shown to drive mixing in the upper water column (Pellichero et al., 2017; Vogt
 675 et al., 2022) and may be drivers of intrusions of MHW in the subsurface. Local parcels
 676 of water carrying the MHW signal may be disconnected from the surface and later re-
 677 connected again by mixing and heating the surface. An example from the hindcast is shown
 678 in Figure S23.

679 Cluster 4 events occur along the Antarctic continent, with colocated MHW and OAX
 680 occurring largely beneath the surface between 100–300 m. Here, MHW-OAX events have
 681 the highest frequency of 21 days per year, the longest mean duration of 19 days, and the
 682 highest maximum intensity index of 3.3. We suggest the upwelling of Circumpolar Deep
 683 Water (CDW) as the primary mechanism for driving the MHW-OAX events of this cluster,
 684 since CDW is warmer and more acidic than the upper waters in the Antarctic zone
 685 (Dinniman et al., 2011; Pellichero et al., 2017; Wang et al., 2023). Such upward intru-
 686 sions of the CDW may be driven by strengthened zonal westerlies (Morrison et al., 2015;
 687 Wilson et al., 2019; Ramadhan et al., 2022) or low sea-ice extent (Ramadhan et al., 2022).
 688 The effect of upwelling on OAX may be enhanced by greater export and remineralisa-
 689 tion of POC, which we identify through logistic regressions (Table S1). An example of
 690 such an event is shown in a Hovmoller diagram (Figure S24).

691 OAX-LOX events are separated into three clusters (see Figure 10 middle column),
 692 where each cluster may be found in the same areas of each ocean basin. Cluster 1 roughly
 693 corresponds to the eastern tropics and the EBUS regions, with OAX and LOX located
 694 together between 50 m and 200 m deep. Cluster 2 events are located deeper in the wa-
 695 ter column, between 100 m and 300 m, and are located along the boundaries of cluster
 696 1, reaching the western side of the basins. Cluster 3 is located along the boundaries of
 697 the subtropical gyres, where the deepest events are found below 100 m. The three clus-
 698 ters are likely driven by the same processes, with the specifics determined by the back-
 699 ground state. This is due to the very strong negative correlation between $[O_2]$ and $[H^+]$
 700 in the ocean interior as a result of the biological pump (Sarmiento & Gruber, 2006; Paul-
 701 mier et al., 2011; Gobler & Baumann, 2016). This negative correlation means that any
 702 lateral or vertical displacement of water masses has the potential to create a combined
 703 OAX and LOX event (Gruber et al., 2021). The specific occurrence of this type of CCX
 704 is modulated by our use of the $150 \mu\text{M}$ threshold for $[O_2]$. This threshold is closest to
 705 the surface in the EBUS, the eastern tropical Pacific, the subarctic Pacific, and the In-
 706 dian Ocean, deeper in the western tropics, and is not reached within the upper 300 m
 707 of the subtropical gyres or the high latitudes (Gilly et al., 2013). Thus, the three clus-
 708 ters track this depth distribution. Our hypothesis of anomalous displacement driving OAX-
 709 LOX events is supported by strongly positive logistic regressions between OAX-LOX oc-
 710 currences and the shoaling of the thermocline depth (Fiedler, 2010) (Table S1). The re-
 711 spective odds ratios of each cluster indicate an increased probability of CCX by 2.10,
 712 1.77, and 1.43 times for every 10 m of thermocline shoaling. The OAX signal may fur-
 713 ther be enhanced by the consequence of increased biological productivity (inferred from
 714 regressions on POC export anomalies) driving additional remineralisation.

715 The clustering separates the MHW-LOX events into 4 clusters (Figure 10 right col-
 716 umn). Very similar clusters are obtained for the triple compound MHW-OAX-LOX events
 717 (Figure 10 bottom row), which is the result of the high spatial correlation between the
 718 MHW-LOX and the triple compound extremes in all characteristics (see Figure 7). As
 719 a consequence, we focus on the clusters of the triple compound extremes.

720 MHW-OAX-LOX cluster 5 (MHW-LOX cluster 4) is found in the central equato-
 721 rial Pacific. It is the most intense of all CCX clusters with a maximum intensity index
 722 of 3.6, but it has a relatively short duration of 9 days and occurs only 4 days per year
 723 on average. The triple compound cluster with the longest duration of 32 days and oc-
 724 ccurring 10 days per year is cluster 4 (MHW-LOX cluster 2), found in the Bering Sea. In
 725 the eastern tropical Indian ocean, we find MHW-OAX-LOX cluster 3 (MHW-LOX clus-
 726 ter 2) occurring 7 days per year. Finally, MHW-OAX-LOX clusters 1 and 2 (MHW-LOX
 727 clusters 1 and 3) occupy the largest area fraction of 86.8%, and border the other clus-
 728 ters in the tropics and North Pacific.

729 In MHW-OAX-LOX clusters 1 and 2, surface intensified extreme signals in tem-
 730 perature are clearly separated from the depth intensified signals in acidity and oxygen,
 731 as vertical entrainment and/or mixing is restricted across the thermocline. We suspect

732 that the anomalous heating of the surface stratifies the surface layer and confines the MHW
 733 signal to the top 100–150 m of the column. Meanwhile, OAX and LOX are intensified
 734 below the MHW. Changes in biological production and export cannot be the primary
 735 driver of these subsurface changes, since we find in cluster 2 a significant odds ratio of
 736 0.64, which means that biological production, export, and remineralisation are reduced
 737 during these events, thus adding less $[H^+]$ to the water column and removing less $[O_2]$.
 738 In cluster 1 the correlation with POC export is relatively weaker but still negative, and
 739 thus also not explaining the co-occurrence. Instead, we propose that these subsurface
 740 extremes are a consequence of the increased efficiency of the biological pump (Sarmiento
 741 & Gruber, 2006) driven by surface stratification. In this situation, a lower amount of mix-
 742 ing between the subsurface and the surface increases the vertical gradient of DIC and
 743 $[O_2]$, causing the subsurface concentrations of DIC to increase and that of $[O_2]$ to de-
 744 crease (Sarmiento & Gruber, 2006).

745 In contrast, certain conditions allow heat to transfer below the thermocline, lead-
 746 ing to distinctive CCX depth profiles. The MHW-OAX-LOX Cluster 5 in the central trop-
 747 ical Pacific is one such example, where MHW is intensified at the surface (0–50 m), and
 748 at depth (150–300 m). Meanwhile, OAX and LOX occupy the gap between 50–150 m.
 749 During El Niño periods, strong anomalous surface heating occurs in the eastern trop-
 750 ical Pacific, deepening the thermocline and inducing MHW throughout the water col-
 751 umn (Fiedler & Lavín, 2017). On the western side of the Pacific, the thermocline shoals,
 752 causing subsurface OAX and LOX to extend into the central tropical Pacific (Xu et al.,
 753 2017; Leung, Thompson, et al., 2019). Thus, the triple compound occurs when all three
 754 stressors occur in the same column, albeit at different vertical locations. When the sur-
 755 face heating tapers towards the end of El Niño, the MHW signal at the bottom of the
 756 column remains below the thermocline and is cut off from surface ventilation, leading
 757 to the characteristic depth profile seen in Figure 10. This subsurface MHW signal per-
 758 sists even into the succeeding La Niña event, where the shoaling thermocline in the east
 759 leads to intensified OAX and LOX above the MHW. This process is illustrated through
 760 a video (Movie S1). The logistic regression supports the described process occurring dur-
 761 ing La Niña with a strong correlation between shoaled thermocline depth, decreased strat-
 762 ification, and increased biological productivity (Table S1).

763 In the eastern tropical Indian ocean and the Bering Sea, corresponding to MHW-
 764 OAX-LOX clusters 3 and 4, an unusual combination of all three stressors co-occur in the
 765 subsurface below 100 m with little to no concurrent surface-MHW expression. One pos-
 766 sible cause of MHW-OAX-LOX in cluster 4 is preceding warm atmospheric conditions
 767 that cause sea ice retreat and surface MHW (Carvalho et al., 2021). Another source of
 768 warm waters in the specific case of 2018 could be the Pacific Blob event in 2014–2016,
 769 which saw intense MHW covering the northeastern Pacific, mixing into the subsurface
 770 and persisting below the mixed layer, then advecting northward. Subsequently, lower sea-
 771 ice cover in the winter led to weakened stratification and allowed warm water to pen-
 772 etrate the subsurface (Stabeno & Bell, 2019; Basyuk & Zuenko, 2020; Scannell et al., 2020).
 773 OAX and LOX are then partially the result of anomalous temperatures driving an in-
 774 crease $[H^+]$ and a decrease in oxygen solubility. This is seen by the change in temper-
 775 ature accounting for 22% of the change in $[H^+]$ (Figure S22). Later, the increased strat-
 776 ification associated with this cluster (Table S1) hindered the ventilation of the subsur-
 777 face, maintaining the triple compound at depth. An example from this cluster is illus-
 778 trated in a Hovmoller diagram (Figure S25). Although there are no existing works on
 779 subsurface extreme events in the Bering Sea, the subsurface compound extremes found
 780 by Hauri et al. (2024) in the Gulf of Alaska reflect the timing and processes associated
 781 with this cluster in the Bering Sea. Carvalho et al. (2021) also found an increase in the
 782 number of surface MHW in the Bering Sea in the time periods leading up to those of clus-
 783 ter 4 (Figure S20). In cluster 3, the largest event occurred in 1997, corresponding to the
 784 largest event of cluster 5, and a strong El Niño event (S20). This suggests an ENSO tele-
 785 connection in the Indian Ocean leading to subsurface MHW-OAX-LOX. In these two clus-

786 ters, few MHW studies have been conducted and even less so on subsurface MHW, OAX,
 787 and LOX. As research in this space has been gradually gaining attention, we expect to
 788 better understand the mechanisms behind these subsurface triple compound events in
 789 the future.

790 4.5 Enhancement and Suppression of CCX during ENSO Events

791 Further insights into the potential drivers of CCX can be deduced from when the
 792 CCX occur. We have already seen that, on the global scale, most CCX tend to corre-
 793 late positively with ENSO (Figure 6). But we also identified more complex responses with
 794 enhanced occurrences during both strong El Niños and strong La Niñas. Therefore, it
 795 is worth examining this connection in depth, looking at the regional changes in CCX days
 796 during El Niño (Figure 11a,c,e,g) and La Niña (Figure 11b,d,f,h) events. Using the Oceanic
 797 Niño index (ONI), we identified 149 months of El Niño and 180 months of La Niña dur-
 798 ing the hindcast period, with the remaining 373 months classified as ENSO neutral.

799 During ENSO events, there is a slight enhancement of all MHW-related CCX in
 800 the tropics across all basins, starting from 5 days per year in many areas, increasing to
 801 more than 20 days per year in certain regions (Figures 11a-b,e-f,g-h). There are clear
 802 spatial differences between the opposite phases of ENSO for MHW-OAX (Figures 11a-
 803 b). In general, El Niño does not suppress MHW-OAX strongly in any location, but in-
 804 stead enhances it in the tropics and subtropics of all ocean basins by about 20 days per
 805 year on average. There is a particularly strong enhancement of more than 20 days per
 806 year in the Atlantic Ocean and the Arabian Sea, which can be attributed to teleconnec-
 807 tions with ENSO (Holbrook et al., 2019; Sen Gupta et al., 2020; Chatterjee et al., 2022).
 808 During La Niña, enhancement of surface MHW-OAX may be observed in the typical chevron
 809 pattern of the western subtropical Pacific (Holbrook et al., 2019). The highlighted re-
 810 gions belong to MHW-OAX clusters 1 and 2, both of which have a strong surface expres-
 811 sion. Looking southward, there are confined regions of strong enhancement and suppres-
 812 sion in the Subantarctic and Antarctic zones, which mostly fall within MHW-OAX clus-
 813 ters 3 and 4. These clusters have a stronger subsurface expression, but the same regions
 814 can be identified in Holbrook et al. (2019) linking surface MHW to various climate modes.
 815 In these regions, modes such as the southern annular mode (SAM) likely drive variabil-
 816 ity in surface wind stress, leading to changes in the depth of the thermocline and hence
 817 subsurface extremes.

818 With MHW-LOX and MHW-OAX-LOX, there are no distinct spatial differences
 819 between the positive and negative phases of ENSO, with a change of less than 10 days
 820 per year across the globe. This is because the frequency of these CCX is also generally
 821 low, and hence no significant changes may be identified in association with ENSO. One
 822 exception occurs in the central equatorial Pacific. Here, the annual CCX days strongly
 823 increase during El Niño by up to 30 days per year. This corresponds to cluster 5 of the
 824 triple compound event, which has distinctive peaks in volume fraction in the El Niño years
 825 of 1997 and 2016 (Figure S20). Both the surface MHW from the east and the subsur-
 826 face OAX and LOX from the west trace their driver to El Niño, thus having a single com-
 827 mon driver, though operating through different processes on the different sides of the trop-
 828 ical Pacific. The lack of a strong ENSO correlation in the eastern tropical Pacific is dif-
 829 ferent from the surface MHW correlations of Holbrook et al. (2019); Sen Gupta et al.
 830 (2020), where there is a strong response in the eastern equatorial Pacific. This was also
 831 reflected in the co-occurrence propensities of MHW-related CCX (Figure 7. MHW in-
 832 duced on the surface during El Niño strongly stratify the surface, suppressing the up-
 833 welling of deep waters, pushing the thermocline down, and hence reducing the occurrence
 834 of OAX and LOX. While some surface MHW induce co-located OAX due to the tem-
 835 perature effect on $[H^+]$, the associated changes in $[H^+]$ tend to be smaller than those in-
 836 duced by the changes in upwelling, such that the propensity of MHW and OAX is very
 837 low.

838 Among the CCX variations, OAX-LOX events stand out as having the strongest
 839 and most distinct ENSO associations (11c-d). In the tropical Pacific, the opposing effects
 840 of El Niño and La Niña phases are clear. During El Niño, OAX-LOX events are enhanced
 841 in the west by more than 30 days (cluster 2), representing a doubling in annual CCX days.
 842 Meanwhile, a strong suppression of up to 30 days is observed in the eastern tropical Pa-
 843 cific (cluster 1). Conversely during La Niña, the eastern tropical Pacific (cluster 1) ex-
 844periences an enhancement of OAX-LOX of a similar magnitude and a weaker suppres-
 845sion in the west (cluster 2). These events can be strongly linked to ENSO with the shoal-
 846ing and deepening of the thermocline, as highlighted in the previous section. The effects
 847of ENSO on OAX-LOX in other regions are also strong, though not as distinctly dichoto-
 848mous between phases. They are typically facilitated by atmospheric teleconnections (Roy
 849& Reason, 2001) and ocean currents (Susanto et al., 2001; Feng et al., 2018), through
 850mechanisms such as thermocline and upwelling modulations.

851 5 Discussion

852 Most studies on marine extremes have focused so far on surface MHW, limiting their
 853 analyses to the drivers and impacts occurring in the surface layer. With the CCX de-
 854tected in this study, there is a need to infer surface and subsurface drivers. Furthermore,
 855CCX in this study with surface expressions extend at least 50 m into the subsurface, prompt-
 856ing an investigation of surface stratification and the mixed layer. Similarly, the associ-
 857ated impacts of CCX are relevant not only to organisms residing at a certain depth, but
 858also to those who inhabit the entire upper ocean water column. These migrating organ-
 859isms are impacted to a greater extent as CCX shrink and divide their habitable space.

860 5.1 Climatic Drivers of Column-Compound Extreme Events

861 The most significant CCX clusters identified in Section 4.4 are summarised in Fig-
 862ure 12, with their corresponding metrics and vertical structure. With the analysis, we
 863have also repeatedly identified ENSO events as the main driver of a large proportion of
 864CCX. This is due to the large area of the Pacific Ocean that is typically affected by ENSO
 865and the atmospheric and oceanic connections it has with other ocean basins. However,
 866the mechanisms through which ENSO drives CCX vary by region. Furthermore, ENSO
 867events can drive CCX through multiple mechanisms.

868 Some of these ENSO-driven CCX have been identified as being spatially co-occurring,
 869where their constituent single extremes co-occur in the same grid cells and tend to be
 870driven by similar mechanisms. The most prominent example is OAX-LOX, which oc-
 871curs primarily in the subsurface. OAX-LOX clusters 1 and 2 exhibit this effect at dif-
 872ferent depths, depending on the location of the thermocline. La Niña events associated
 873with an increase in surface winds drive anomalous upwelling of low-pH and low-oxygen
 874waters in the California and Humboldt current systems, leading to events in the OAX-
 875LOX 1 cluster. Furthermore, the increased biological productivity induced by the up-
 876welled waters can further deplete oxygen through remineralisation and enrich the wa-
 877ter with carbon, driving OAX. The depth of OAX and LOX during OAX-LOX events
 878in the EBUS and east tropics cluster lies between 50 –200 m, which is consistent with
 879the typical coastal and offshore upwelling source waters of 150 –280 m (Chhak & Di Lorenzo,
 8802007; Frischknecht et al., 2018; Bograd et al., 2015), and sits beneath the mean mixed
 881layer depth (Ando & McPhaden, 1997; Fiedler & Talley, 2006). Furthermore, the shoal-
 882ing of the thermocline in the east tropics intensifies OAX and LOX in the subsurface.
 883The co-occurrence propensity and vertical location of these events correspond roughly
 884with the locations of low oxygen zones or shadow zones (Luyten et al., 1983; Paulmier
 885& Ruiz-Pino, 2009), which are often associated with low pH (Paulmier et al., 2011). In
 886the western tropical Pacific corresponding to OAX-LOX cluster 2, El Niño events lead
 887to the shoaling of the thermocline, bringing low pH and low oxygen waters closer to the

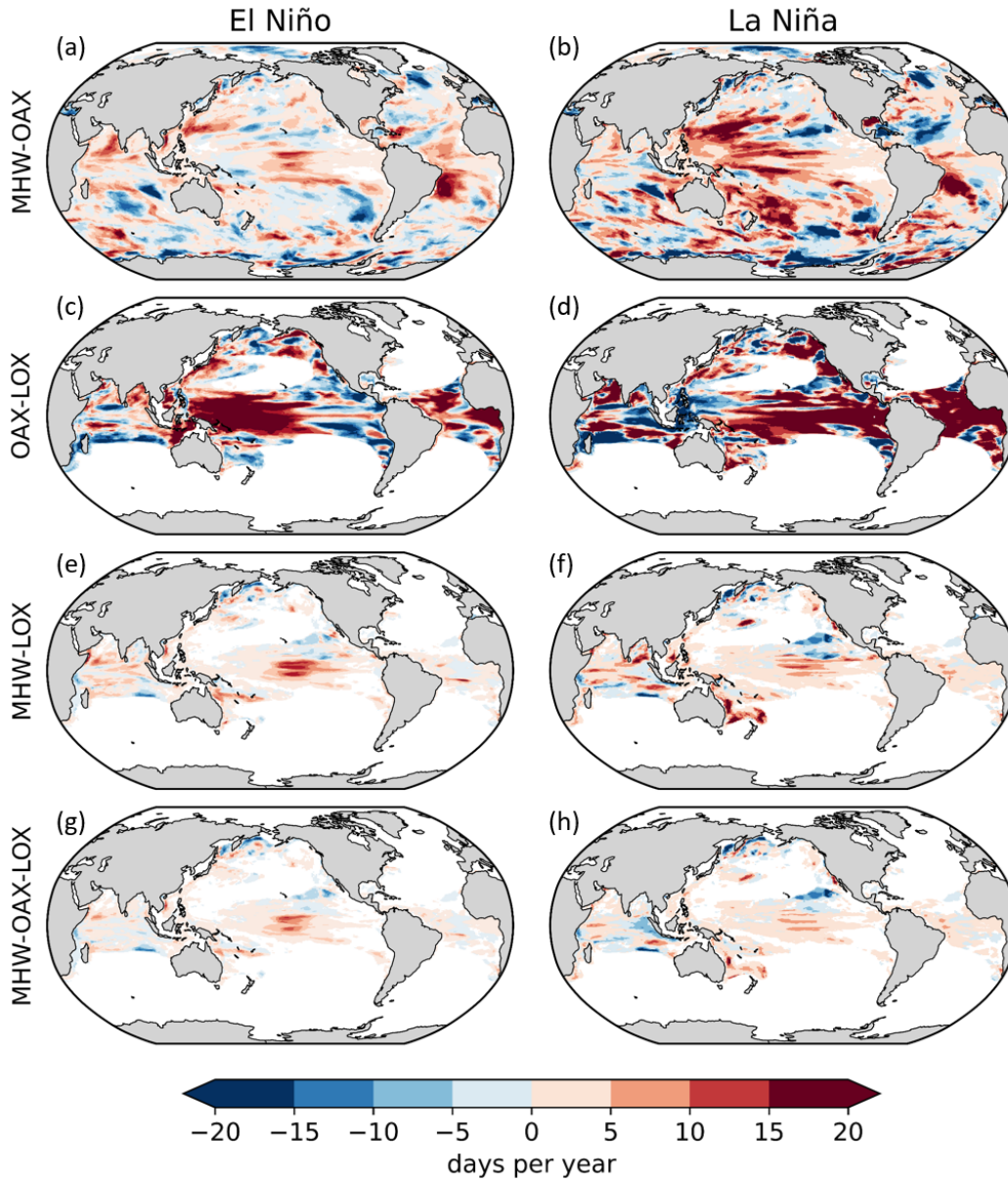


Figure 11. Maps illustrating the impact of ENSO on the number of extreme days for each CCX type. Shown are changes of annual CCX days during positive (left column) and negative (right column) ENSO phases, compared to a neutral ENSO phase. Each row corresponds to one CCX type, i.e. (a-b): MHW-OAX, (c-d): OAX-LOX, (e-f): MHW-LOX, (g-h): MHW-OAX-LOX. In this figure, a year is defined to begin in July and end in June of the next year, permitting to better capture the impact of ENSO as it peaks around Christmas.

888 surface, with mean depths corresponding to the mean mixed layer depth (Ando & McPhaden,
 889 1997; Fiedler & Talley, 2006). In general, these events are deeper in the column than their
 890 eastern counterparts due to the deeper mixed layer depths in the western tropical Pa-
 891 cific. These events have the highest days per year among the identified clusters, increas-
 892 ing the most during ENSO events. The association of OAX-LOX events with a shallower

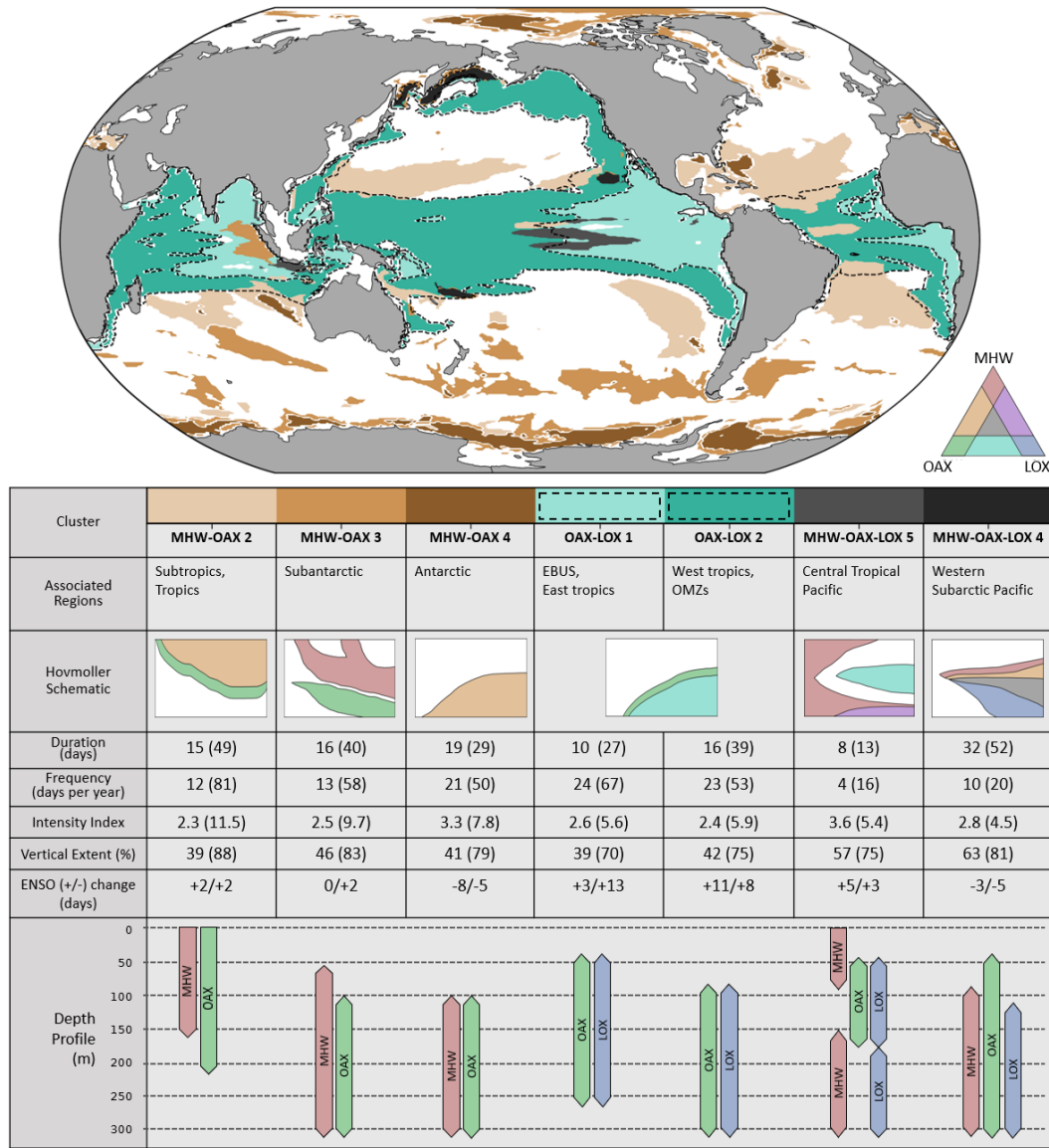


Figure 12. Synthesis figure of CCX properties in selected clusters. Map: Selected clusters of CCX in a composite plot. The extent of OAX-LOX 1 and OAX-LOX 2 are marked by dashed lines to indicate their overlap with other clusters. Table (from top to bottom): Cluster names and their associated regions. Hovmoller schematics that are drawn to illustrate actual extreme conditions seen in the hindcast. Cluster mean values of mean duration, mean frequency, mean maximum intensity index, mean vertical extent, and change in number of CCX days during positive and negative ENSO periods. Values in parentheses are of the fixed baseline. Lastly, the approximate vertical locations of single extremes during CCX are represented with simplified bars.

893 thermocline and increased biological productivity has been shown in Section 4.4 through
 894 the odds ratio values of logistic regressions.

895 Another example of spatially co-occurring CCX driven by ENSO is MHW-OAX
 896 cluster 2, predominantly in the subtropics. Within this cluster we see a positive asso-

897 ciation with both phases of ENSO (Figure 11. ENSO-driven temperature anomalies lead
 898 to MHW (Holbrook et al., 2019), which then induces OAX through shifts in the carbon-
 899 ate chemistry equilibrium (Zeebe & Wolf-Gladrow, 2001; Burger et al., 2022). The ar-
 900 eas where MHW-OAX 2 occur tend to be areas without a tendency for deep water up-
 901 welling or thermocline shifts. The contribution of temperature to increases in $[H^+]$ was
 902 shown in Section 4.4 by computing the fraction contribution of temperature anomalies.
 903 For all MHW-OAX clusters, the temperature contribution is high (>0.6), but the high-
 904 est is seen in MHW-OAX-2 with a value of 1.38

905 ENSO events can also drive CCX through multiple mechanisms, as seen in MHW-
 906 OAX-LOX cluster 5. MHW is induced throughout the column by strong surface heat-
 907 ing during El Niño in the eastern tropical Pacific. Meanwhile, El Niño also drives the
 908 shoaling of the thermocline in the western tropical Pacific, inducing OAX and LOX
 909 in the subsurface. A deep MHW also persists in the subsurface even after being disconnected
 910 from the surface MHW. The resulting CCX is one that occupies the entire water column,
 911 driven by El Niño through different mechanisms. The MHW-OAX-LOX cluster 4 is an-
 912 other peculiar example, of which one occurrence in 2018 has been linked an El Niño event
 913 in 2014-2016 (Basyuk & Zuenko, 2020). Lateral advection of a warm water mass, enhanced
 914 southerly winds, and lower sea ice cover could be factors that lead to surface MHW in
 915 the Bering Sea. Anomalously low stratification then allows heat to be transmitted to the
 916 subsurface, possibly inducing OAX and LOX. Since our ENSO analysis does not account
 917 for lag times, it is difficult to link this event to ENSO. CCX in this cluster may also be
 918 driven by local processes and other modes of variability, such as the Pacific Decadal Os-
 919 cillation (PDO). The mechanisms behind events in these two clusters involve vertical and
 920 lateral transfer of heat and/or water, occurring over timescales of months. Thus, it is
 921 a more complex driver attribution than can be achieved through the correlations employed
 922 in this study.

923 The CCX in the Southern Ocean (MHW-OAX clusters 3 and 4) could be driven
 924 by various climate modes. Within these clusters, strong sub-cluster enhancements and
 925 suppression have been found during ENSO events. Due to the regionally varying ENSO
 926 response within the clusters, the cluster-mean change in days per year due to ENSO is
 927 rather muted. These CCX can be inferred to be driven by a combination of surface heat-
 928 ing, strong winds causing diapycnal mixing (Ledwell et al., 2011; Tamsitt et al., 2017),
 929 anomalous sea-ice cover (Ramadhan et al., 2022; Gordon, 1981), and upwelling of the
 930 CDW along the Antarctic divergence zone (Morrison et al., 2015; Wilson et al., 2019;
 931 Ramadhan et al., 2022). In particular, we attributed the increased biological productiv-
 932 ity found in these clusters to the CDW through a logistic regression. The inferred mech-
 933 anisms can also be linked to other climate modes, such as the Southern Annular Mode
 934 and the Indian Ocean Dipole.

935 **5.2 Potential Impacts of Column-Compound Extreme Events**

936 Compounded extreme events can cause severe impacts when stressors interact syn-
 937 ergistically (Gruber et al., 2021). This synergism can occur in different ways. The most
 938 direct effects occur when an organism experiences multiple stressors in the same place
 939 and time (Le Grix et al., 2021; Burger et al., 2022). In our study, we additionally con-
 940 sider the contraction of habitable space within the water column during CCX, where ex-
 941 tremes may occur at different depths. This contraction may lead to indirect impacts re-
 942 lated to predator evasion or food availability.

943 Co-located and co-temporal events exacerbate impacts on organisms to which mul-
 944 tiple stressors are synergistically detrimental and are highly dependent on species and
 945 life stage (Kroeker et al., 2013; Deutsch et al., 2015; Gobler & Baumann, 2016). Dur-
 946 ing compounded MHW and LOX, thermal stress increases metabolism and drives ad-
 947 ditional oxygen demand in ectotherms (Pörtner, 2002; K. E. Smith et al., 2023). The co-

948 inciding low-oxygen environment further hinders the ability of organisms to survive, grow,
949 or recruit. Recent work has quantified this effect into a composite "metabolic" or "aer-
950 obic growth" index (Deutsch et al., 2015; Clarke et al., 2021). MHW and LOX occur-
951 ring at the same place and time will pose a large threat in this case, although they have
952 been shown to be relatively uncommon in this work. However, a strong MHW can si-
953 multaneously induce lower oxygen (due to lower solubility) and reduce the low oxygen
954 tolerance threshold of the organism (through increased metabolism), effectively increas-
955 ing the oxygen threshold beyond those used in this study. Furthermore, acidic conditions
956 have been shown to increase metabolic stress (Pan et al., 2015; Engström-Öst et al., 2019;
957 Tai et al., 2021; Lattuca et al., 2023). Thus, the co-occurrence of OAX adds another layer
958 of metabolic demand. Every organism has a different metabolic threshold (Deutsch et
959 al., 2015), and it is beyond the range of this study to identify the impacts on any par-
960 ticular species. However, higher resolution regional studies (Franco et al., 2022) in con-
961 junction with laboratory studies (Seibel et al., 2016) will be able to identify the impacts
962 on metabolism of any given species.

963 Up to now, there has been very little work on the compression of marine habitats
964 due to extreme events (Desmet et al., 2022; Köhn et al., 2022), and much less so with
965 compounded extreme stressors. In this study, we show that when CCX occur, the re-
966 maining contiguous habitable space is less than half of the upper ocean water column
967 on average. This fraction is reduced further when multiple extremes occur in different
968 parts of the water column. Vertically migrating organisms are expected to be especially
969 affected by CCX, as they depend on the habitable water column for essential biological
970 activities. Diel vertical migration (DVM) is understood to be performed by planktonic
971 species for the purpose of food gathering and predator avoidance (Ritz et al., 2011), and
972 is a behavioural response to light (Cohen & Forward, 2019). Little is known about the
973 impact of marine extremes on DVM, except that some species regularly migrate to low
974 oxygen and low pH environments (Riquelme-Bugueño et al., 2020). When extreme con-
975 ditions occur close to the surface, the habitable space of migrating organisms is reduced.
976 They may avoid extreme conditions on the surface, thereby reducing food availability,
977 or simply continue to migrate upward into extreme conditions, increasing metabolism
978 and food demand. In either case, the ability of organisms to grow and survive is reduced.
979 In the event of a CCX that covers both the surface and the subsurface, the migrating
980 organisms have no good choice to make and are simply subject to extreme conditions
981 wherever they are. Habitat contraction may further affect organisms in more indirect
982 ways. Extreme conditions on the surface may force marine fish to migrate to the sub-
983 surface (Jorda et al., 2020), decreasing the survivability of zooplankton species that use
984 the darker environment to avoid predators. The impact of column extreme events on such
985 vertically migrating organisms can be quantified with the choice of threshold. While a
986 small vertical displacement of $[H^+]$ or $[O_2]$ anomalies may not lead to much impact, a
987 choice of at least 50 m in this study implies that organisms could be 50 m away from wa-
988 ters with normal conditions, increasing the amount of time spent in extreme conditions.

989 Although we cannot yet identify the specific biological impacts of the compound
990 extremes that we identified and described in this study, we point out that these CCX
991 occur in ecologically and biogeochemically sensitive regions. Of particular concern is the
992 tropical nature of many CCX, given that these regions contain the highest diversity across
993 nearly all trophic levels (Tittensor et al., 2010), ranging from phytoplankton (Righetti
994 et al., 2019), zooplankton (Benedetti et al., 2021), fish (Stuart-Smith et al., 2013), to top
995 predators (Worm & Tittensor, 2018). Furthermore, these tropical regions are also the
996 locations of major fisheries (Watson, 2017). The co-occurrence of many double and triple
997 compound extremes in the central and eastern tropical Pacific make this region among
998 the most vulnerable. Also of concern are the western tropical Pacific, Southeast Asian
999 seas, and the Coral Sea where MHW-OAX and OAX-LOX are found to occur, while be-
1000 ing characterised as the world's region with the highest marine biodiversity (Tittensor
1001 et al., 2010). Furthermore, the EBUS, home to some of the highest fishery catches, are

subject to regular compound extremes (especially OAX-LOX). In addition, the frequent occurrence of very intense MHW-OAX events in the high-latitude Southern Ocean hits a very sensitive ecosystem, with a relatively high diversity (Chown et al., 2015) and home to very unique organisms and ecosystems (Hill et al., 2006; Constable et al., 2014).

5.3 Caveats and Limitations

In this study, extreme events in the model hindcast were evaluated with respect to surface MHW and OAX only. The evaluation of surface OAX with OceanSODA-ETHZ (Gregor & Gruber, 2021) showed a tendency of the model towards longer and more intense events on the surface. A large fraction of this bias is located in regions with strong thermocline variability, and hence we also expect it to apply to detected LOX, due to their high co-occurrence with OAX. On the other hand, some part of this bias may also be attributed to the relatively lower variability in the OceanSODA-ETHZ product (Ma et al., 2023). Overall, we expect the impact of potential biases on our results to be restricted to particular metrics, perhaps most importantly the intensity and duration of the events. In contrast, the spatial structure of the CCX and their co-occurrence propensity is likely much less affected, as these are related to their underlying physical and biogeochemical processes, which we consider well captured by the model. One option for the subsurface evaluation of these properties is emerging from the rapidly increasing number of observations from the Biogeochemical Argo float program (Johnson & Claustre, 2016). These observations could be used to evaluate $[\text{H}^+]$ and $[\text{O}_2]$ in the subsurface. In particular, we used the GOBAI-O2 product (Sharp et al., 2022) to evaluate the mean state of $[\text{O}_2]$, although the time period covered is too short to establish a baseline for LOX. We found that the CESM hindcast has a tendency to overestimate $[\text{O}_2]$ in confined regions within all ocean basins, particularly in oxygen-deficient zones, while making an underestimation elsewhere, such as in the west Pacific. This leads to biases in the 150 μM depth of $[\text{O}_2]$, by up to ± 40 m, and should be taken into account when considering the subsurface OAX and LOX. Still, we do not expect the main findings to be different, since the subsurface column extremes tend to extend over 100 m in range.

A second caveat concerns the relatively low spatial resolution of the CESM hindcast, particularly near the poles. Small-scale, local processes are not captured by the model, and thus we are unable to conduct analyses regarding such physical mechanisms. The CCX identified in the Southern Ocean have been linked to variations in the upwelling of the CDW and surface wind stress, which are large enough to be represented by the CESM hindcast. Still, considering the moderate resolution of our model, our results are biased towards CCX extending over substantial spatial scales, and represent the low to mid latitudes better with a higher resolution.

The third caveat concerns the choice of criteria used to identify extremes. Our choices were made with the intention to investigate the co-occurrence of multiple stressors within the vertical column in a systematic and consistent manner, linking them to drivers and mechanisms based on their spatiotemporal characteristics. For this work, the moving baseline was primarily used, as it is more suitable for the investigation of drivers behind extreme events. However, in Figures 5 and 6, it was shown that the detected volume fraction is vastly different between the fixed and moving baselines. The results on the moving baseline are unable to show the worsening conditions of the global ocean under climate change, nor the change in propensity of extreme events under such conditions. For such an analysis, the fixed baseline may be a better choice.

Furthermore, the chosen extreme criteria are not targeted toward specific biological thresholds or marine organisms. Therefore, the biological impacts of the extremes identified in this study cannot be directly quantified. For example, MHW-OAX CCX are generally absent in the EBUS, even though temperature-induced OAX are known to occur during MHW. This is likely because the OAX occurrences in these regions are

1053 dominated by anomalous upwelling events, which increase $[H^+]$ more strongly compared
1054 to MHW. Thus, we see more OAX-LOX occurring in the EBUS. However, this does not
1055 mean that the MHW-induced high $[H^+]$ is irrelevant, as organisms may still be affected.
1056 In such scenarios, it is better to rely on species-specific thresholds as the basis for ex-
1057 treme detection (Le Grix et al., 2023). This limitation on biological impacts also extends
1058 to the definition of CCX, where a vertical extent of at least 50 m of each extreme type
1059 is required. An organism whose metabolism is affected by temperature could be affected
1060 by either MHW or LOX, and not necessarily only when both occur. It may then be a
1061 better choice to define extreme conditions based on the metabolic rate of the particu-
1062 lar organism and oxygen concentration in the water.

1063 6 Summary and Conclusions

1064 With this work on CCX, we took a first step in characterising extremes that are
1065 compounded in the vertical water column. CCX are detected in the global ocean on a
1066 CESM-BEC daily hindcast from 1961 to 2020. Key characteristics such as frequency, du-
1067 ration, intensity, and reduction of habitable space are assessed, to determine the regions
1068 where CCX are the most severe. These are the subtropics and Southern Ocean for MHW-
1069 OAX, and the tropics and north Pacific for OAX-LOX, MHW-LOX, and MHW-OAX-
1070 LOX. All CCX substantially increase in their intensity, frequency, and spatial extent, pri-
1071 marily driven by ocean warming and the increase in ocean acidity due to the oceanic up-
1072 take of anthropogenic CO_2 from the atmosphere.

1073 Within the vertical column, the depths where single extremes occur during CCX
1074 are analysed to determine the mechanisms behind them. We find that ENSO-associated
1075 CCX tend to be driven by a single mechanism such as increased air-sea heat flux or in-
1076 creased upwelling, resulting in colocated compounded events. On the other hand, there
1077 is a significant proportion of CCX in which the single constitutive extremes occur in dif-
1078 ferent parts of the vertical column. These tend to be driven by separate drivers and have
1079 a reduced association with ENSO events.

1080 Marine extreme events can have a large impact on pelagic organisms, which are usu-
1081 ally affected by multiple stressors, rather than a single stressor. These organisms swim
1082 or migrate vertically, experiencing various physical and chemical conditions. Therefore,
1083 the study of vertically compounded extremes advances our understanding of the impacts
1084 of extreme events on marine organisms. Furthermore, these extremes are likely to be-
1085 come more frequent and intense with the climate trend of increasing temperatures and
1086 atmospheric CO_2 . Extreme conditions of the past may well become the mean state of
1087 the ocean in the future. Further analysis of such column-compound events on regional
1088 scales or with regard to specific organisms will extend our understanding of their future
1089 impacts.

1090 Open Research

1091 All data to reproduce the plots can be found in the following repository: <https://doi.org/10.3929/ethz-b-000654113>. The standard monthly output of the CESM model
1092 simulations is available through the RECCAP2 Zenodo repository (Müller, 2023): <https://zenodo.org/records/7990823>.
1093
1094

1095 Conflict of Interest Statement

1096 The authors have no conflicts of interest to declare.

1097 **Acknowledgments**

1098 This project has received funding from the European Union's Horizon 2020 research and
1099 innovation programme under grant agreement No 820989 (COMFORT). The authors thank
1100 Dr. Damian Loher for his modeling support, and Dr. Eike Köhn, Dr. Luke Gregor, and
1101 Dr. Fabio Benedetti for useful discussions. The authors also thank the two reviewers for
1102 their time and expertise in improving the quality and clarity of this manuscript.

1103

References

1104

Amaya, D. J., Jacox, M. G., Alexander, M. A., Scott, J. D., Deser, C., Capotondi, A., & Phillips, A. S. (2023, March). Bottom marine heatwaves along the continental shelves of North America. *Nature Communications*, *14*(1), 1038. doi: 10.1038/s41467-023-36567-0

1107

1108

Ando, K., & McPhaden, M. J. (1997). Variability of surface layer hydrography in the tropical Pacific Ocean. *Journal of Geophysical Research: Oceans*, *102*(C10), 23063–23078. doi: 10.1029/97JC01443

1109

1110

Basyuk, E., & Zuenko, Y. (2020). Extreme oceanographic conditions in the northwestern Bering Sea in 2017–2018. *Deep-Sea Research Part II: Topical Studies in Oceanography*, *181-182*. doi: 10.1016/j.dsr2.2020.104909

1111

1112

1113

Bednaršek, N., Feely, R. A., Beck, M. W., Glippa, O., Kanerva, M., & Engström-Öst, J. (2018). El Niño-related thermal stress coupled with upwelling-related ocean acidification negatively impacts cellular to population-level responses in pteropods along the California current system with implications for increased bioenergetic costs. *Frontiers in Marine Science*, *5*, 1–17. doi: 10.3389/fmars.2018.00486

1116

1117

1118

1119

Benedetti, F., Vogt, M., Elizondo, U. H., Righetti, D., Zimmermann, N. E., & Gruber, N. (2021). Major restructuring of marine plankton assemblages under global warming. *Nature Communications*, *12*(1), 5226. doi: 10.1038/s41467-021-25385-x

1120

1121

1122

1123

Bertrand, A., Ballón, M., & Chaigneau, A. (2010). Acoustic observation of living organisms reveals the upper limit of the oxygen minimum zone. *PLoS ONE*, *5*(4). doi: 10.1371/journal.pone.0010330

1124

1125

1126

Bianchi, D., & Mislán, K. A. (2016). Global patterns of diel vertical migration times and velocities from acoustic data. *Limnology and Oceanography*, *61*(1), 353–364. doi: 10.1002/lno.10219

1127

1128

1129

Bianchi, D., Stock, C., Galbraith, E. D., & Sarmiento, J. L. (2013). Diel vertical migration: Ecological controls and impacts on the biological pump in a one-dimensional ocean model. *Global Biogeochemical Cycles*, *27*(2), 478–491. doi: 10.1002/gbc.20031

1130

1131

1132

1133

Bograd, S. J., Buil, M. P., Lorenzo, E. D., Castro, C. G., Schroeder, I. D., Goericke, R., ... Whitney, F. A. (2015). Changes in source waters to the Southern California Bight. *Deep-Sea Research Part II: Topical Studies in Oceanography*, *112*, 42–52. doi: 10.1016/j.dsr2.2014.04.009

1134

1135

1136

1137

Boyd, P. W., & Brown, C. J. (2015). Modes of interactions between environmental drivers and marine biota. *Frontiers in Marine Science*, *2*, 1–7. doi: 10.3389/fmars.2015.00009

1138

1139

1140

Braun, C. D., Kaplan, M. B., Horodysky, A. Z., & Llopiz, J. K. (2015). Satellite telemetry reveals physical processes driving billfish behavior. *Animal Biotelemetry*, *3*(1). doi: 10.1186/s40317-014-0020-9

1141

1142

1143

Burger, F. A., & Frölicher, T. L. (2023). Drivers of Surface Ocean Acidity Extremes in an Earth System Model. *Global Biogeochemical Cycles*, *37*(9), e2023GB007785. doi: 10.1029/2023GB007785

1144

1145

1146

Burger, F. A., John, J. G., & Frölicher, T. L. (2020). Increase in ocean acidity variability and extremes under increasing atmospheric CO₂. *Biogeosciences*, *17*(18), 4633–4662. doi: 10.5194/bg-17-4633-2020

1147

1148

1149

Burger, F. A., Terhaar, J., & Frölicher, T. L. (2022). Compound marine heatwaves and ocean acidity extremes. *Nature Communications*, 1–12. doi: 10.1038/s41467-022-32120-7

1150

1151

1152

Carvalho, K. S., Smith, T. E., & Wang, S. (2021, September). Bering Sea marine heatwaves: Patterns, trends and connections with the Arctic. *Journal of Hydrology*, *600*, 126462. doi: 10.1016/j.jhydrol.2021.126462

1153

1154

1155

Chan, F., Barth, J. A., Lubchenco, J., Kirincich, A., Weeks, H., Peterson, W. T., & Menge, B. A. (2008). Emergence of anoxia in the California current large

1156

1157

- 1158 marine ecosystem. *Science*, *319*(5865), 920. doi: 10.1126/science.1149016
- 1159 Chatterjee, A., Anil, G., & Shenoy, L. R. (2022). Marine heatwaves in the Arabian
1160 Sea. *Ocean Science*, *18*(3), 639–657. doi: 10.5194/os-18-639-2022
- 1161 Chhak, K., & Di Lorenzo, E. (2007). Decadal variations in the California Cur-
1162 rent upwelling cells. *Geophysical Research Letters*, *34*(14), 1–6. doi: 10.1029/
1163 2007GL030203
- 1164 Chiswell, S. M. (2022). Global Trends in Marine Heatwaves and Cold Spells: The
1165 Impacts of Fixed Versus Changing Baselines. *Journal of Geophysical Research:
1166 Oceans*, *127*(10), e2022JC018757. doi: 10.1029/2022JC018757
- 1167 Chown, S. L., Clarke, A., Fraser, C. I., Cary, S. C., Moon, K. L., & McGeoch, M. A.
1168 (2015). The changing form of Antarctic biodiversity. *Nature*, *522*(7557),
1169 431–438. doi: 10.1038/nature14505
- 1170 Clarke, T. M., Wabnitz, C. C., Striegel, S., Frölicher, T. L., Reygondeau, G., & Che-
1171 ung, W. W. (2021). Aerobic growth index (AGI): An index to understand
1172 the impacts of ocean warming and deoxygenation on global marine fisheries
1173 resources. *Progress in Oceanography*, *195*. doi: 10.1016/j.pocean.2021.102588
- 1174 Cohen, J. H., & Forward, R. B. (2019). Vertical Migration of Aquatic Animals.
1175 In J. C. Choe (Ed.), *Encyclopedia of Animal Behavior (Second Edition)* (pp.
1176 546–552). Oxford: Academic Press. doi: 10.1016/B978-0-12-809633-8.01257-7
- 1177 Collins, M., Sutherland, M., Bouwer, L., Cheong, S.-M., Frölicher, T., Des Combes,
1178 H. J., ... Tibig, L. (2019). *Extremes, Abrupt Changes and Managing Risks*
1179 (Tech. Rep.).
- 1180 Constable, A. J., Melbourne-Thomas, J., Corney, S. P., Arrigo, K. R., Barbraud, C.,
1181 Barnes, D. K. A., ... Ziegler, P. (2014). Climate change and Southern Ocean
1182 ecosystems I: how changes in physical habitats directly affect marine biota.
1183 *Global Change Biology*, *20*(10), 3004–3025. doi: 10.1111/gcb.12623
- 1184 Crain, C. M., Kroeker, K., & Halpern, B. S. (2008). Interactive and cumulative ef-
1185 fects of multiple human stressors in marine systems. *Ecology Letters*, *11*(12),
1186 1304–1315. doi: 10.1111/j.1461-0248.2008.01253.x
- 1187 Desmet, F., Gruber, N., Köhn, E. E., Münnich, M., & Vogt, M. (2022). Tracking the
1188 space-time evolution of ocean acidification extremes in the California Current
1189 System and Northeast Pacific. *Journal of Geophysical Research: Oceans*, 1–30.
1190 doi: 10.1029/2021jc018159
- 1191 Desmet, F., Münnich, M., & Gruber, N. (2023). *Spatiotemporal heterogeneity in
1192 the increase of ocean acidity extremes in the Northeast Pacific*. doi: 10.5194/bg
1193 -2023-60
- 1194 Deutsch, C., Ferrel, A., Seibel, B., Pörtner, H.-O., & Huey, R. B. (2015). Climate
1195 change tightens a metabolic constraint on marine habitats. *Science*, *348*(6239),
1196 1132–1136. doi: DOI:10.1126/science.aaa1605
- 1197 DeVries, T., Yamamoto, K., Wanninkhof, R., Gruber, N., Hauck, J., Müller, J. D.,
1198 ... Zeng, J. (2023). Magnitude, Trends, and Variability of the Global Ocean
1199 Carbon Sink From 1985 to 2018. *Global Biogeochemical Cycles*, *37*(10). doi:
1200 10.1029/2023GB007780
- 1201 Diaz, R. J., & Rosenberg, R. (2008). Spreading Dead Zones and Consequences
1202 for Marine Ecosystems. *Science*, *321*(5891), 926–929. doi: 10.1126/science
1203 .1156401
- 1204 Di Lorenzo, E., & Mantua, N. (2016). Multi-year persistence of the 2014/15 North
1205 Pacific marine heatwave. *Nature Climate Change*, *6*(11), 1042–1047. doi: 10
1206 .1038/nclimate3082
- 1207 Dinniman, M. S., Klinck, J. M., & Smith, W. O. (2011). A model study of Circum-
1208 polar Deep Water on the West Antarctic Peninsula and Ross Sea continental
1209 shelves. *Deep Sea Research Part II: Topical Studies in Oceanography*, *58*(13-
1210 16), 1508–1523. doi: 10.1016/j.dsr2.2010.11.013
- 1211 Ebita, A., Kobayashi, S., Ota, Y., Moriya, M., Kumabe, R., Onogi, K., ... Ishimizu,
1212 T. (2011). The Japanese 55-year Reanalysis “JRA-55”: An Interim Report.

- 1213 *Sola*, 7, 149–152. doi: 10.2151/sola.2011-038
- 1214 Elzahaby, Y., Schaeffer, A., Roughan, M., & Delaux, S. (2021). Oceanic Circula-
1215 tion Drives the Deepest and Longest Marine Heatwaves in the East Australian
1216 Current System. *Geophysical Research Letters*, 48(17), e2021GL094785. doi:
1217 10.1029/2021GL094785
- 1218 Engström-Öst, J., Glippa, O., Feely, R. A., Kanerva, M., Keister, J. E., Alin, S. R.,
1219 ... Bednaršek, N. (2019). Eco-physiological responses of copepods and
1220 pteropods to ocean warming and acidification. *Scientific Reports*, 9(1), 1–
1221 13. doi: 10.1038/s41598-019-41213-1
- 1222 Feng, M., Zhang, N., Liu, Q., & Wijffels, S. (2018). The Indonesian throughflow, its
1223 variability and centennial change. *Geoscience Letters*, 5(1), 3. doi: 10.1186/
1224 s40562-018-0102-2
- 1225 Fiedler, P. C. (2010). Comparison of objective descriptions of the thermocline.
1226 *Limnology and Oceanography: Methods*, 8(6), 313–325. doi: 10.4319/lom.2010
1227 .8.313
- 1228 Fiedler, P. C., & Lavín, M. F. (2017). Oceanographic Conditions of the Eastern
1229 Tropical Pacific. In P. W. Glynn, D. P. Manzello, & I. C. Enochs (Eds.),
1230 *Coral Reefs of the Eastern Tropical Pacific: Persistence and Loss in a Dy-*
1231 *namic Environment* (pp. 59–83). Dordrecht: Springer Netherlands. doi:
1232 10.1007/978-94-017-7499-4_3
- 1233 Fiedler, P. C., & Talley, L. D. (2006). Hydrography of the eastern tropical Pacific:
1234 A review. *Progress in Oceanography*, 69(2-4), 143–180. doi: 10.1016/j.pocean
1235 .2006.03.008
- 1236 Filho, W. L. F. C., Lucio, P. S., & Spyrides, M. H. C. (2013). Precipitation Ex-
1237 tremes Analysis over the Brazilian Northeast via Logistic Regression. *Atmo-*
1238 *spheric and Climate Sciences*, 2014. doi: 10.4236/acs.2014.41007
- 1239 Fragkopoulou, E., Sen Gupta, A., Costello, M. J., Wernberg, T., Araújo, M. B.,
1240 Serrão, E. A., ... Assis, J. (2023, September). Marine biodiversity exposed to
1241 prolonged and intense subsurface heatwaves. *Nature Climate Change*, 1–8. doi:
1242 10.1038/s41558-023-01790-6
- 1243 Franco, A. C., Kim, H., Frenzel, H., Deutsch, C., Ianson, D., Sumaila, U. R., &
1244 Tortell, P. D. (2022). Impact of warming and deoxygenation on the habitat
1245 distribution of Pacific halibut in the Northeast Pacific. *Fisheries Oceanogra-*
1246 *phy*, 31(6), 601–614. doi: 10.1111/fog.12610
- 1247 Friedlingstein, P., Jones, M. W., Sullivan, M. O., Andrew, R. M., Bakker, D. C. E.,
1248 Hauck, J., ... Peters, W. (2022). Global Carbon Budget 2021. *Earth System*
1249 *Science Data*, 1917–2005. doi: 10.5194/essd-14-4811-2022
- 1250 Frischknecht, M., Münnich, M., & Gruber, N. (2018). Origin, Transformation,
1251 and Fate: The Three-Dimensional Biological Pump in the California Current
1252 System. *Journal of Geophysical Research: Oceans*, 123(11), 7939–7962. doi:
1253 10.1029/2018JC013934
- 1254 Frölicher, T. L., Fischer, E. M., & Gruber, N. (2018). Marine heatwaves under
1255 global warming. *Nature*, 560(7718), 360–364. doi: 10.1038/s41586-018-0383-9
- 1256 Gent, P. R., Danabasoglu, G., Donner, L. J., Holland, M. M., Hunke, E. C., Jayne,
1257 S. R., ... Zhang, M. (2011). The Community Climate System Model Version
1258 4. *Journal of Climate*, 24(19), 4973–4991. doi: 10.1175/2011JCLI4083.1
- 1259 Gilly, W. F., Michael Beman, J., Litvin, S. Y., & Robison, B. H. (2013). Ocea-
1260 nographic and biological effects of shoaling of the oxygen minimum zone. *Annual*
1261 *Review of Marine Science*, 5, 393–420. doi: 10.1146/annurev-marine-120710
1262 -100849
- 1263 Gleckler, P. J., Durack, P. J., Stouffer, R. J., Johnson, G. C., & Forest, C. E.
1264 (2016). Industrial-era global ocean heat uptake doubles in recent decades.
1265 *Nature Climate Change*, 6(4), 394–398. doi: 10.1038/nclimate2915
- 1266 Gobler, C. J., & Baumann, H. (2016). Hypoxia and acidification in ocean ecosys-
1267 tems: Coupled dynamics and effects on marine life. *Biology Letters*, 12(5). doi:

- 1268 10.1098/rsbl.2015.0976
- 1269 Gordon, A. L. (1981). Seasonality of Southern Ocean Sea Ice. *Journal of Geophysical*
1270 *Research*, 86(C5), 4193–4197. doi: 10.1029/JC086iC05p04193
- 1271 Gregor, L., & Gruber, N. (2021). OceanSODA-ETHZ: A global gridded data
1272 set of the surface ocean carbonate system for seasonal to decadal studies
1273 of ocean acidification. *Earth System Science Data*, 13(2), 777–808. doi:
1274 10.5194/essd-13-777-2021
- 1275 Gruber, N., Boyd, P. W., Frölicher, T. L., & Vogt, M. (2021). Ocean Biogeochemical
1276 Extremes and Compound Events. *Nature*, 600, 395–407. doi: 10.1038/s41586
1277 -021-03981-7
- 1278 Hauck, J., Gregor, L., Nissen, C., Patara, L., Hague, M., Mongwe, P., ... Ter-
1279 haar, J. (2023). The Southern Ocean Carbon Cycle 1985–2018: Mean, Sea-
1280 sonal Cycle, Trends, and Storage. *Global Biogeochemical Cycles*, 37(11),
1281 e2023GB007848. doi: 10.1029/2023GB007848
- 1282 Hauck, J., Zeising, M., Le Quéré, C., Gruber, N., Bakker, D. C. E., Bopp, L., ...
1283 Séférian, R. (2020). Consistency and Challenges in the Ocean Carbon Sink
1284 Estimate for the Global Carbon Budget. *Frontiers in Marine Science*, 7.
- 1285 Hauri, C., Gruber, N., McDonnell, A. M., & Vogt, M. (2013). The intensity, du-
1286 ration, and severity of low aragonite saturation state events on the California
1287 continental shelf. *Geophysical Research Letters*, 40(13), 3424–3428. doi:
1288 10.1002/grl.50618
- 1289 Hauri, C., Pagès, R., Hedstrom, K., Doney, S. C., Dupont, S., Ferriss, B., &
1290 Stuecker, M. F. (2024). More Than Marine Heatwaves: A New Regime of
1291 Heat, Acidity, and Low Oxygen Compound Extreme Events in the Gulf of
1292 Alaska. *AGU Advances*, 5(1), e2023AV001039. doi: 10.1029/2023AV001039
- 1293 Hauri, C., Pagès, R., McDonnell, A. M., Stuecker, M. F., Danielson, S. L., Hed-
1294 strom, K., ... Doney, S. C. (2021). Modulation of ocean acidification by
1295 decadal climate variability in the Gulf of Alaska. *Communications Earth*
1296 *and Environment*, 2(1), 1–7. Retrieved from [http://dx.doi.org/10.1038/
1297 s43247-021-00254-z](http://dx.doi.org/10.1038/s43247-021-00254-z) doi: 10.1038/s43247-021-00254-z
- 1298 Hill, S. L., Murphy, E. J., Reid, K., Trathan, P. N., & Constable, A. J. (2006). Mod-
1299 elling Southern Ocean ecosystems: krill, the food-web, and the impacts of har-
1300 vesting. *Biological Reviews*, 81(4), 581–608. doi: 10.1017/S1464793106007123
- 1301 Hobday, A. J., Alexander, L. V., Perkins, S. E., Smale, D. A., Straub, S. C.,
1302 Oliver, E. C., ... Wernberg, T. (2016). A hierarchical approach to defin-
1303 ing marine heatwaves. *Progress in Oceanography*, 141, 227–238. doi:
1304 10.1016/j.pocean.2015.12.014
- 1305 Hobday, A. J., Oliver, E. C., Gupta, A. S., Benthuisen, J. A., Burrows, M. T.,
1306 Donat, M. G., ... Smale, D. A. (2018). Categorizing and naming marine
1307 heatwaves. *Oceanography*, 31(2), 162–173. doi: 10.5670/oceanog.2018.205
- 1308 Hofmann, A. F., Peltzer, E. T., Walz, P. M., & Brewer, P. G. (2011). Hypoxia by
1309 degrees: Establishing definitions for a changing ocean. *Deep-Sea Research Part*
1310 *I: Oceanographic Research Papers*, 58(12), 1212–1226. doi: 10.1016/j.dsr.2011
1311 .09.004
- 1312 Holbrook, N. J., Claar, D. C., Hobday, A. J., McInnes, K. L., Oliver, E. C. J.,
1313 Gupta, A. S., ... Zhang, X. (2020). ENSO-Driven Ocean Extremes and Their
1314 Ecosystem Impacts. *El Niño Southern Oscillation in a Changing Climate*,
1315 409–428.
- 1316 Holbrook, N. J., Scannell, H. A., Sen Gupta, A., Benthuisen, J. A., Feng, M.,
1317 Oliver, E. C., ... Wernberg, T. (2019). A global assessment of marine
1318 heatwaves and their drivers. *Nature Communications*, 10(1), 1–13. doi:
1319 10.1038/s41467-019-10206-z
- 1320 Holbrook, N. J., Sen Gupta, A., Oliver, E. C. J., Hobday, A. J., Benthuisen,
1321 J. A., Scannell, H. A., ... Wernberg, T. (2020). Keeping pace with ma-
1322 rine heatwaves. *Nature Reviews Earth & Environment*, 1(9), 482–493. doi:

- 10.1038/s43017-020-0068-4
- 1323 Huang, B., Liu, C., Banzon, V., Freeman, E., Graham, G., Hankins, B., . . . Zhang,
1324 H.-M. (2021, April). Improvements of the Daily Optimum Interpolation
1325 Sea Surface Temperature (DOISST) Version 2.1. *Journal of Climate*, *34*(8),
1326 2923–2939. doi: 10.1175/JCLI-D-20-0166.1
- 1327
- 1328 Hunke, E., & Lipscomb, W. (2008). *CICE: The Los Alamos sea ice model documen-*
1329 *tation and software user’s manual version 4.0* (Tech. Rep.). Los Alamos NM
1330 87545: T-3 Fluid Dynamics Group, Los Alamos National Laboratory.
- 1331 Jacox, M. G. (2019). Marine heatwaves in a changing climate. *Nature*, *571*(7766),
1332 485–487. doi: 10.1038/d41586-019-02196-1
- 1333 Johnson, K., & Claustre, H. (2016). The scientific rationale, design, and implemen-
1334 tation plan for a Biogeochemical-Argo float array. *Biogeochemical-Argo Plan-*
1335 *ning Group*. doi: 10.13155/46601
- 1336 Jorda, G., Marbà, N., Bennett, S., Santana-Garcon, J., Agustí, S., & Duarte,
1337 C. M. (2020). Ocean warming compresses the three-dimensional habi-
1338 tat of marine life. *Nature Ecology and Evolution*, *4*(1), 109–114. doi:
1339 10.1038/s41559-019-1058-0
- 1340 Kroeker, K. J., Kordas, R. L., Crim, R., Hendriks, I. E., Ramajo, L., Singh, G. S.,
1341 . . . Gattuso, J. P. (2013). Impacts of ocean acidification on marine organisms:
1342 Quantifying sensitivities and interaction with warming. *Global Change Biology*,
1343 *19*(6), 1884–1896. doi: 10.1111/gcb.12179
- 1344 Kwiatkowski, L., & Orr, J. C. (2018). Diverging seasonal extremes for ocean acidifi-
1345 cation during the twenty-first century. *Nature Climate Change*, *8*(2), 141–145.
1346 doi: 10.1038/s41558-017-0054-0
- 1347 Kwiatkowski, L., Torres, O., Bopp, L., Aumont, O., Chamberlain, M., Christian,
1348 J. R., . . . Ziehn, T. (2020). Twenty-first century ocean warming, acidifica-
1349 tion, deoxygenation, and upper-ocean nutrient and primary production decline
1350 from CMIP6 model projections. *Biogeosciences*, *17*(13), 3439–3470. doi:
1351 10.5194/bg-17-3439-2020
- 1352 Köhn, E. E., Münnich, M., Vogt, M., Desmet, F., & Gruber, N. (2022). Strong
1353 Habitat Compression by Extreme Shoaling Events of Hypoxic Waters in the
1354 Eastern Pacific. *Journal of Geophysical Research: Oceans*, *127*(6). doi:
1355 10.1029/2022jc018429
- 1356 Köhn, E. E., Vogt, M., Münnich, M., & Gruber, N. (2024). On the Vertical
1357 Structure and Propagation of Marine Heatwaves in the Eastern Pacific.
1358 *Journal of Geophysical Research: Oceans*, *129*(1), e2023JC020063. doi:
1359 10.1029/2023JC020063
- 1360 Lattuca, M. E., Vanella, F. A., Malanga, G., Rubel, M. D., Manríquez, P. H.,
1361 Torres, R., . . . Fernández, D. A. (2023). Ocean acidification and sea-
1362 sonal temperature extremes combine to impair the thermal physiology
1363 of a sub-Antarctic fish. *Science of the Total Environment*, *856*. doi:
1364 10.1016/j.scitotenv.2022.159284
- 1365 Lauvset, S. K., Key, R. M., Olsen, A., van Heuven, S., Velo, A., Lin, X., . . . Wa-
1366 telet, S. (2016, August). A new global interior ocean mapped climatology: the
1367 1° × 1° GLODAP version 2. *Earth System Science Data*, *8*(2), 325–340. doi:
1368 10.5194/essd-8-325-2016
- 1369 Ledwell, J. R., St. Laurent, L. C., Girton, J. B., & Toole, J. M. (2011). Diapycnal
1370 mixing in the antarctic circumpolar current. *Journal of Physical Oceanography*,
1371 *41*(1), 241–246. doi: 10.1175/2010JPO4557.1
- 1372 Le Grix, N., Cheung, W. L., Reygondeau, G., Zscheischler, J., & Frölicher, T. L.
1373 (2023). Extreme and compound ocean events are key drivers of projected
1374 low pelagic fish biomass. *Global Change Biology*, *29*(23), 6478–6492. doi:
1375 10.1111/gcb.16968
- 1376 Le Grix, N., Zscheischler, J., Laufkötter, C., Rousseaux, C. S., & Frölicher, T. L.
1377 (2021). Compound high-temperature and low-chlorophyll extremes in the

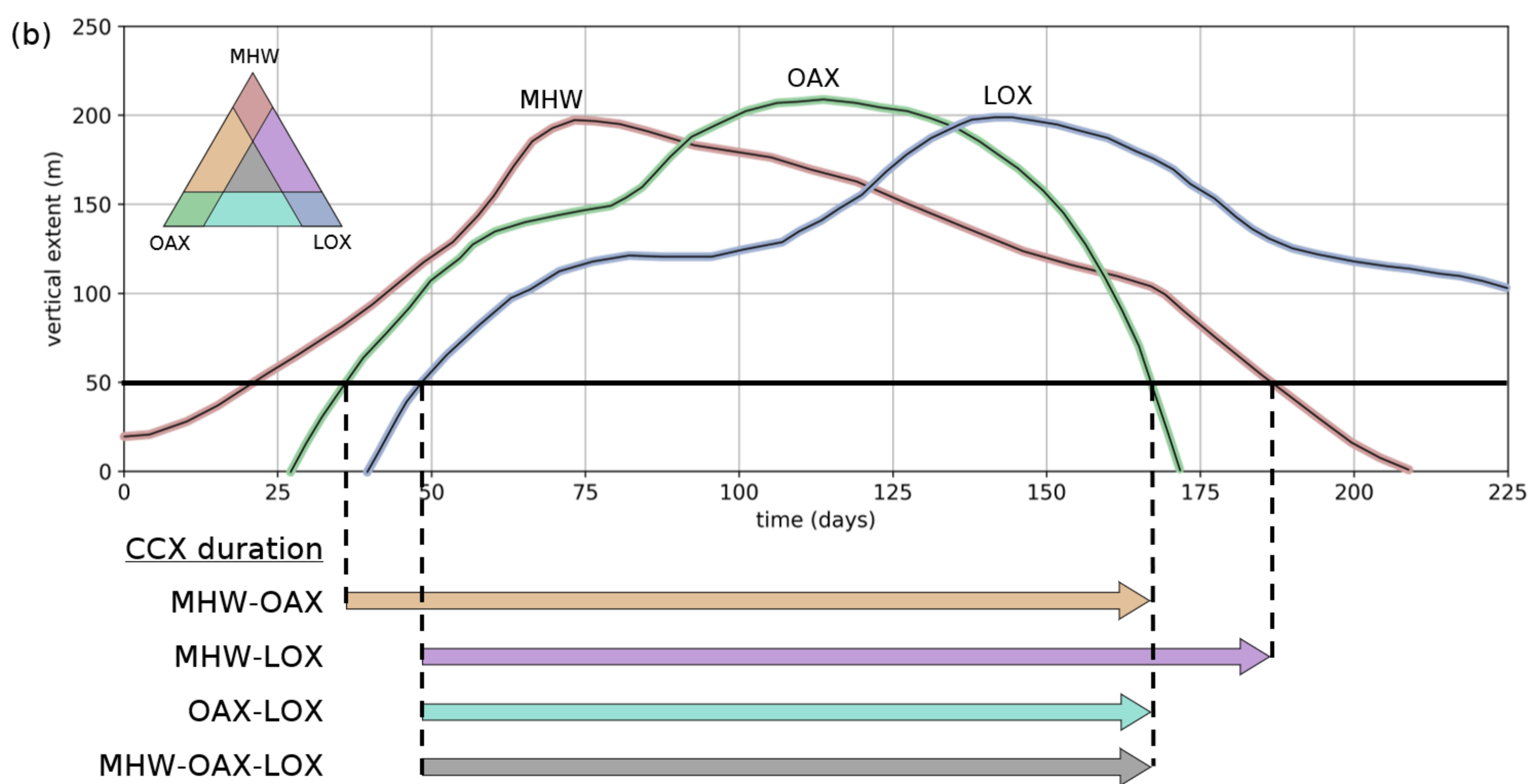
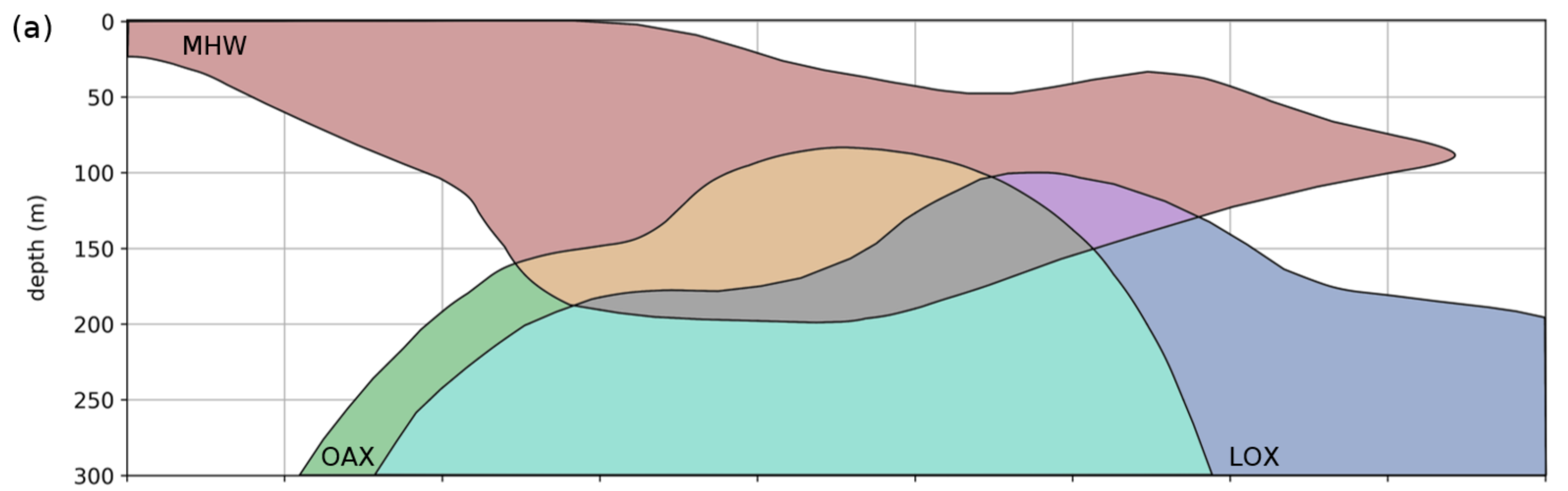
- 1378 ocean over the satellite period. *Biogeosciences*, 18(6), 2119–2137. doi:
 1379 10.5194/bg-18-2119-2021
- 1380 Le Grix, N., Zscheischler, J., Rodgers, K. B., Yamaguchi, R., & Frölicher, T. L.
 1381 (2022). Hotspots and drivers of compound marine heatwaves and low net
 1382 primary production extremes. *Biogeosciences*, 19(24), 5807–5835. doi:
 1383 10.5194/bg-19-5807-2022
- 1384 Leung, S., Mislán, K. A. S., Muhling, B., & Brill, R. (2019). The significance of
 1385 ocean deoxygenation for open ocean tunas and billfishes. In *Laffoley, D.*
 1386 *& Baxter, J.M. (eds.) (2019). Ocean deoxygenation: Everyone’s problem -*
 1387 *Causes, impacts, consequences and solutions.* (pp. 277–308). IUCN, Gland,
 1388 Switzerland. doi: 10.2305/IUCN.CH.2019.13.en
- 1389 Leung, S., Thompson, L. A., McPhaden, M. J., & Mislán, K. A. (2019). ENSO
 1390 drives near-surface oxygen and vertical habitat variability in the tropical Pa-
 1391 cific. *Environmental Research Letters*, 14(6). doi: 10.1088/1748-9326/ab1c13
- 1392 Luo, J. J., Zhang, R., Behera, S. K., Masumoto, Y., Jin, F. F., Lukas, R., & Ya-
 1393 magata, T. (2010). Interaction between El Niño and extreme Indian Ocean
 1394 dipole. *Journal of Climate*, 23(3), 726–742. doi: 10.1175/2009JCLI3104.1
- 1395 Luyten, R., J., Pedlosky, J., & Stommel, J. (1983). The Ventilated Thermocline.
 1396 *Journal of Physical Oceanography*. doi: 10.1175/1520-0485(1983)013(0292:
 1397 TVT)2.0.CO;2
- 1398 Ma, D., Gregor, L., & Gruber, N. (2023). Four Decades of Trends and Drivers
 1399 of Global Surface Ocean Acidification. *Global Biogeochemical Cycles*, 37(7),
 1400 e2023GB007765. doi: 10.1029/2023GB007765
- 1401 MacQueen, J. (1967). Some methods for classification and analysis of multivariate
 1402 observations. In *Proceedings of the fifth Berkeley symposium on mathematical*
 1403 *statistics and probability* (Vol. 1, pp. 281–297). Oakland, CA, USA.
- 1404 Mahlstein, I., Martius, O., Chevalier, C., & Ginsbourger, D. (2012). Changes
 1405 in the odds of extreme events in the Atlantic basin depending on the posi-
 1406 tion of the extratropical jet. *Geophysical Research Letters*, 39(22). doi:
 1407 10.1029/2012GL053993
- 1408 Marin, M., Feng, M., Bindoff, N. L., & Phillips, H. E. (2022). Local Drivers of
 1409 Extreme Upper Ocean Marine Heatwaves Assessed Using a Global Ocean
 1410 Circulation Model. *Frontiers in Climate*, 4. doi: 10.3389/fclim.2022.788390
- 1411 Masson-Delmotte, V., P. Z., A. Pirani, S. L. Connors, C. Péan, S. Berger, . . . B.
 1412 Zhou (eds.) (2021). *IPCC, 2021: Summary for Policymakers. In: Climate*
 1413 *Change 2021: The Physical Science Basis. Contribution of Working Group*
 1414 *I to the Sixth Assessment Report of the Intergovernmental Panel on Climate*
 1415 *Change* (Tech. Rep.).
- 1416 Maulida, T., Wirasatriya, A., Ismunarti, D. H., & Puryajati, A. D. (2022). Physi-
 1417 cal drivers of the 2013 marine heatwave in the seas of the southern Java-Nusa
 1418 Tenggara. *Geographia Technica*, 17, 129–139. doi: 10.21163/GT_2022.171.10
- 1419 McAdam, R., Masina, S., & Gualdi, S. (2022). Seasonal forecasting of subsurface
 1420 marine heat waves. *Submitted to Nature Communications*(2023), 1–11. doi: 10
 1421 .1038/s43247-023-00892-5
- 1422 Moore, J. K., Doney, S. C., & Lindsay, K. (2004). Upper ocean ecosystem dynam-
 1423 ics and iron cycling in a global three-dimensional model. *Global Biogeochemical*
 1424 *Cycles*, 18(4), 1–21. doi: 10.1029/2004GB002220
- 1425 Moore, J. K., Lindsay, K., Doney, S. C., Long, M. C., & Misumi, K. (2013). Marine
 1426 ecosystem dynamics and biogeochemical cycling in the community earth sys-
 1427 tem model [CESM1(BGC)]: Comparison of the 1990s with the 2090s under the
 1428 RCP4.5 and RCP8.5 scenarios. *Journal of Climate*, 26(23), 9291–9312. doi:
 1429 10.1175/JCLI-D-12-00566.1
- 1430 Morrison, A. K., Frölicher, T. L., & Sarmiento, J. L. (2015). Upwelling in the South-
 1431 ern Ocean. *Physics Today*, 68(1), 27–32. doi: 10.1063/PT.3.2654
- 1432 Müller, J. D. (2023). *RECCAP2-ocean data collection*. Zenodo. doi: 10.5281/zenodo

- 1433 .7990823
- 1434 Nam, S., Kim, H. J., & Send, U. (2011). Amplification of hypoxic and acidic events
1435 by la Niña conditions on the continental shelf off California. *Geophysical Re-*
1436 *search Letters*, *38*(22), 1–5. doi: 10.1029/2011GL049549
- 1437 Negrete-García, G., Lovenduski, N. S., Hauri, C., Krumhardt, K. M., & Lauvset,
1438 S. K. (2019). Sudden emergence of a shallow aragonite saturation hori-
1439 zon in the Southern Ocean. *Nature Climate Change*, *9*(4), 313–317. doi:
1440 10.1038/s41558-019-0418-8
- 1441 Oliver, E. C., Benthuisen, J. A., Darmaraki, S., Donat, M. G., Hobday, A. J., Hol-
1442 brook, N. J., . . . Gupta, A. S. (2021). Marine Heatwaves. *Annual Review of*
1443 *Marine Science*, *13*(1), 1–30. doi: 10.1146/annurev-marine-032720-095144
- 1444 Oliver, E. C., Donat, M. G., Burrows, M. T., Moore, P. J., Smale, D. A., Alexan-
1445 der, L. V., . . . Wernberg, T. (2018). Longer and more frequent marine
1446 heatwaves over the past century. *Nature Communications*, *9*(1), 1–12. doi:
1447 10.1038/s41467-018-03732-9
- 1448 Orr, J. C., & Epitalon, J. M. (2015). Improved routines to model the ocean carbon-
1449 ate system: Mocsy 2.0. *Geoscientific Model Development*, *8*(3), 485–499. doi:
1450 10.5194/gmd-8-485-2015
- 1451 Orr, J. C., Fabry, V. J., Aumont, O., Bopp, L., Doney, S. C., Feely, R. A., . . . Yool,
1452 A. (2005). Anthropogenic ocean acidification over the twenty-first centu-
1453 ry and its impact on calcifying organisms. *Nature*, *437*, 681–686. doi:
1454 10.1038/nature04095
- 1455 Pan, T. C., Applebaum, S. L., & Manahan, D. T. (2015). Experimental ocean acid-
1456 ification alters the allocation of metabolic energy. *Proceedings of the National*
1457 *Academy of Sciences of the United States of America*, *112*(15), 4696–4701. doi:
1458 10.1073/pnas.1416967112
- 1459 Paulmier, A., & Ruiz-Pino, D. (2009). Oxygen minimum zones (OMZs) in
1460 the modern ocean. *Progress in Oceanography*, *80*(3-4), 113–128. Re-
1461 trieved from <http://dx.doi.org/10.1016/j.pocean.2008.08.001> doi:
1462 10.1016/j.pocean.2008.08.001
- 1463 Paulmier, A., Ruiz-Pino, D., & Garçon, V. (2011). CO₂ maximum in the oxygen
1464 minimum zone (OMZ). *Biogeosciences*, *8*(2), 239–252. doi: 10.5194/bg-8-239
1465 -2011
- 1466 Pellichero, V., Sallée, J.-B., Schmidtko, S., Roquet, F., & Charrassin, J.-B. (2017).
1467 The ocean mixed layer under Southern Ocean sea-ice: Seasonal cycle and
1468 forcing. *Journal of Geophysical Research: Oceans*, *122*(2), 1608–1633. doi:
1469 10.1002/2016JC011970
- 1470 Pirota, E., Thomas, L., Costa, D. P., Hall, A. J., Harris, C. M., Harwood, J., . . .
1471 Tyack, P. L. (2022). Understanding the combined effects of multiple stres-
1472 sors: A new perspective on a longstanding challenge. *Science of the Total*
1473 *Environment*, *821*, 153322. doi: 10.1016/j.scitotenv.2022.153322
- 1474 Pörtner, H. O. (2002). Climate variations and the physiological basis of temperature
1475 dependent biogeography: Systemic to molecular hierarchy of thermal toler-
1476 ance in animals. *Comparative Biochemistry and Physiology - A Molecular and*
1477 *Integrative Physiology*, *132*(4), 739–761. doi: 10.1016/S1095-6433(02)00045-4
- 1478 Pörtner, H. O., & Knust, R. (2007). Climate Change Affects Marine Fishes Through
1479 the Oxygen Limitation of Thermal Tolerance. *Science*, *315*, 95–97. doi: 10
1480 .1259/0007-1285-53-633-920-b
- 1481 Qi, R., Zhang, Y., Du, Y., & Feng, M. (2022). Characteristics and Drivers of Ma-
1482 rine Heatwaves in the Western Equatorial Indian Ocean. *Journal of Geophysi-*
1483 *cal Research: Oceans*, *127*(10), e2022JC018732. doi: 10.1029/2022JC018732
- 1484 Ramadhan, A., Marshall, J., Meneghello, G., Illari, L., & Speer, K. (2022). Obser-
1485 vations of Upwelling and Downwelling Around Antarctica Mediated by Sea Ice.
1486 *Frontiers in Marine Science*, *9*. doi: 10.3389/fmars.2022.864808
- 1487 Righetti, D., Vogt, M., Gruber, N., Psomas, A., & Zimmermann, N. E. (2019).

- 1488 Global pattern of phytoplankton diversity driven by temperature and environ-
 1489 mental variability. *Science Advances*, 5(5). doi: 10.1126/sciadv.aau6253
- 1490 Riquelme-Bugueño, R., Pérez-Santos, I., Alegria, N., Vargas, C. A., Urbina, M. A.,
 1491 & Escribano, R. (2020). Diel vertical migration into anoxic and high-pCO₂
 1492 waters: acoustic and net-based krill observations in the Humboldt Current.
 1493 *Scientific Reports*, 10(1), 1–11. doi: 10.1038/s41598-020-73702-z
- 1494 Ritz, D. A., Hobday, A. J., Montgomery, J. C., & Ward, A. J. W. (2011). Chapter
 1495 Four - Social Aggregation in the Pelagic Zone with Special Reference to Fish
 1496 and Invertebrates. In M. Lesser (Ed.), *Advances in Marine Biology* (Vol. 60,
 1497 pp. 161–227). Academic Press. doi: 10.1016/B978-0-12-385529-9.00004-4
- 1498 Rose, K., Gutiérrez, D., Breitburg, D., Conley, D., Craig, K., Froehlich, H., ...
 1499 Prema, D. (2019). Impacts of ocean deoxygenation on fisheries. In *Laffoley,*
 1500 *D. & Baxter, J.M. (eds.) (2019). Ocean deoxygenation: Everyone's problem*
 1501 *- Causes, impacts, consequences and solutions.* (pp. 519–544). IUCN, Gland,
 1502 Switzerland. doi: 10.2305/IUCN.CH.2019.13.en
- 1503 Rosselló, P., Pascual, A., & Combes, V. (2023). Assessing marine heat waves in the
 1504 Mediterranean Sea: a comparison of fixed and moving baseline methods. *Fron-*
 1505 *tiers in Marine Science*, 10, 1168368. doi: 10.3389/fmars.2023.1168368
- 1506 Roy, C., & Reason, C. (2001). ENSO related modulation of coastal upwelling in the
 1507 eastern Atlantic. *Progress in Oceanography*, 49(1-4), 245–255. doi: 10.1016/
 1508 S0079-6611(01)00025-8
- 1509 Samuels, T., Rynearson, T. A., & Collins, S. (2021). Surviving Heatwaves: Thermal
 1510 Experience Predicts Life and Death in a Southern Ocean Diatom. *Frontiers in*
 1511 *Marine Science*, 8. doi: 10.3389/fmars.2021.600343
- 1512 Santoso, A., Mcphaden, M. J., & Cai, W. (2017). The Defining Characteristics
 1513 of ENSO Extremes and the Strong 2015/2016 El Niño. *Reviews of Geophysics*,
 1514 55(4), 1079–1129. doi: 10.1002/2017RG000560
- 1515 Sarmiento, J. L., & Gruber, N. (2006). *Ocean Biogeochemical Dynamics*. Princeton
 1516 University Press. doi: 10.2307/j.ctt3fgxqx
- 1517 Scannell, H. A., Johnson, G. C., Thompson, L., Lyman, J. M., & Riser, S. C.
 1518 (2020). Subsurface Evolution and Persistence of Marine Heatwaves in
 1519 the Northeast Pacific. *Geophysical Research Letters*, 47(23), 1–10. doi:
 1520 10.1029/2020GL090548
- 1521 Schaeffer, A., & Roughan, M. (2017). Subsurface intensification of marine heatwaves
 1522 off southeastern Australia: The role of stratification and local winds. *Geophysi-*
 1523 *cal Research Letters*, 44(10), 5025–5033. doi: 10.1002/2017GL073714
- 1524 Seibel, B. A. (2011). Critical oxygen levels and metabolic suppression in oceanic
 1525 oxygen minimum zones. *Journal of Experimental Biology*, 214(2), 326–336.
 1526 doi: 10.1242/jeb.049171
- 1527 Seibel, B. A., Schneider, J. L., Kaartvedt, S., Wishner, K. F., & Daly, K. L.
 1528 (2016). Hypoxia Tolerance and Metabolic Suppression in Oxygen Mini-
 1529 mum Zone Euphausiids: Implications for Ocean Deoxygenation and Biogeo-
 1530 chemical Cycles. *Integrative and Comparative Biology*, 56(4), 510–523. doi:
 1531 10.1093/icb/icw091
- 1532 Sen Gupta, A. (2023). *Marine heatwaves: definition duel heats up.*
- 1533 Sen Gupta, A., Thomsen, M., Benthuisen, J. A., Hobday, A. J., Oliver, E., Alexan-
 1534 der, L. V., ... Smale, D. A. (2020). Drivers and impacts of the most
 1535 extreme marine heatwaves events. *Scientific Reports*, 10(1), 1–15. doi:
 1536 10.1038/s41598-020-75445-3
- 1537 Sharp, J. D., Fassbender, A. J., Carter, B. R., Johnson, G. C., Schultz, C., &
 1538 Dunne, J. P. (2022). GOBAI-O₂ : temporally and spatially resolved fields
 1539 of ocean interior dissolved oxygen over nearly two decades.
 1540 doi: 10.5194/essd-2022-308
- 1541 Smale, D. A., Wernberg, T., Oliver, E. C. J., Thomsen, M., Harvey, B. P., Straub,
 1542 S. C., ... Moore, P. J. (2019). Marine heatwaves threaten global biodiver-

- 1543 sity and the provision of ecosystem services. *Nature Climate Change*, *9*(4),
 1544 306–312. doi: 10.1038/s41558-019-0412-1
- 1545 Smith, K. E., Burrows, M. T., Hobday, A. J., King, N. G., Moore, P. J., Sen Gupta,
 1546 A., . . . Smale, D. A. (2023). Biological Impacts of Marine Heatwaves. *Annual*
 1547 *review of marine science*, *15*, 119–145. doi: 10.1146/annurev-marine-032122
 1548 -121437
- 1549 Smith, R., & Gent, P. (2010). *The Parallel Ocean Program (POP) reference manual*
 1550 (Tech. Rep.). National Center for Atmospheric Research Boulder, Colorado:
 1551 National Center for Atmospheric Research Boulder, Colorado.
- 1552 Stabeno, P. J., & Bell, S. W. (2019). Extreme Conditions in the Bering Sea
 1553 (2017–2018): Record-Breaking Low Sea-Ice Extent. *Geophysical Research*
 1554 *Letters*, *46*(15), 8952–8959. doi: 10.1029/2019GL083816
- 1555 Stuart-Smith, R. D., Bates, A. E., Lefcheck, J. S., Duffy, J. E., Baker, S. C., Thom-
 1556 son, R. J., . . . Edgar, G. J. (2013). Integrating abundance and functional
 1557 traits reveals new global hotspots of fish diversity. *Nature*, *501*(7468), 539–542.
 1558 doi: 10.1038/nature12529
- 1559 Susanto, R. D., Gordon, A. L., & Zheng, Q. (2001). Upwelling along the coasts
 1560 of Java and Sumatra and its relation to ENSO. *Geophysical Research Letters*,
 1561 *28*(8), 1599–1602. doi: 10.1029/2000GL011844
- 1562 Tai, T. C., Sumaila, U. R., & Cheung, W. W. (2021). Ocean Acidification Ampli-
 1563 fies Multi-Stressor Impacts on Global Marine Invertebrate Fisheries. *Frontiers*
 1564 *in Marine Science*, *8*, 1–12. doi: 10.3389/fmars.2021.596644
- 1565 Tamsitt, V., Drake, H. F., Morrison, A. K., Talley, L. D., Dufour, C. O., Gray,
 1566 A. R., . . . Weijer, W. (2017). Spiraling pathways of global deep waters to
 1567 the surface of the Southern Ocean. *Nature Communications*, *8*(1), 1–10. doi:
 1568 10.1038/s41467-017-00197-0
- 1569 Tittensor, D. P., Mora, C., Jetz, W., Lotze, H. K., Ricard, D., Berghe, E. V., &
 1570 Worm, B. (2010). Global patterns and predictors of marine biodiversity across
 1571 taxa. *Nature*, *466*(7310). doi: 10.1038/nature09329
- 1572 Turi, G., Alexander, M., Lovenduski, N. S., Capotondi, A., Scott, J., Stock, C., . . .
 1573 Jacox, M. (2018). Response of O₂ and pH to ENSO in the California Current
 1574 System in a high-resolution global climate model. *Ocean Science*, *14*(1), 69–86.
 1575 doi: 10.5194/os-14-69-2018
- 1576 Vogt, L., Burger, F. A., Griffies, S. M., & Frölicher, T. L. (2022). Local Drivers of
 1577 Marine Heatwaves: A Global Analysis With an Earth System Model. *Frontiers*
 1578 *in Climate*, *4*. doi: 10.3389/fclim.2022.847995
- 1579 Wang, Y., Zhou, M., Zhang, Z., & Dinniman, M. S. (2023). Seasonal variations in
 1580 Circumpolar Deep Water intrusions into the Ross Sea continental shelf. *Frontiers*
 1581 *in Marine Science*, *10*.
- 1582 Watson, R. A. (2017). A database of global marine commercial, small-scale, illegal
 1583 and unreported fisheries catch 1950–2014. *Scientific Data*, *4*(1), 170039. doi:
 1584 10.1038/sdata.2017.39
- 1585 Wilson, E. A., Riser, S. C., Campbell, E. C., & Wong, A. P. (2019). Winter
 1586 upper-ocean stability and ice-ocean feedbacks in the sea ice-covered South-
 1587 ern Ocean. *Journal of Physical Oceanography*, *49*(4), 1099–1117. doi:
 1588 10.1175/JPO-D-18-0184.1
- 1589 Worm, B., & Tittensor, D. P. (2018). *A theory of global biodiversity* (No. 60).
 1590 Princeton, New Jersey: Princeton University Press.
- 1591 Xu, K., Huang, R. X., Wang, W., Zhu, C., & Lu, R. (2017). Thermocline fluctua-
 1592 tions in the equatorial Pacific related to the two types of El Niño events. *Jour-
 1593 nal of Climate*, *30*(17), 6611–6627. doi: 10.1175/JCLI-D-16-0291.1
- 1594 Yang, S., & Gruber, N. (2016). The anthropogenic perturbation of the marine ni-
 1595 trogen cycle by atmospheric deposition: Nitrogen cycle feedbacks and the 15N
 1596 Haber-Bosch effect. *Global Biogeochemical Cycles*, *30*(10), 1418–1440. doi:
 1597 10.1002/2016GB005421

- 1598 Zeebe, R. E., & Wolf-Gladrow, D. (2001). *CO₂ in seawater : equilibrium, kinetics,*
 1599 *isotopes*. Burlington: Elsevier Burlington.
- 1600 Zhang, Y., Du, Y., Feng, M., & Hu, S. (2021). Long-Lasting Marine Heat-
 1601 waves Instigated by Ocean Planetary Waves in the Tropical Indian Ocean
 1602 During 2015–2016 and 2019–2020. *Geophysical Research Letters*, *48*(21),
 1603 e2021GL095350. doi: 10.1029/2021GL095350
- 1604 Zscheischler, J., & Seneviratne, S. I. (2017). Dependence of drivers affects risks as-
 1605 sociated with compound events. *Science Advances*, *3*(6), 1–11. doi: 10.1126/
 1606 sciadv.1700263
- 1607 Zuo, H., Balmaseda, M. A., Tietsche, S., Mogensen, K., & Mayer, M. (2019). The
 1608 ECMWF operational ensemble reanalysis–analysis system for ocean and sea
 1609 ice: a description of the system and assessment. *Ocean Science*, *15*(3), 779–
 1610 808. doi: 10.5194/os-15-779-2019



Column-single extreme (CSX)

Column-compound extreme (CCX) variations

Surface

(a)

(b)

(c)

(d)

(e)

Each grid cell exceeds thresholds

$\geq 50m$

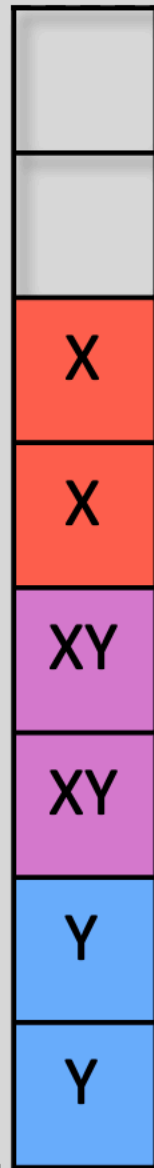
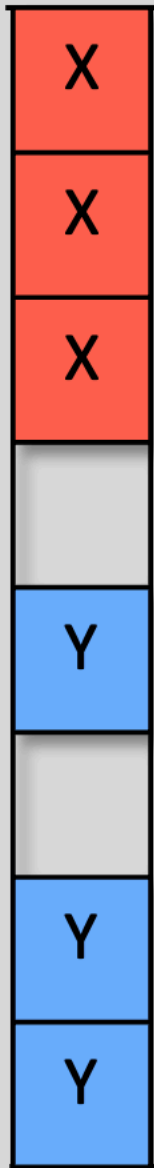
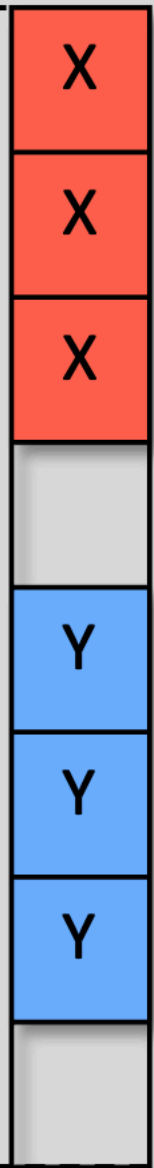
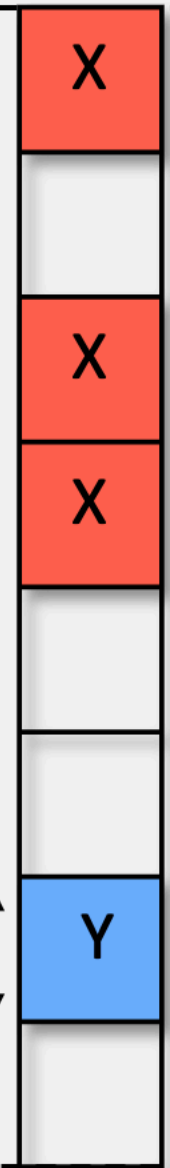
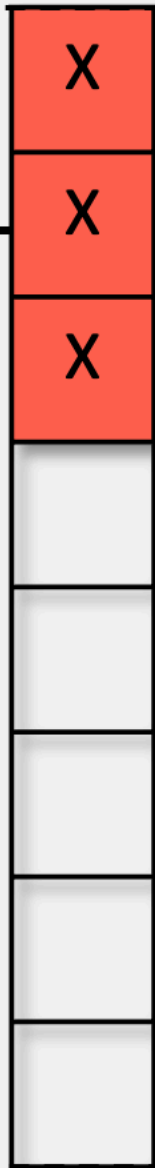
$\geq 50m$

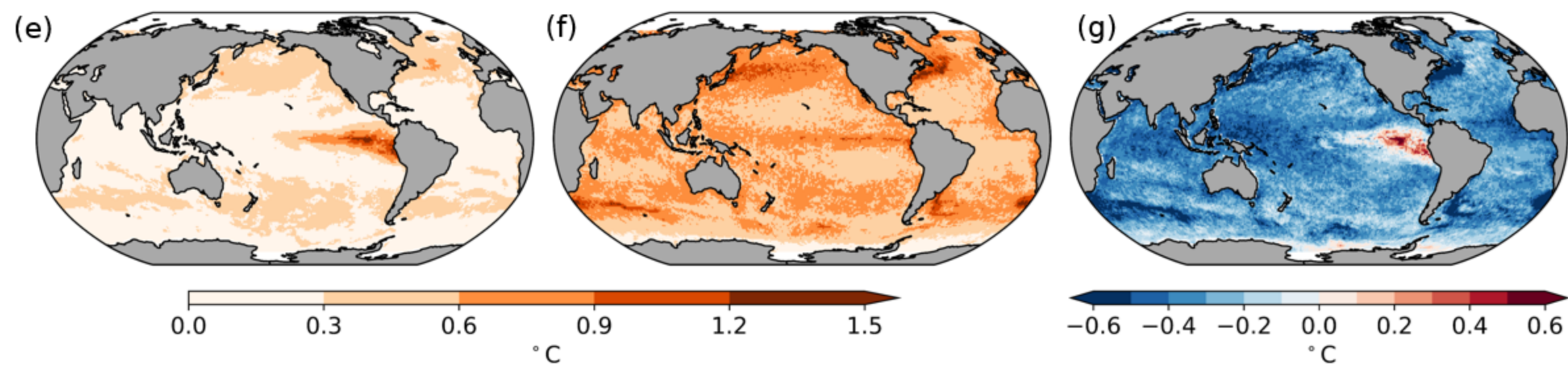
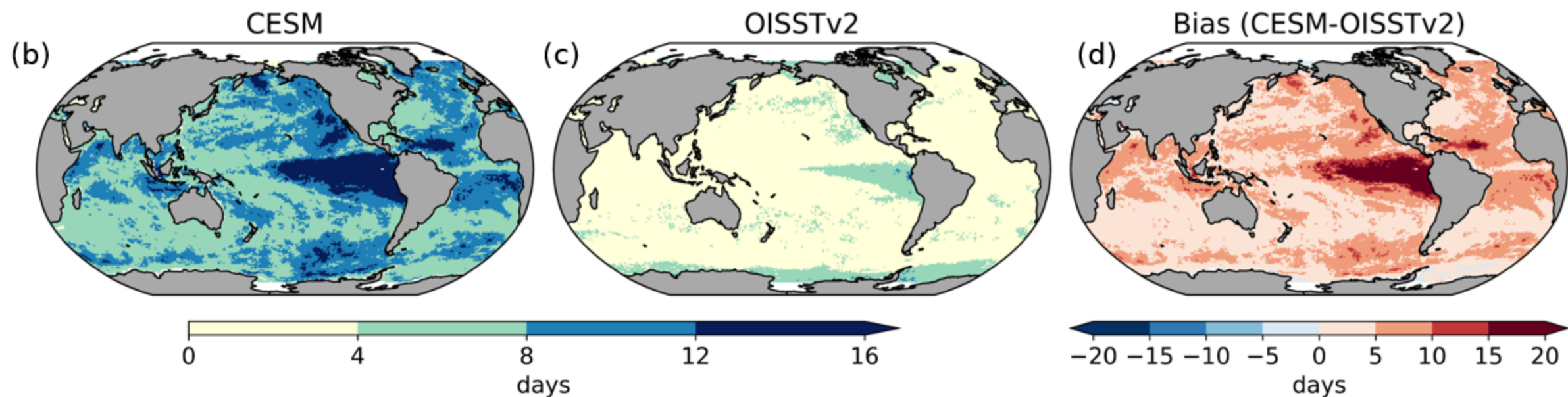
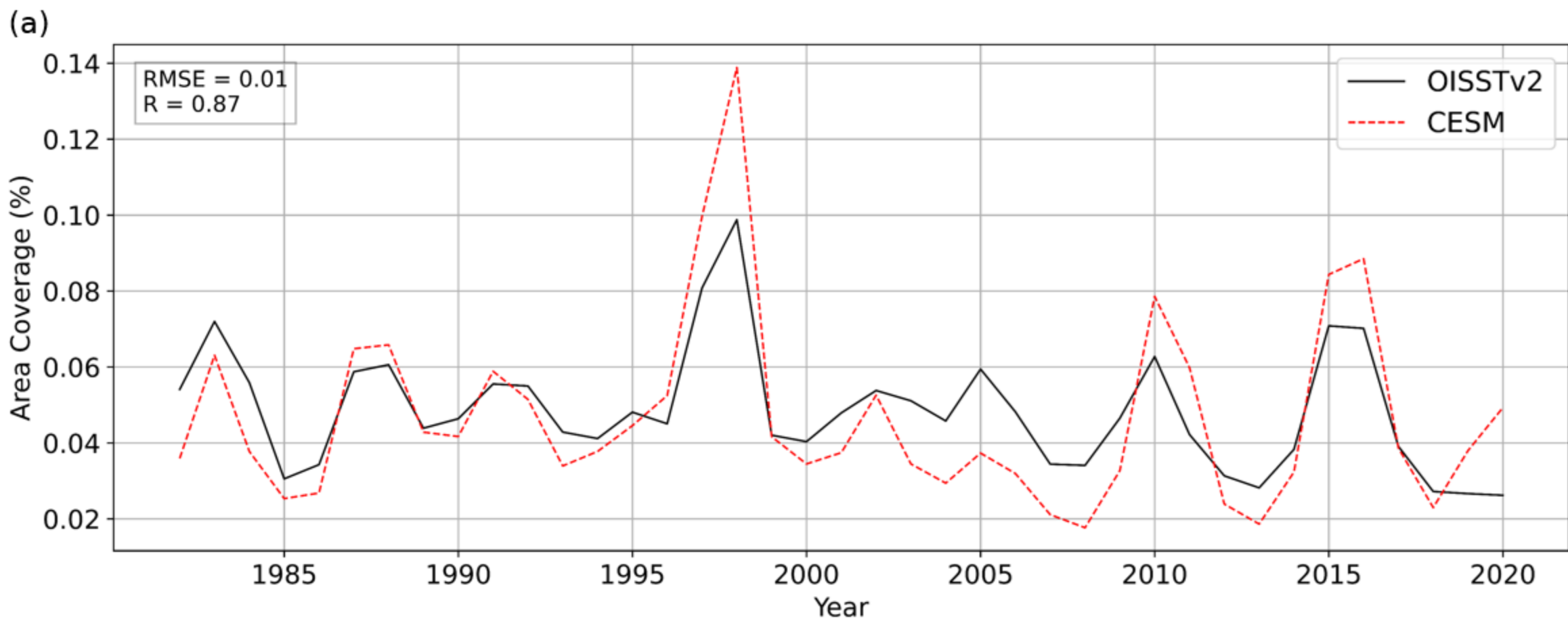
$< 50m$

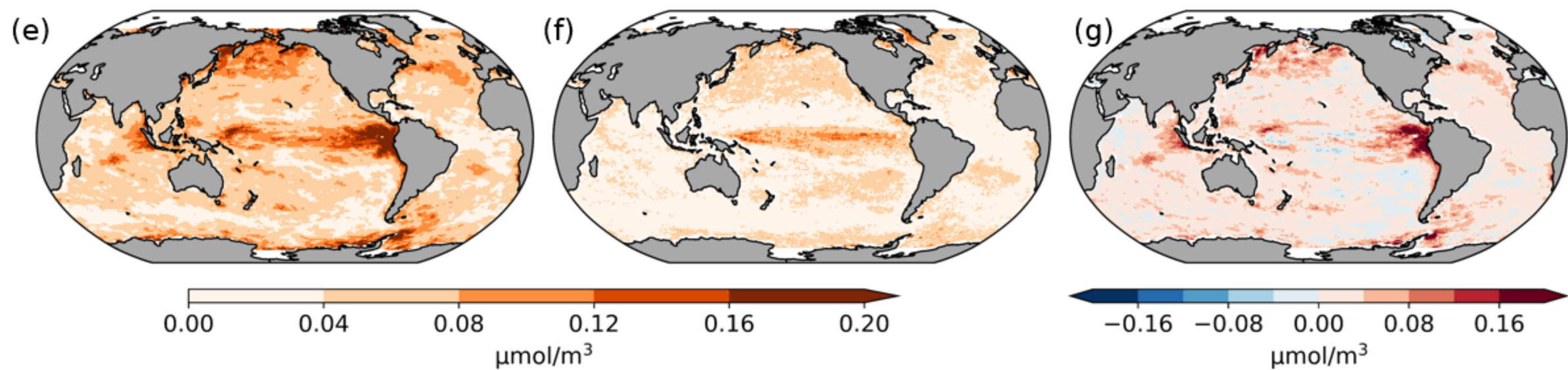
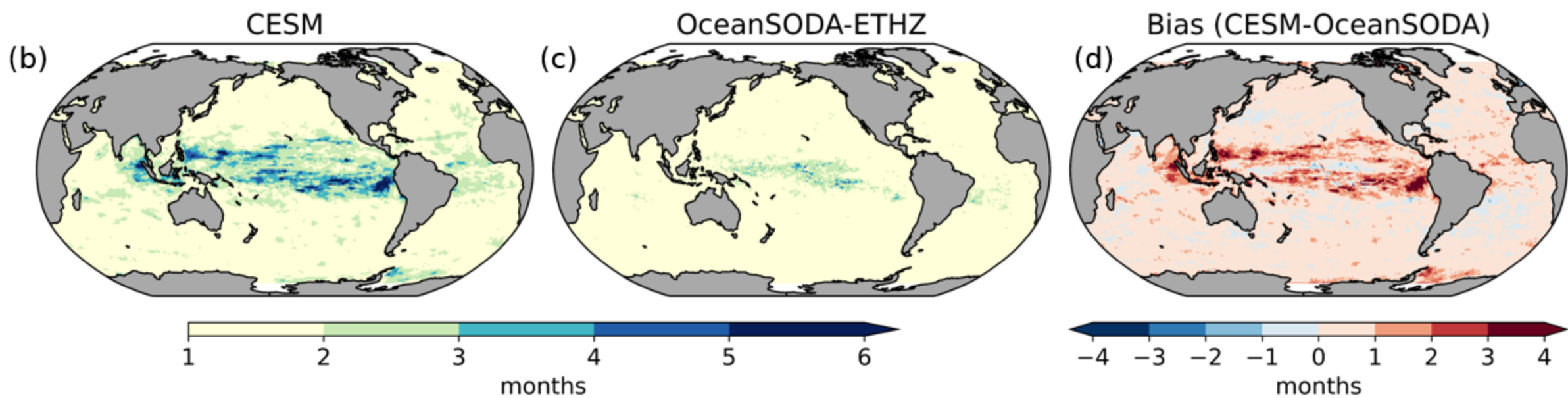
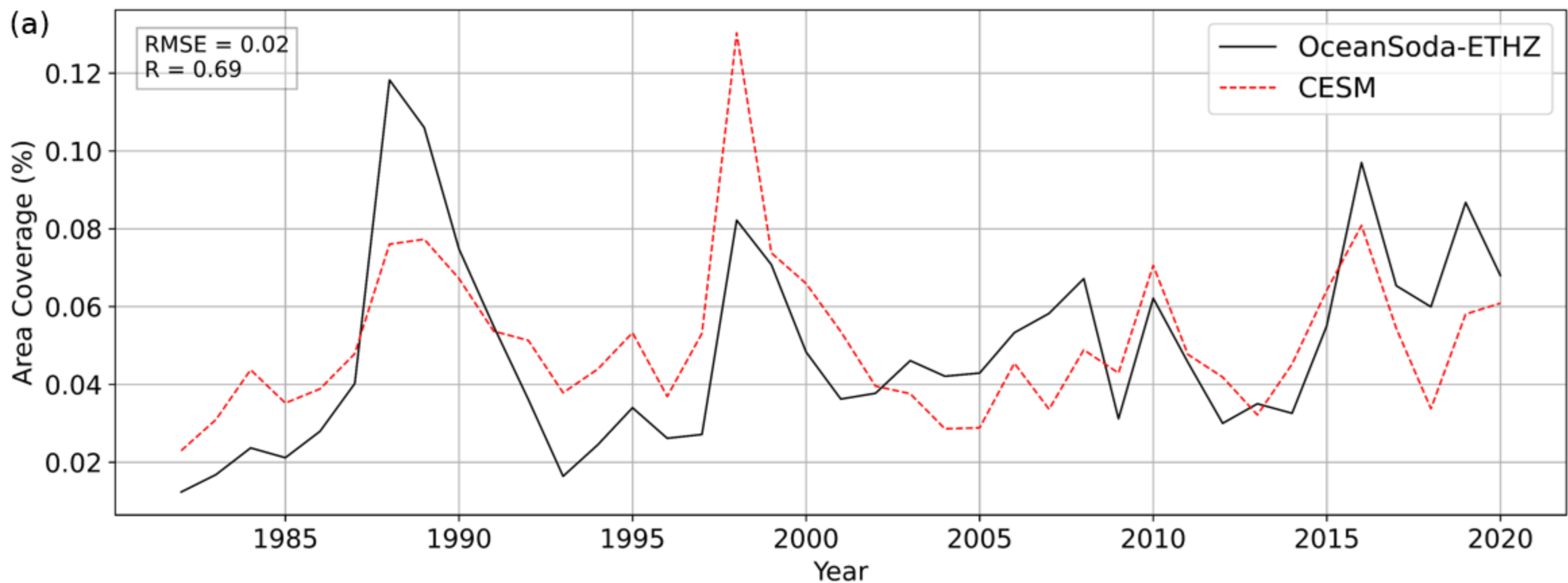
Not column extreme

$\geq 50m$

300m

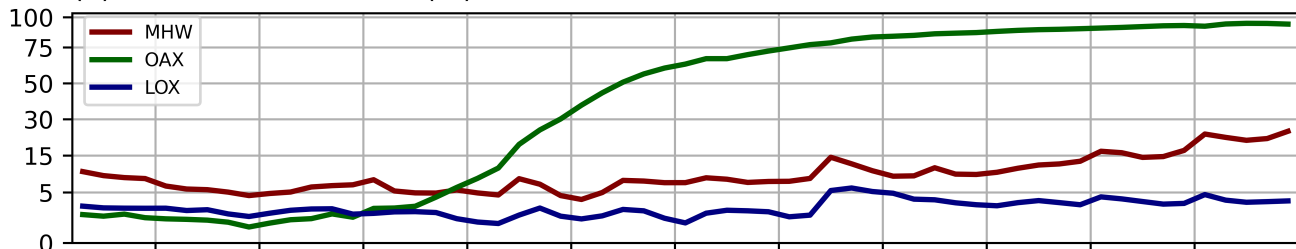




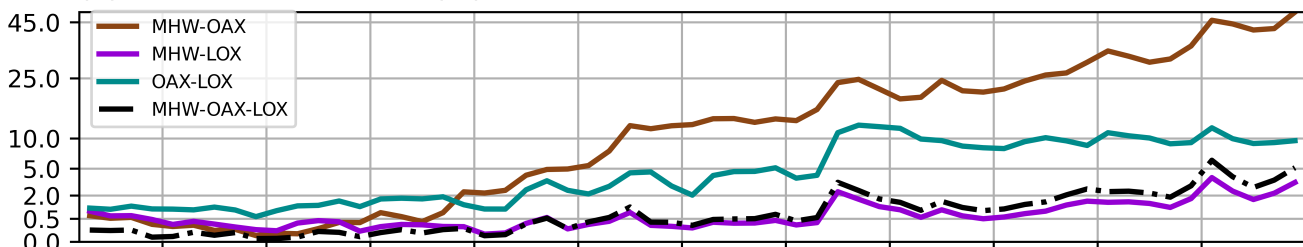


Fixed Baseline

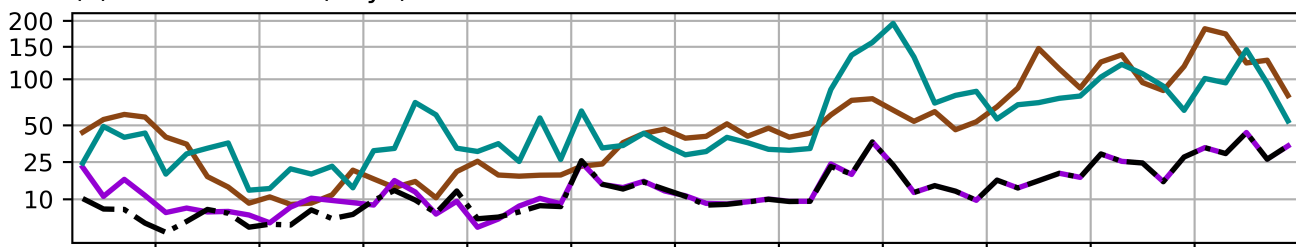
(a) CSX volume fraction (%)



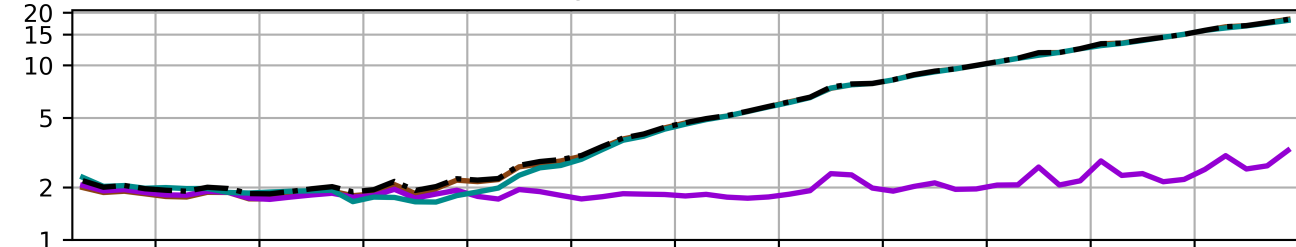
(b) CCX volume fraction (%)



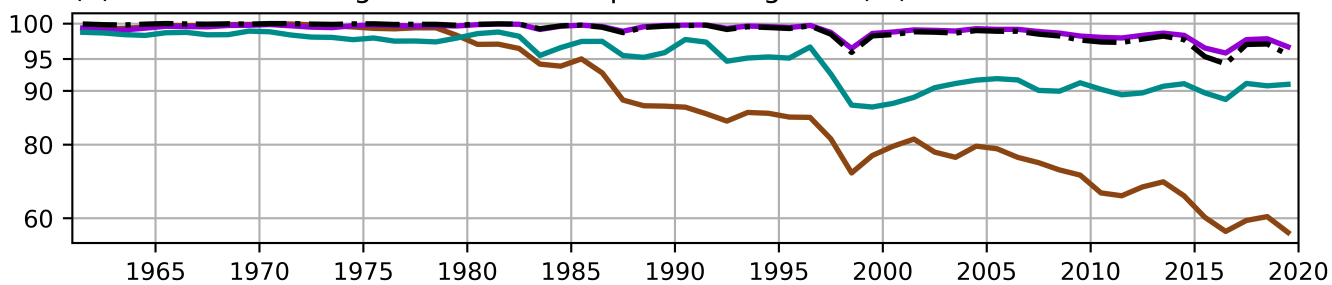
(c) CCX duration (days)



(d) Column-maximum CCX intensity index

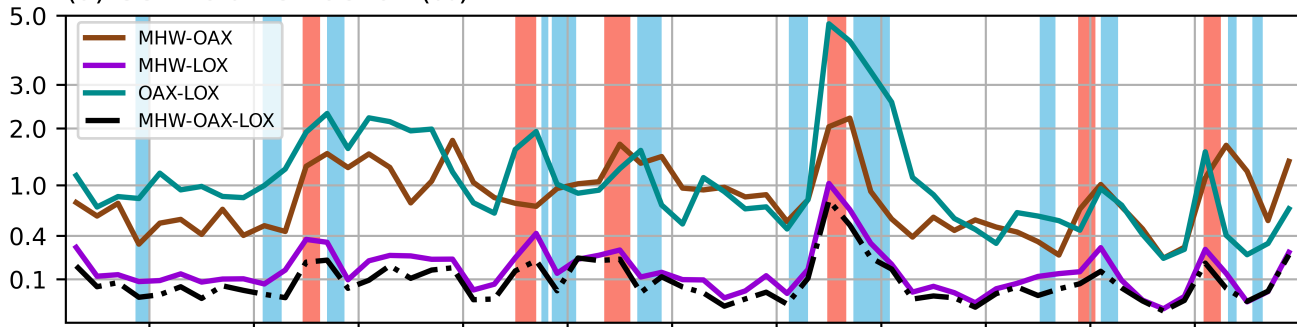


(e) Fraction of contiguous habitable space during CCX (%)

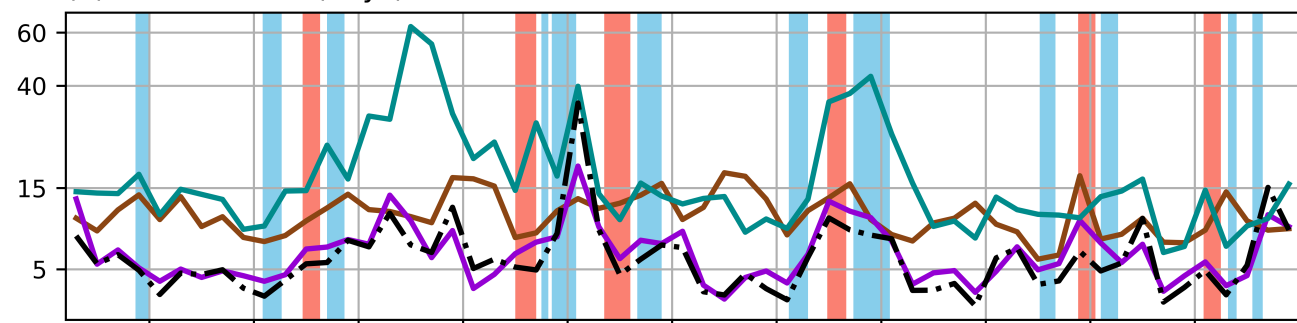


Moving Baseline

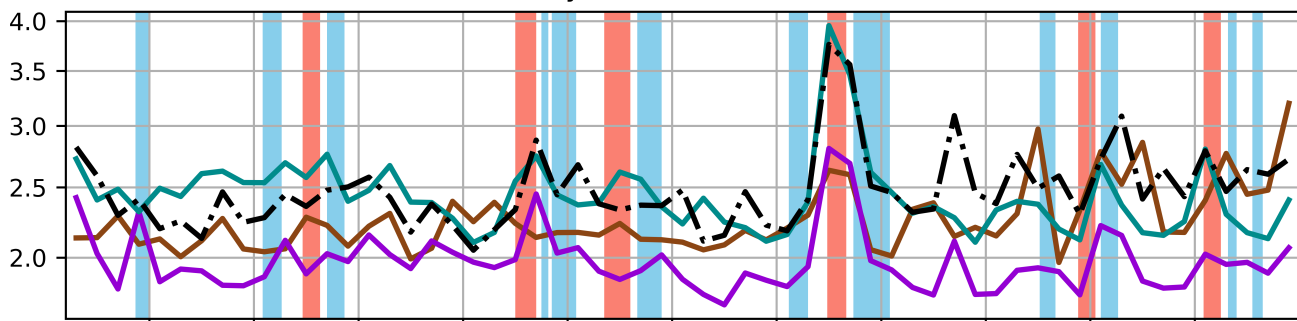
(a) CCX volume fraction (%)



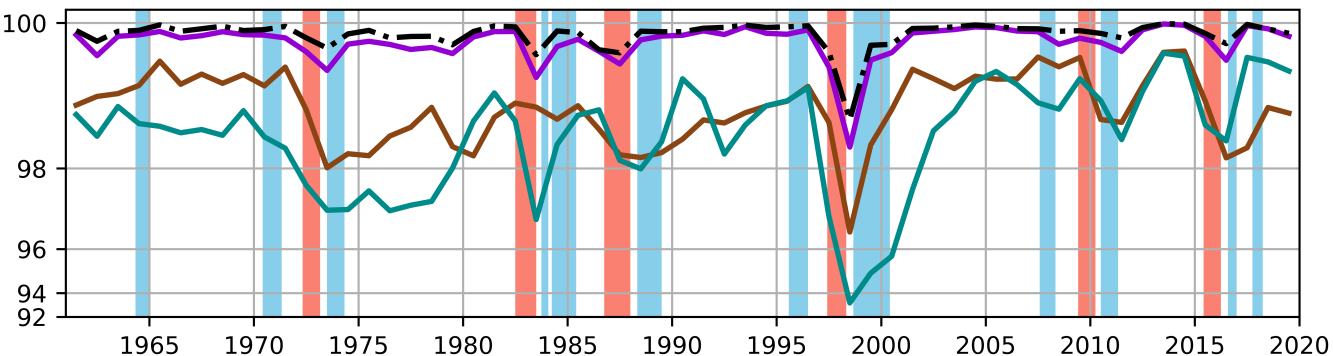
(b) CCX duration (days)



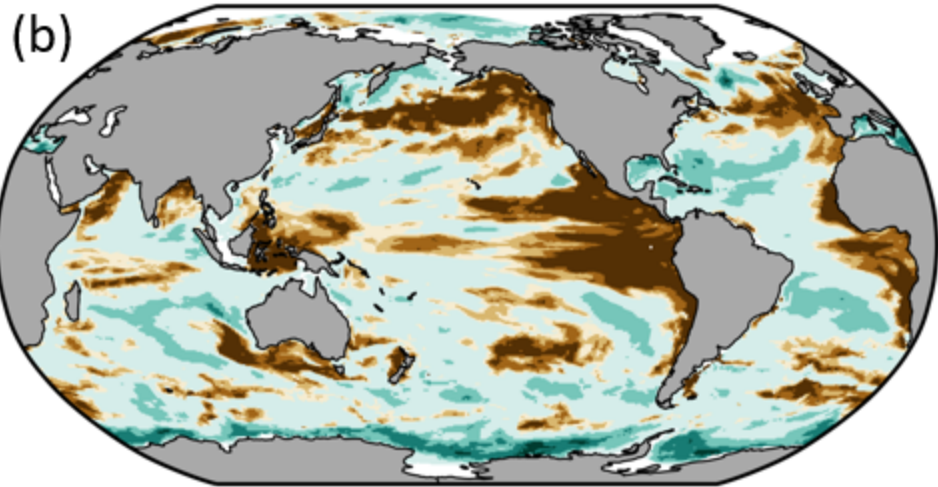
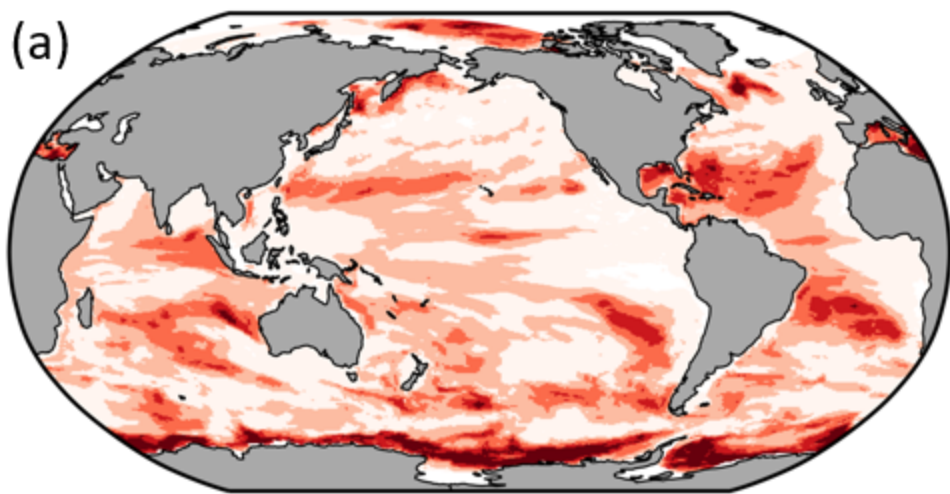
(c) Column-maximum CCX intensity index



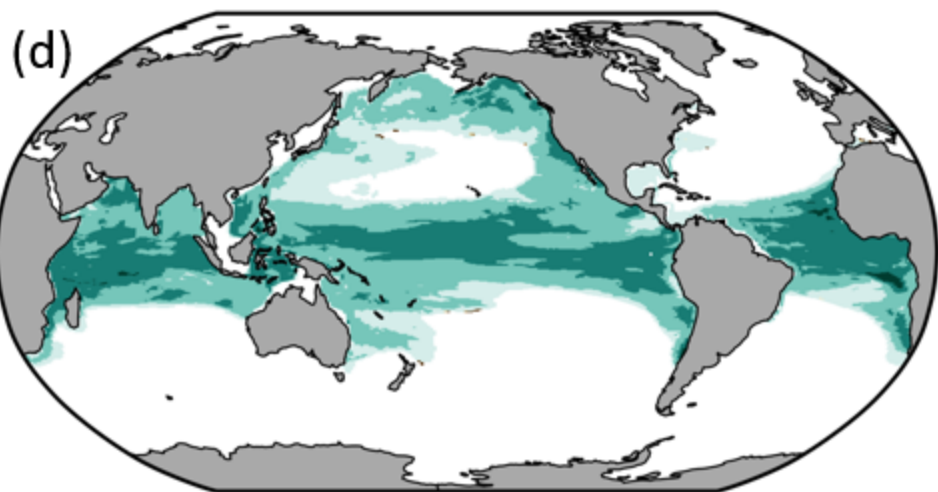
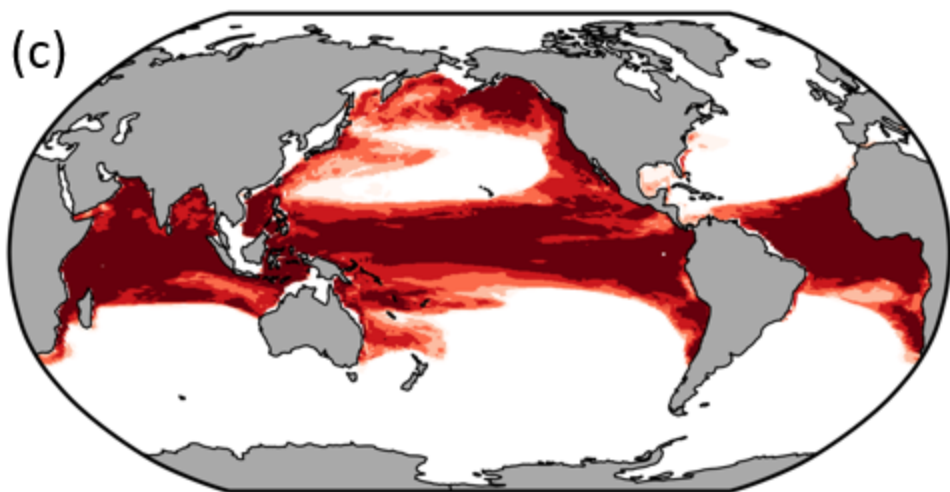
(d) Fraction of contiguous habitable space during CCX (%)



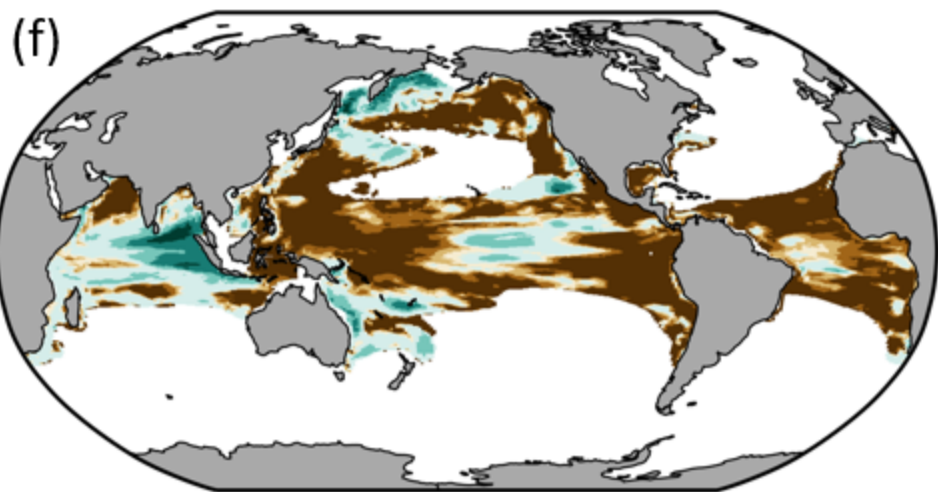
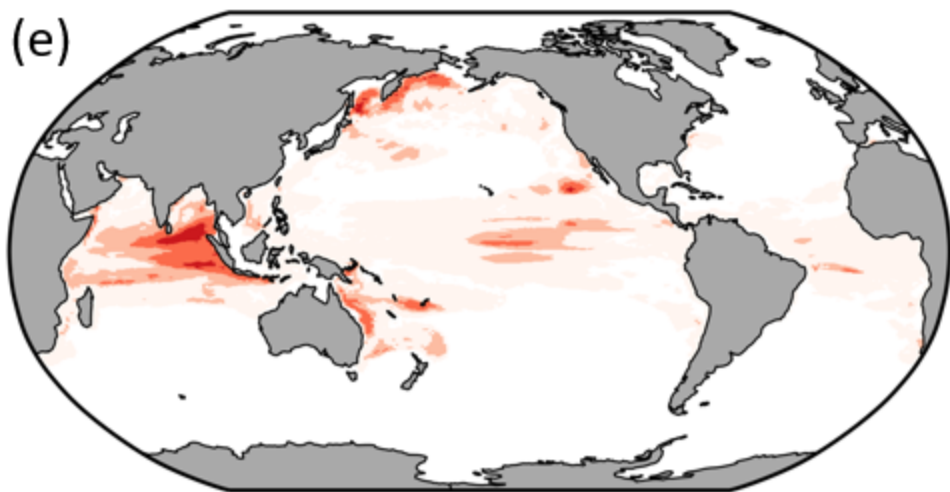
MHW-OAX



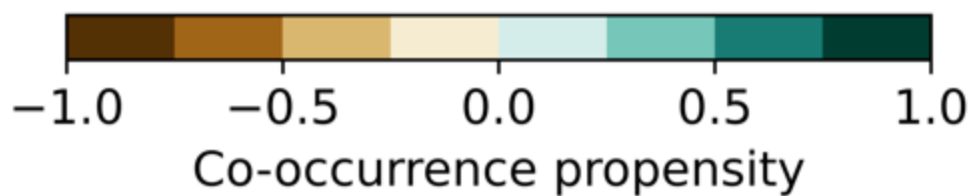
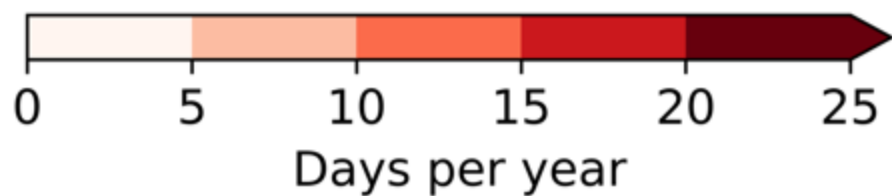
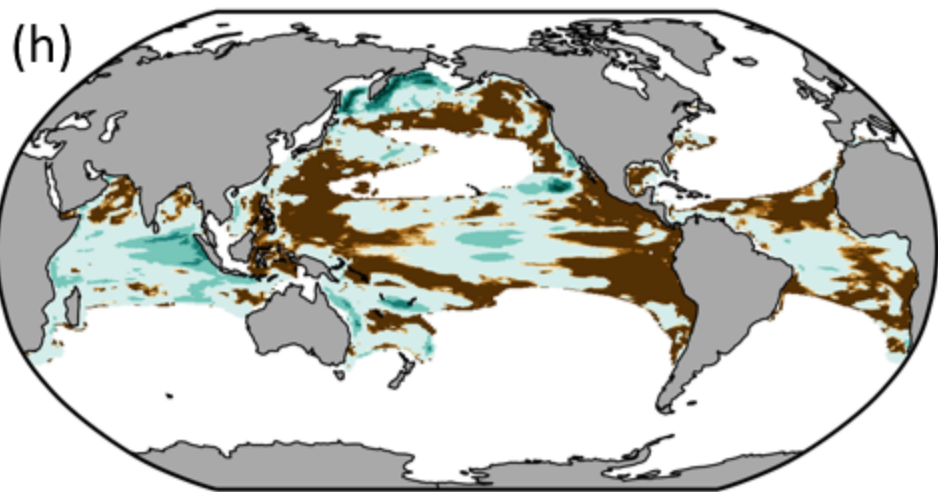
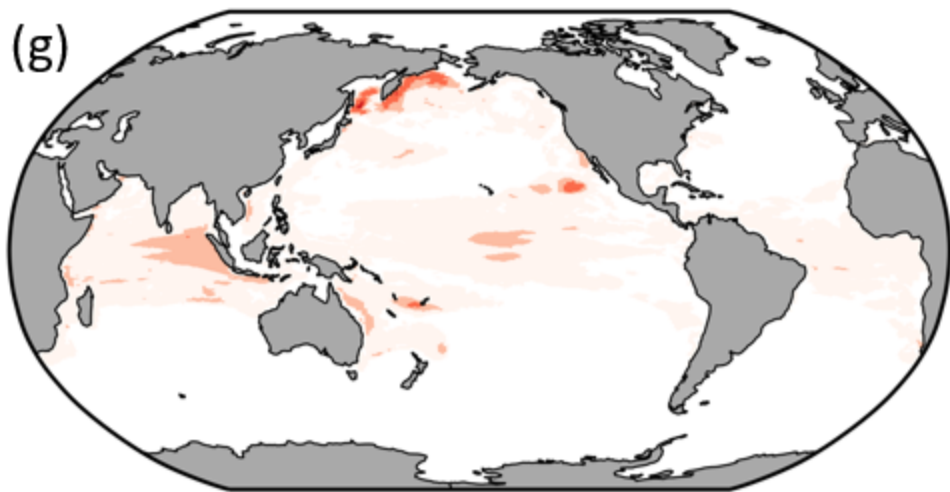
OAX-LOX



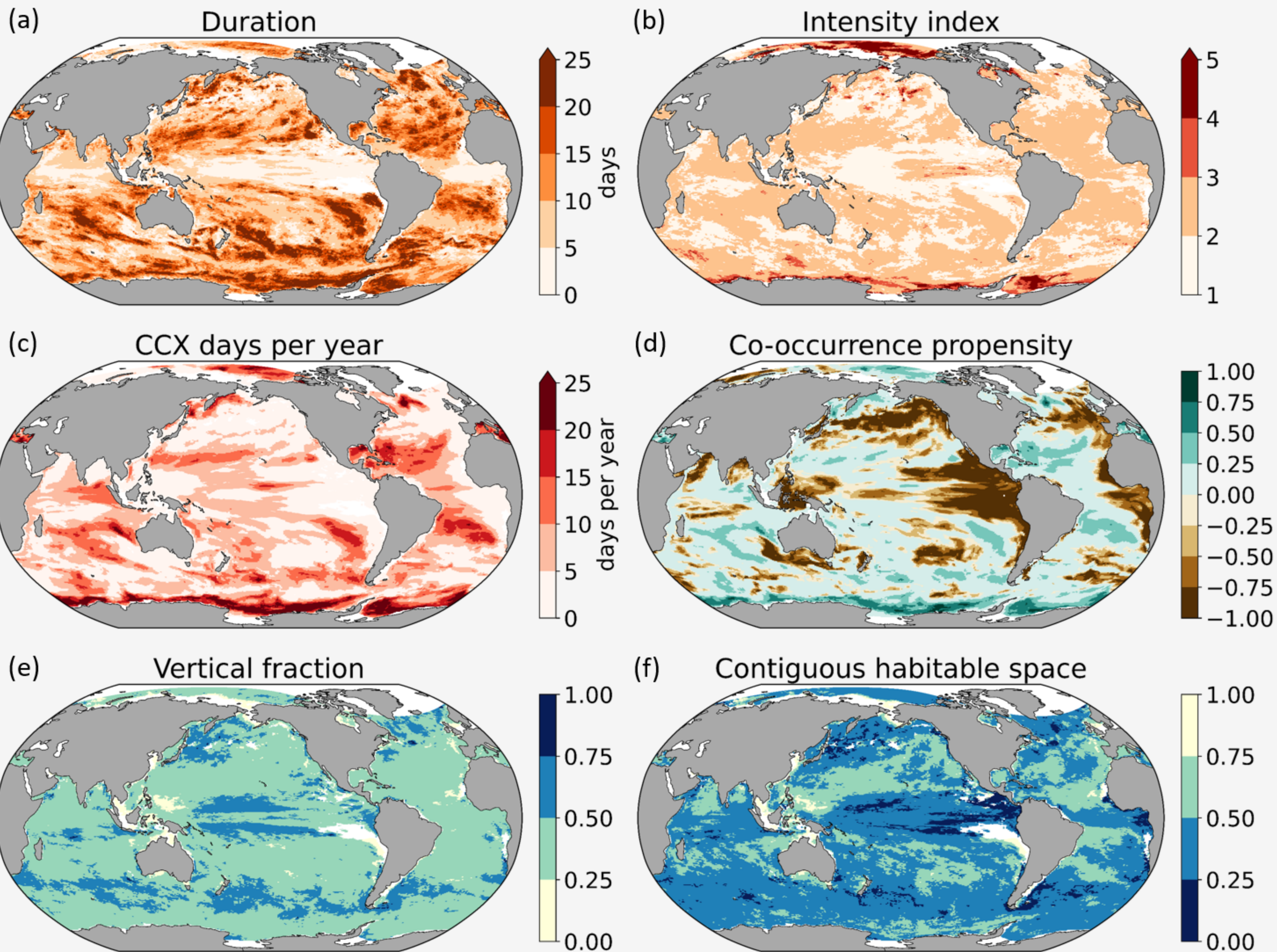
MHW-LOX



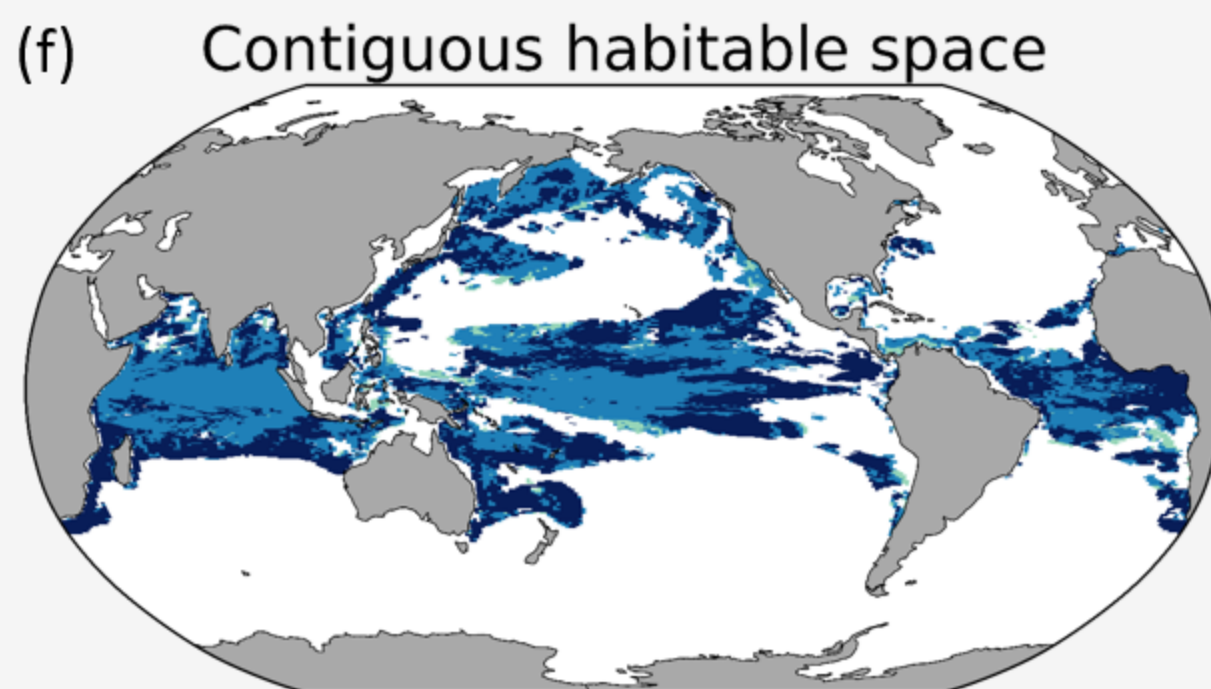
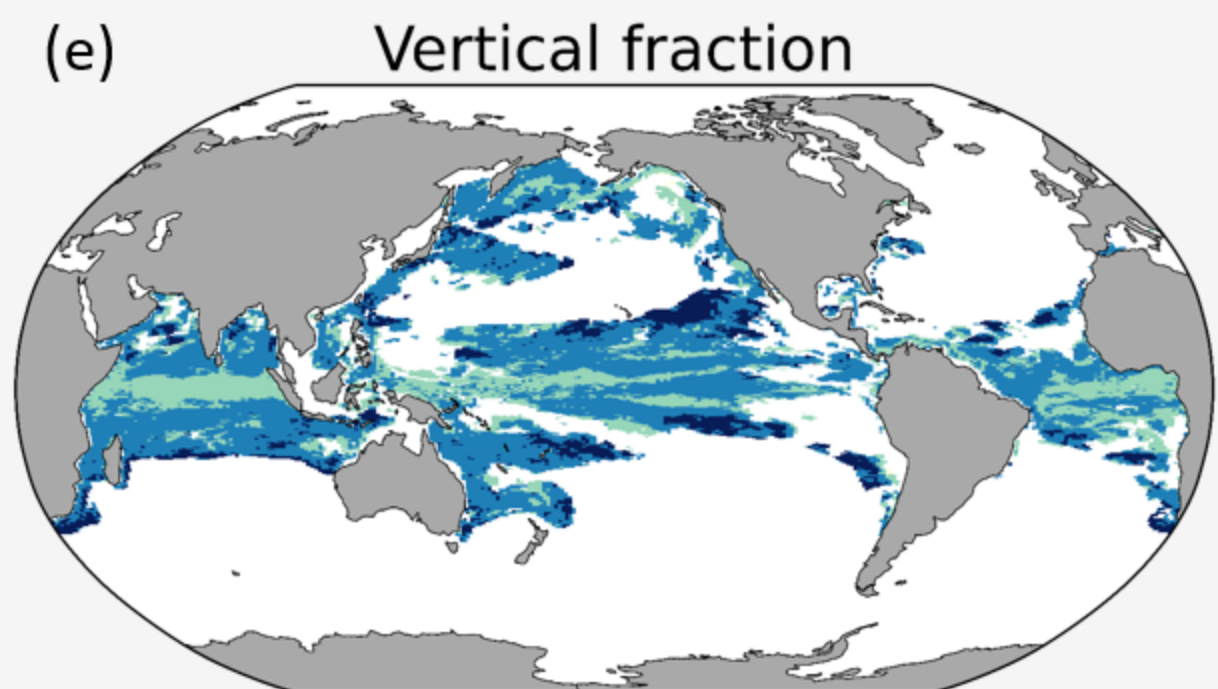
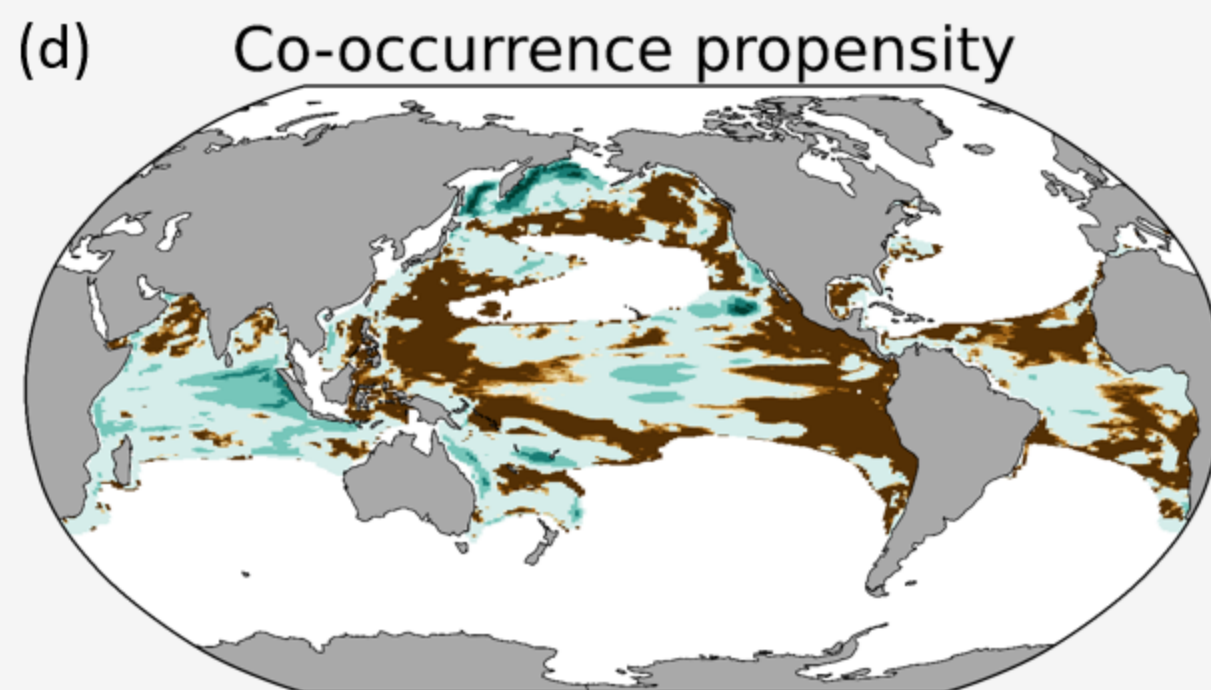
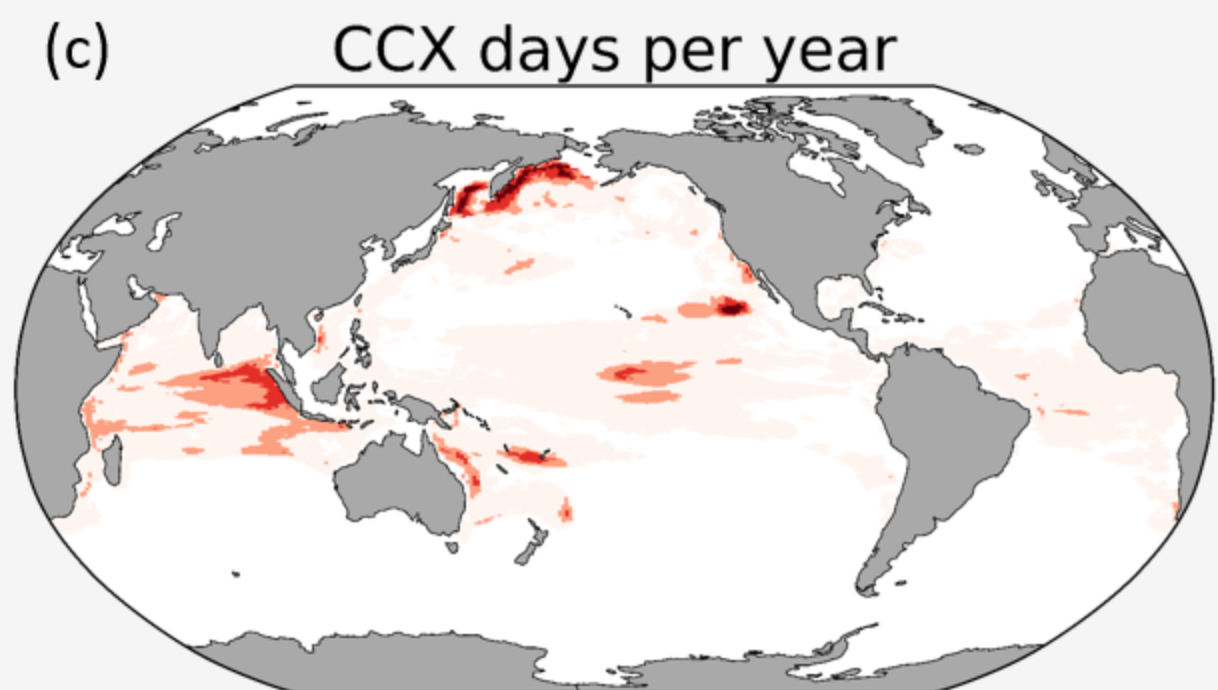
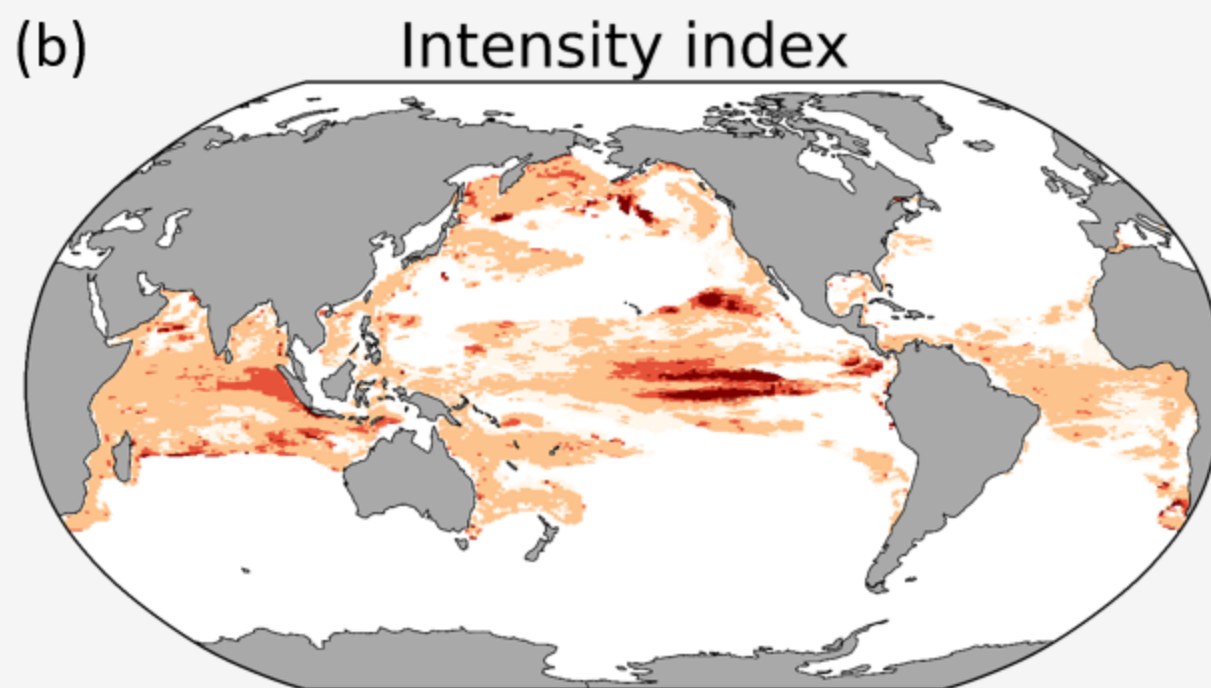
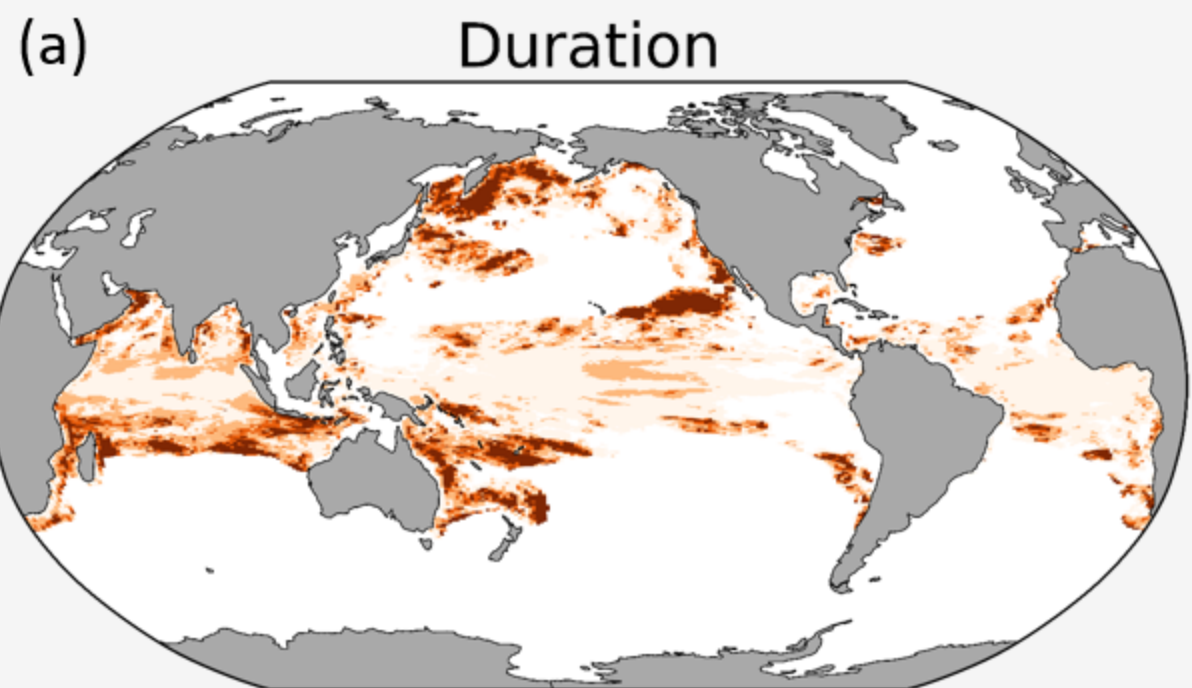
MHW-OAX-LOX

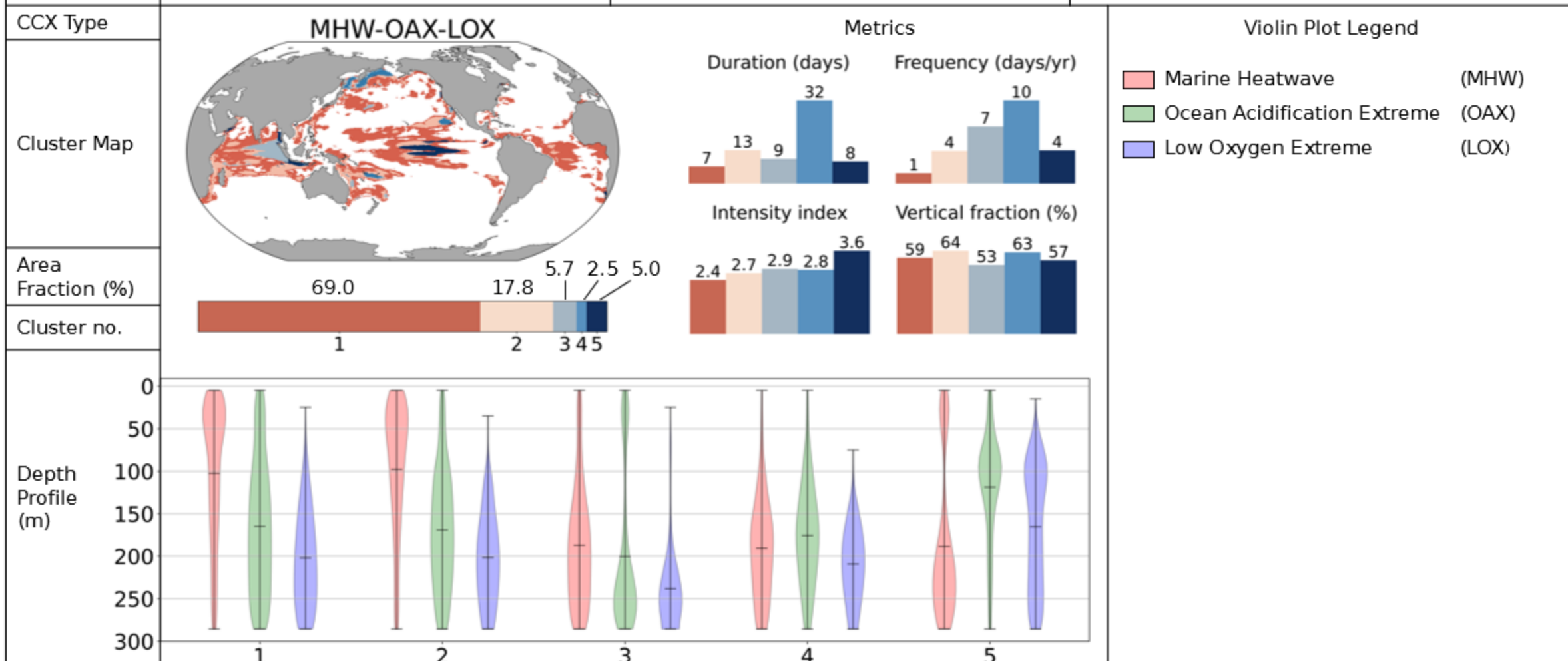
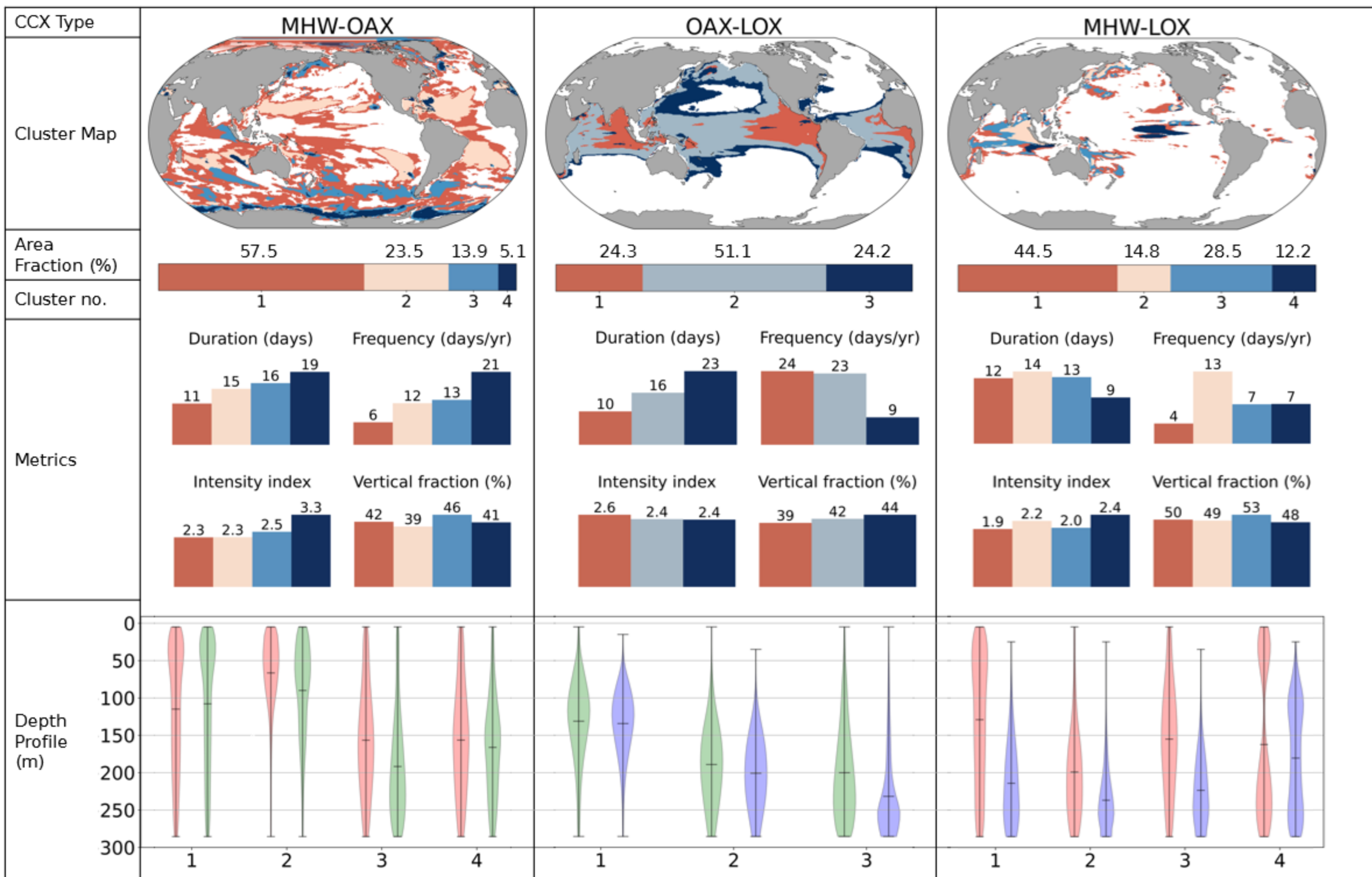


Key Metrics of the **MHW-OAX** Column-Compound Extreme



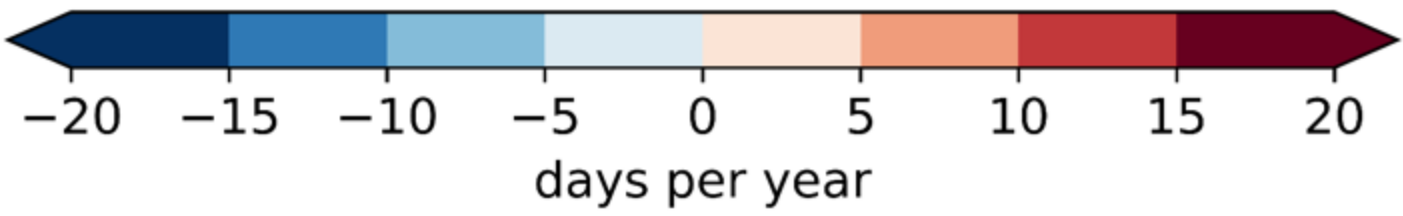
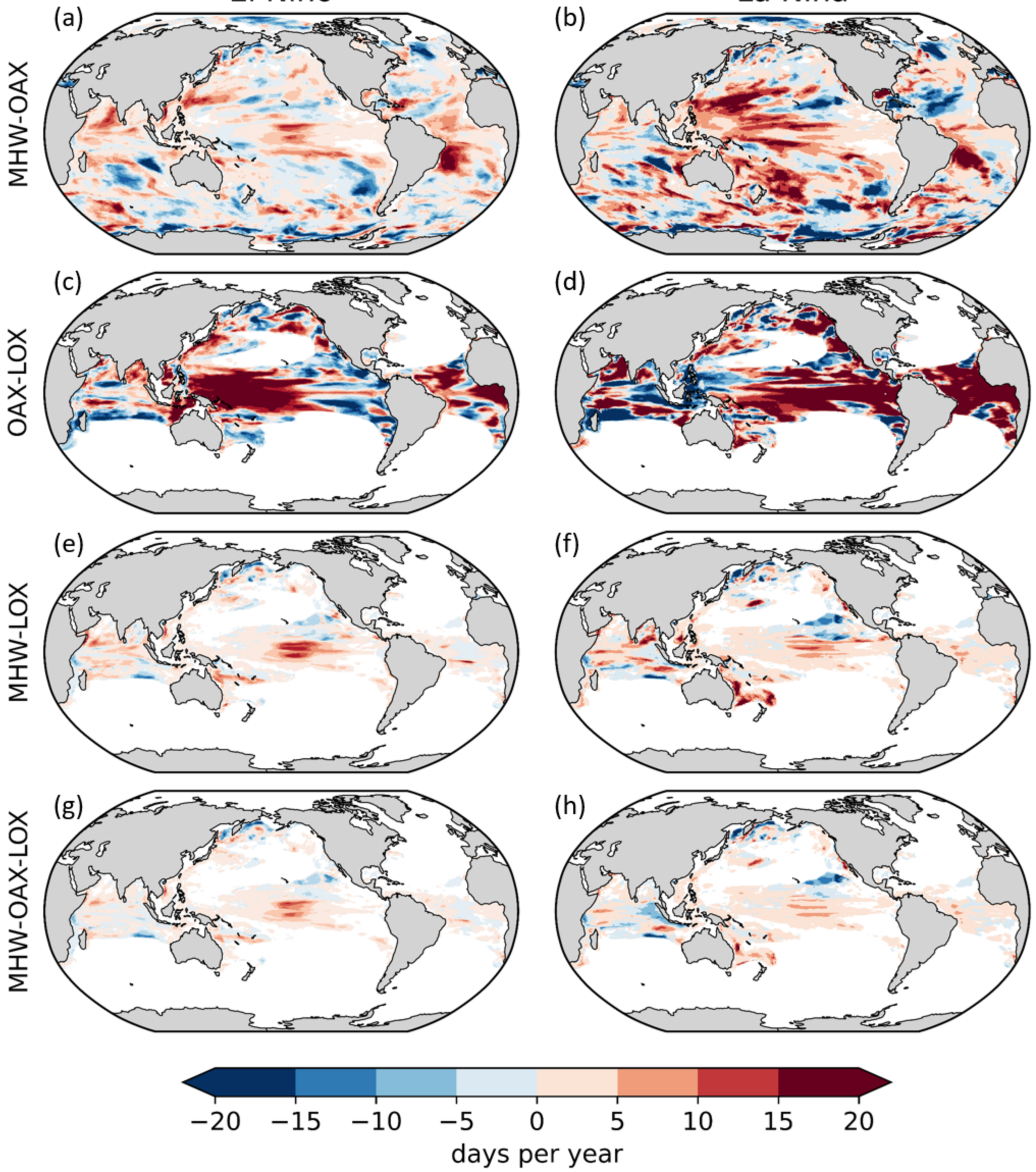
Key Metrics of the **MHW-OAX-LOX** Column-Compound Extreme

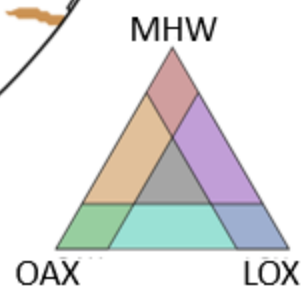
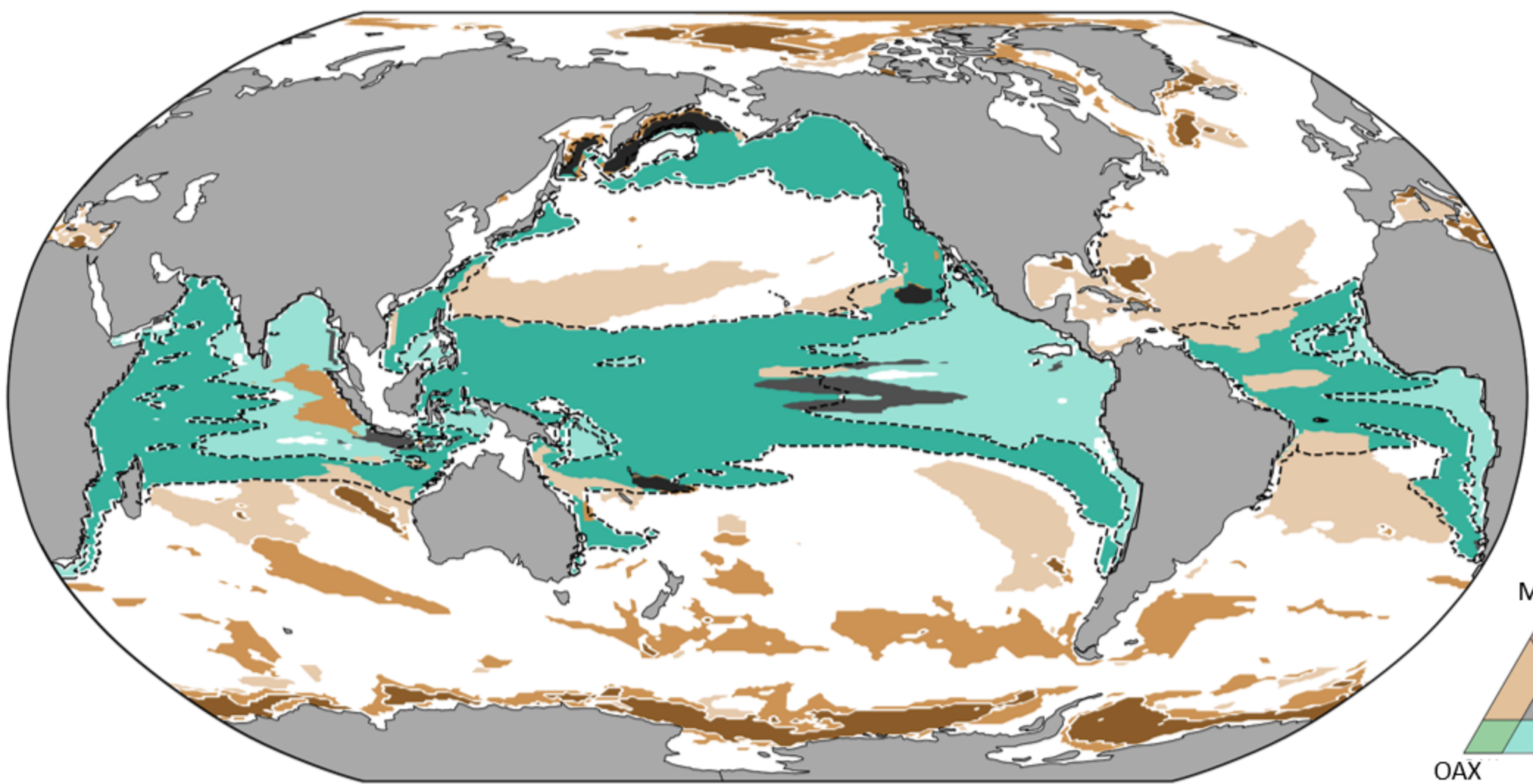




El Niño

La Niña





Cluster							
	MHW-OAX 2	MHW-OAX 3	MHW-OAX 4	OAX-LOX 1	OAX-LOX 2	MHW-OAX-LOX 5	MHW-OAX-LOX 4
Associated Regions	Subtropics, Tropics	Subantarctic	Antarctic	EBUS, East tropics	West tropics, OMZs	Central Tropical Pacific	Western Subarctic Pacific
Hovmoller Schematic							
Duration (days)	15 (49)	16 (40)	19 (29)	10 (27)	16 (39)	8 (13)	32 (52)
Frequency (days per year)	12 (81)	13 (58)	21 (50)	24 (67)	23 (53)	4 (16)	10 (20)
Intensity Index	2.3 (11.5)	2.5 (9.7)	3.3 (7.8)	2.6 (5.6)	2.4 (5.9)	3.6 (5.4)	2.8 (4.5)
Vertical Extent (%)	39 (88)	46 (83)	41 (79)	39 (70)	42 (75)	57 (75)	63 (81)
ENSO (+/-) change (days)	+2/+2	0/+2	-8/-5	+3/+13	+11/+8	+5/+3	-3/-5

